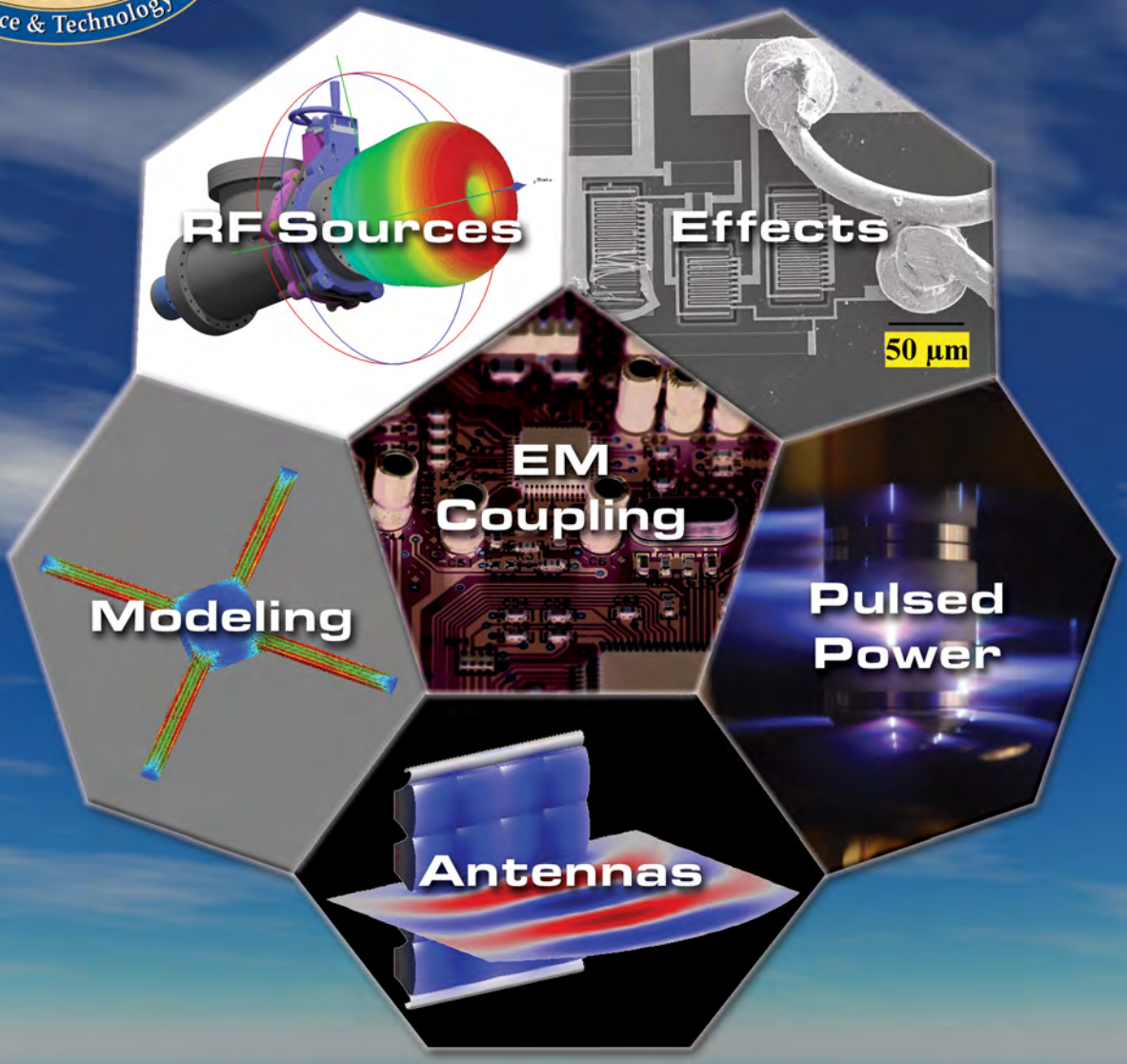

DIRECTED ENERGY WEAPONS (DEW)
HIGH POWER MICROWAVE (HPM)
6.1 PROGRAMS
FY18 ANNUAL REPORT

Mr. Ryan Hoffman, Program Manager

DCN#: 43-6161-20

NAVAL SCIENCE & TECHNOLOGY

Directed Energy Weapons (DEW) High Power Microwave (HPM) Program
Annual Report for FY18

Table of Contents

Directed Energy Weapons (DEW) High Power Microwave (HPM) Fundamental Research Program Annual Report for FY18

Introduction

Program Officer
Ryan Hoffman, Office of Naval Research

The Directed Energy Weapons (DEW) Program of ONR was initiated in response to the rapid development and growing threat of directed energy technologies by adversaries. Directed energy weapons are defined as electromagnetic systems capable of converting chemical or electrical energy to radiated energy and focusing it on a target, resulting in physical damage that degrades, neutralizes, defeats, or destroys an adversarial capability. The U.S. Navy uses HPM to gain and sustain tactical, operational, and strategic advantage in the arena of EM Maneuver Warfare and Integrated Defense for U.S. forces across the full range of military operations, including power projection and integrated defense missions. The ability to focus radiated energy reliably and repeatedly at range, with precision and controllable effects, while producing measured physical damage, is the measure of DEW system effectiveness. In anticipation of DEW advancements, the ONR HPM Program comprises a portfolio of initiatives and research projects which seek to provide the science and engineering basis for means and methodologies to provide the Navy advanced HPM technologies, systems, and techniques enabling a new class of weapons that will be highly effective in the battlespace. The goal is to be the most effective steward of DEW systems.

Asymmetric threats are proliferating worldwide and likely will continue to do so until such time as effective countermeasures are deployed. Often enough, Rules of Engagement will restrict kinetic engagement with asymmetric threats contingent on the particulars of the scenario. DEW systems – or more specifically for this report, HPM weapons – are expected to allow Naval commanders significantly more flexible responses to a number of asymmetric threats, including various small surface craft and unmanned aerial vehicle (UAV) threats. This flexibility is possible since the restrictions on engaging targets might be removed or reduced based on recognition of 1) the low collateral damage and 2) the non-lethal and reversible effects associated with HPM weapons.

HPM weapons create pulses of electromagnetic energy over a broad spectrum of known radio and microwave frequencies, causing either temporary or permanent results on electronics within targeted systems at scalable effects. HPM weapon systems can be used to disrupt, disable, or potentially destroy critical electronic circuitry in target systems, even in restricted scenarios, while also having the advantage of low cost per shot. HPM weapons deliver electromagnetic energy through coupling of the electromagnetic wave to target circuits through aperture or cable points of entry, thereby inducing currents in the circuitry capable of causing a variety of effects. Potential effects include erroneous signals, system lock-up, shutdown, loss of communications between systems, and physical damage.

As DEW falls within the Fundamental Research part of the broad ONR Science & Technology Investment Portfolio, projects funded are long-term initiatives, covering basic research or applied science. These investigations can have a five to twenty year horizon. Across the HPM technology thrust areas, research projects within the program include performers from academia, industry,

government laboratories, and small businesses. Moreover, the program includes performers whose research is financed through Navy SBIR/STTR funding. In addition, science and technology solutions from an international technical community are afforded through ONR Global, which funds projects that foster cooperation in areas of mutual interest with global partners. The program encourages the cross-pollination of ideas and collaboration among performers worldwide, and offers an annual review where performers provide updates on the status of their research and present results to their DEW peers. Furthermore, data and facilities sharing are encouraged within the program. This approach contributes to increased success for the program and for the Navy.

The portfolio is binned across technology thrust areas of materials, sources/devices, and target interaction. Further description on areas of interest and research include:

- Vulnerability and Lethality. Prediction of weapon effects through target vulnerability and lethality testing, data collection, and analysis that investigates HPM coupling mechanisms by utilizing modeling and simulation (M&S), and experimental validation.
- Improved Prediction Capability. Engagement level modeling, weaponeering, and battle damage assessment (BDA) co-located with HPM. Target interaction physics, advanced sensing, waveform optimization research, and improved prediction confidence with less target effects data (reduced program costs).
- Pulsed Power/Power Electronics. Pulsed power/power electronics, including high energy density batteries, power conditioning, switches, and modulator pulse forming networks that enable RF source development (vacuum and solid state).
- Advanced HPM and RF Sources that include novel generation methods. Increased effectiveness through higher rep-rate and frequency tunability. High power, low profile, conformal antenna design and radome materials, including very high power RF propagation and air breakdown modeling. Distributed arrays and beam combining.

RF Coupling Revisited

Grant No. N00014 -17-1-2932

Annual Summary Report for Fiscal year 2018

Period of Performance: September, 1, 2017 to August 31, 2020

Prepared by:

Professor Anthony Caruso, Principal Investigator
University of Missouri, Kansas City, MO
Department of Physics and Astronomy
5110 Rockhill Rd.
Flarsheim Hall, Room 257
Kansas City, MO 64110
Tel: (816) 235-2505
Fax: (816) 235-5221
Email: carusoan@umkc.edu

This work was sponsored by the Office of Naval Research (ONR), under grant number N00014 -17-1-2932. The views and conclusions contained herein are those of the authors only and should not be interpreted as representing those of ONR, the U.S. Navy or the U.S. Government.

Grant or Contract Number: N00014-17-1-2932
Date Prepared: November 30, 2018
Project Title: RF Coupling Revisited
Annual Summary Report: CY2018
Principle Investigator: Anthony N. Caruso, 816-235-2505, carusoan@umkc.edu
Department of Physics and Astronomy
University of Missouri, Kansas City, MO.

Section I: Project Summary

1. Overview of Project

Abstract:
The problem of undesirable RF coupling to wires and electronics has received high interest for several decades. Coupling can be unintentional, originating from nearby radiators, especially in the rising congestion in the wireless spectrum, or due to the rising threat of High Power Microwave (HPM) weapons. In this work, we develop a combined experimental and modeling approach to quantify coupling to realistic wire systems and we also develop general guidelines to protect wires and electronic circuity from unintentional and intentional interference.

Objective:
The objective of the proposed work is to develop rules-of-thumb to predict HPM source dependent effect coupling parameters for any arbitrary collection/geometry of wires/traces/wire-bonds, in a dielectric or metallic enclosure. Such studies are directly applicable to UAVs or circuits composed of printed circuit boards (PCBs)/wire-bundles. The work is a combined experimental, simulation and theory effort.

The underlying physics is based on the fundamental modes or eigen-currents induced in sections of wire(s) from impinging RF, and their nearest neighbor interactions. This may be viewed as charge flowing through a scatterer which can be decomposed into a weighted summation of fundamental modes. It is the support and strength of these modes that forms the basis for their frequency dependent coupling and primary/secondary induction.

The current-state-of-research in RF effects/coupling work focuses on the prediction of the statistical coupling properties which can be setup within arbitrary enclosures. Such efforts do not address the actual coupling to the electronics within these enclosures, although that is the future-art in development.

Introduction:
Electromagnetic weapons in the radio frequency range (700-MHz to 95-GHz) at on-target power densities that induce tenths- to ones-of-volts onto a printed circuit board trace, free wire, or other integrated circuit input (hereafter high-power microwaves or HPM) represent a single event effect (SEE) threat to microelectronics and their downstream applications. Developing a deeper understanding of the means by which HPM couple to wires, traces, chasses, integrated circuits, and/or their enclosures, as a function of the source properties, is the objective of this proposed effort. A stretch objective is to further understand the secondary and tertiary coupling effects, including direct and inductive coupling. At the conclusion of this work, the vision is a balance of

empirical- and simulation-derived results that will drive a generally applicable and pragmatic model (i.e., rules-of-thumb) that may be used to inform both the offensive and defensive side of HPM design and electronics and their enclosures.

Since at least the mid-1960s through today, electronic warfare – and to a lesser extent HPM – testing has been a staple for what is now MIL STD 464C. Empirical testing has and will likely continue to be used as there is no current ability to generate sufficient (i.e., simple, but mostly accurate) models. This effects testing has been employed against assets ranging from motor vehicles to desktop computers to unmanned aerial vehicles to smartphones to instrument landing systems. While with enough detail and empirical feedback data, some models have been developed, the models are not generalizable. Of those models that seek to be generalizable, they are too complex to set up, inaccurate and/or ill-pragmatic. A new approach, which stands on the shoulders of this previous work, but harnesses the utility/power of new capabilities, is needed.

New capabilities, whose confluence will take the above work to a new level, including the ability to: (a) map or predict the three-dimensional layout of complex electrical structures (e.g., wiring harness but not necessarily multilayer printed circuit boards); (b) automatically transfer the physical maps into simulation; (c) automatically approximate the complex permittivity/permeability of the materials; (d) run multi-source-parameter permutations on supercomputers inexpensively (through the ability to parallelize and run on an order-of-magnitude more cores/memory than two years earlier); (e) validate simulations through automated empirical measurements; and, (f) most of all, use machine learning methods to extract trends that humans cannot.

In this work, we will design, build and test an empirical measurement and simulation system capable of demonstrating the new capabilities described above to develop a predictive capability that is both simple and accurate enough to be useful for HPM effects and design needs.

Background:

One of the main techniques for predicting interference in metallic enclosures is the Random Coupling Model (RCM). The RCM addresses enclosures or cavities that are much larger than the wavelength of concern. Under this condition, the wave propagation inside the cavity is chaotic, meaning that any small change in the cavity or its components will lead to highly different outcomes. Based on the properties of the enclosure or cavity, such as its quality factor, statistical information about the voltages generated at the ports can be induced. In RCM, the ports can represent apertures in the enclosures or the input ports of devices and electronic circuitry inside the enclosure. Therefore, RCM aims to quantify the statistics of the interactions between the enclosures and its constituents. There are a number of other models (e.g., Dynamical Energy Analysis) and their predecessors that are important and form the basis for the work proposed here. We refer the reader to an exhaustive compilation of these works if greater background is desired (http://anlage.umd.edu/RCM/), as it is important that we shift gears to describe the background of the new effort proposed here.

In this work, we will focus on studying the constituents within an enclosure, primarily wiring systems and printed circuit boards. We will study the fundamental modes that these wiring systems and PCBs can support, how these modes vary with dimensions, material, and geometrical properties, before finally quantifying how the metallic enclosures will affect these modes. More importantly, we also propose a combined approach where computational electromagnetics modeling will go hand-in-hand with experimental measurements.

2. Activities and Accomplishments

During the reporting period, 10/1/2017–9/30/2018, the team: (1) Quantified the coupling to an individual wire with arbitrary shape using the Characteristic Mode Analysis (CMA), (2) Developed a preliminary experimental setup for the fully automatic quantification of crosstalk between a few wires with arbitrary shapes, (3) Studied coupling and crosstalk to PCB traces with realistic shapes, and (4) Initiated the employment of Big Data techniques to speed-up the computational models developed to allow the simulations of large systems of wires in a feasible computational time.

(1) Practical wiring systems typically exhibit non-straight wires or metallic traces. Therefore, the effect of wire shapes needs to be quantified to accurately assess the field-to-wire coupling and crosstalk in practical wiring systems. One of the approaches of constructing these arbitrary wires is the Random Walking Chains (RWC) model [1]. In RWC, each wire is divided into equal segments with a pre-defined length. Each segment changes its direction, by randomly varying its alignment angle β as shown in Fig. 1. By controlling the length of the segments and the range of variations in the angle β, a large variety of random wire shapes with varying waviness or curvature can be generated. To explain the variations in the field to wire coupling, we performed the Characteristic Mode Analysis (CMA) of the wires, decomposing the response into the first three fundamental modes. At low frequencies, where the incident wavelength is much larger than the size of the wire, the first mode dominates the response. As the frequency of the incident wave increases, higher order modes start to contribute to the overall response. So far we focused on the first 3 modes since they showed similar behavior as the wires became more wavy due to the increase in β in the RWC model. The results showed that as the wires became more crumpled, there was a slight increase in the average resonance frequency of the wire, a significant decrease in the bandwidth of each mode, and an increase in the amplitude of each modal current. Therefore, CMA explains why, on average, crumpled wires have larger coupling currents than straight wires. Moreover, it shows that this higher coupling current does not occur at a specific angle of incidence or polarization but that it is an inherent feature of non-straight wires. Therefore, the average coupled current over multiple angles of incidence and polarizations is higher for a curved wire than for a straight wire as shown in Fig. 1 albeit over a narrower bandwidth. Both wires in Fig. 1 are perfectly conducting and they have identical dimensions, length = 1 m and radius = 0.25 mm.

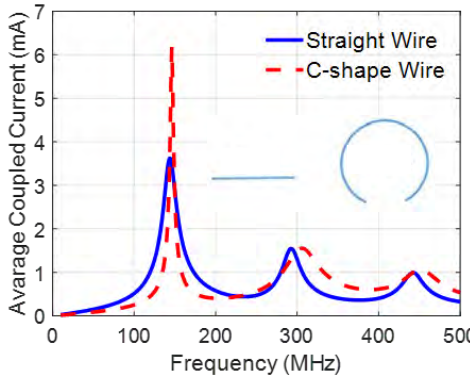

Fig. 1: The Average magnitude of the coupled current of an unterminated 1 m C-shaped wire versus straight wire in free space.

We are currently extending the CMA studies to include multiple wires. We selected an unterminated perfectly conducting wire pair with length L = 18 m, radius a = 1.25 mm, and separation d = 0.4 m, as shown in Fig. 2, similar to the dimensions described in [2]. We performed the CMA where we showed that the first mode of a single wire splits into two modes for a wire-pair: Mode 1 and Additional Mode 1. Fig. 3 shows the modal significance of Mode 1 and Additional Mode 1.

The current distribution of Mode 1 and Additional Mode 1 has a sin(πx) behavior where x is the normalized length of each wire $0 < x < 1$. However, for Mode 1, the currents in the two wires are in phase whereas for the Additional Mode 1, the currents are 180° out of phase but at a significantly larger amplitude than that of Mode 1. At 8.3 MHz, Additional Mode 1 has a very high modal significance. Therefore, at this frequency Additional Mode 1, with its large amplitude, will be most efficiently excited causing the total induced current on the wires to reach maximal values. This is confirmed in Fig. 4 which shows the total induced current at the middle of the bottom wire in Fig. 2. The current at 8.3 MHz is an order of magnitude larger than that at other frequencies.

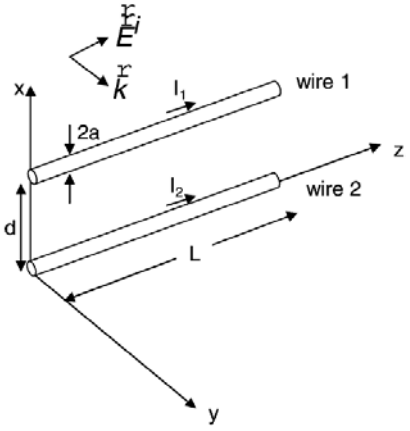

Fig. 2: A wire pair showing two wires of radius a, length L, and inter-wire

At this frequency, the wire is most prone to interference and coupling from external sources. Even though this frequency is hard to detect due to the narrow bandwidth of this resonance, CMA theory predicts the existence of Additional Mode 1 (see for example [3]) and therefore it will facilitate the detection of such frequencies where the currents in a wire pair will peak. In the next MSR we will investigate how the mode behavior will vary with the wires' conductivity, the separation between the wires, and how will it vary if the wires have an arbitrary waviness and are not perfectly straight. The wire-pair analysis will be used as a stepping stone for studying a large wire system with multiple wires.

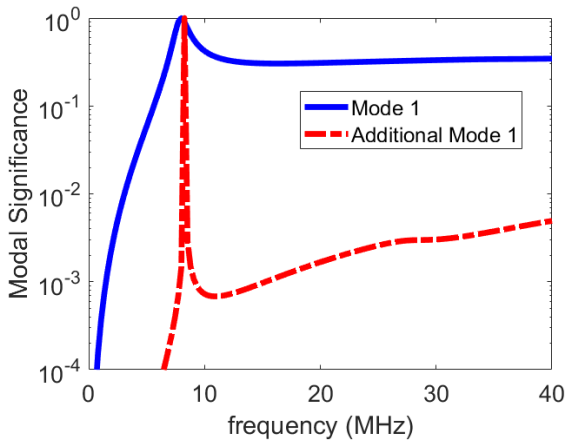

Fig. 3: The Modal Significance of the wire-pair in Fig. 2

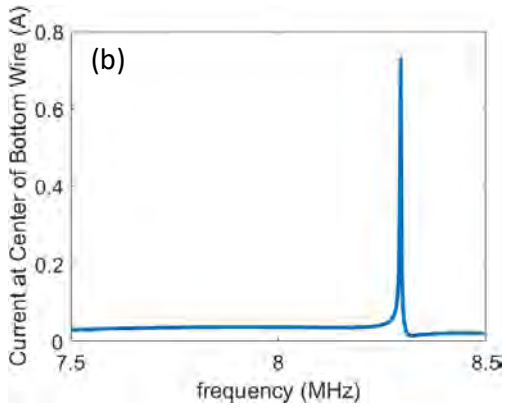

Fig. 4: Total current induced at the center of the bottom wire due to an incident plane wave at an angle of incidence of 60°.

(2) One of the main goals of work is to build a fully automatic experimental system that is capable of verifying our computational coupling and crosstalk predictions. The experimental system should be capable of studying complex wire systems with realistic shapes and distributions. We will progressively increase the number of wires in the experimental setup and extrapolate our conclusions to wire systems with hundreds of wires. However, most Vector Network Analyzers (VNA) have 2 or 4 ports. Therefore, to connect the VNA to numerous wires a switching/multiplexing system is needed as an interface. The switching/multiplexing system should introduce minimal losses and dispersion to maximize the signal that is transferred from the VNA to the wire system.

Fig. 5. ZTVX-8-12-S 2×8 switching system acquired.

We reviewed the commercial switching/multiplexing systems and we acquired the 2×8 ZTVX-8-12-S system shown in Fig. 5. The 2×8 ZTVX-8-12-S system has an Insertion Loss of ~ 1 dB, a Return Loss of ~ 20 dB, and an isolation of 90 dB between the ports over a frequency range that spans DC to 12 GHz, which covers the frequency range of interest in this project. The 2×8 ZTVX-8-12-S system will allow us to automatically collect measurements from a system containing up to 8 terminated wires. Moreover, by using another stage of switches, to be implemented using the 1×2 and 1×4 switches we currently possess, we can extend the number of wires studied experimentally.

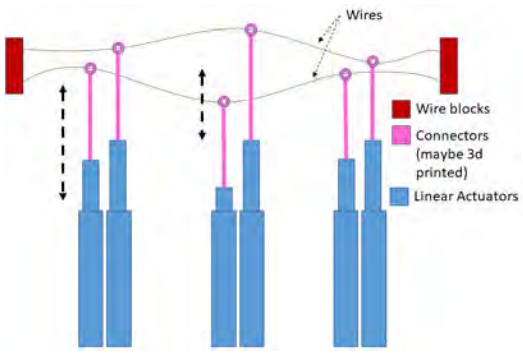

Fig. 6: simplified representation of a 6-linear actuator system with an example of a possible 2-wire configuration.

After automating the data collections using the 2×8 ZTVX-8-12-S switching system, we are currently developing multiple approaches to automatically vary the wire shapes and distributions. We started with a system of 2 wires attached to 6 linear actuators in the configuration shown in Fig. 6. The linear actuators will be connected to the wires via thin rods that are made of a low permittivity dielectric. We investigated different materials for these connectors to make sure they have minimal effect on the crosstalk between the wires. We used rubber and wood connectors and found that wood sticks have minimal effect on the measured scattering parameters from the wires. That is, the addition of wood sticks did not significantly modify the crosstalk values achieved when the wood sticks were absent. A picture of the setup is shown in Fig. 7. An Arduino microcontroller controlled the linear actuators, which translated the wood couplers, and changed the shape of the wires as shown in Fig. 7b. For each shape, the VNA collected the far-end crosstalk. The wire ends

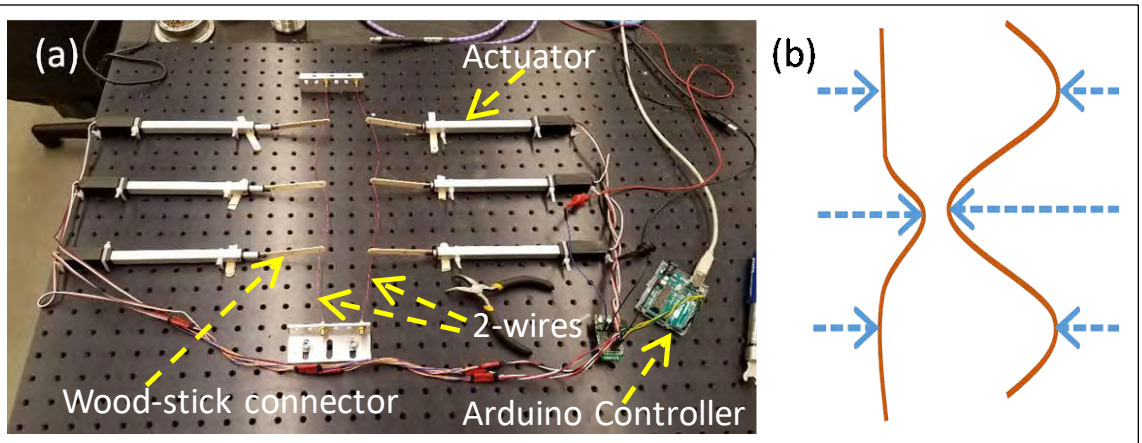

Fig. 7: (a) Experimental setup showing the automatic wire-shape varying system and (b) a sketch showing how the shapes of the 2-wires system are varied using the 6 linear actuators.

not connected to the VNA were terminated with an open circuit. For the initial data collection, we measured the far-end cross-talk for 729 different wire configurations, i.e. 3^6, which is achieved by shifting each of the 6 liner actuators by three different increments. Although a larger number of configurations was possible, 729 different configurations was found to reasonably cover the possible coupling variations, and the data collection required only 90 minutes with no human intervention.

Fig. 8 shows the: (a) average, (b) maximum, and (c) minimum far-end crosstalk calculated from the experimental measurements using the 729 two-wire configurations. The corresponding simulation values are also shown in Fig. 8. Good agreement is achieved between the experimental measurements and the simulations validating the accuracy of our experimental setup. Any discrepancy can be attributed to the fact that the simulatons did not account for the connectors, losses, and the sagging in the wires. Inspite of its simplicity, we plan to use this system to experimentally validate our numerical predictions and simulations for realistic wire configurations in multiple coupling and crosstalk scenarios.

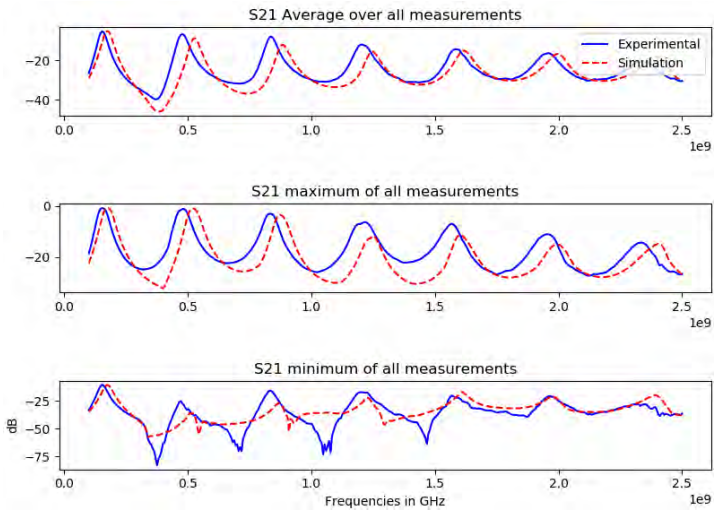

Fig. 8: Comparison between the experimental measurements and the numerical simulations of the average, maximum, and minimum far-end crosstalk.

For the immediate future, we are creating a system that can automatically configure a larger number of wires (8). Thus we will take one step

further in complexity, and become one step closer to understanding how cross-talk affects real wire systems.

(3) To the best of our knowledge, there is no systematic study that accurately quantified the effect of the shapes of PCB metallic traces on the electromagnetic coupling. To perform this analysis, an efficient full wave solver is needed. A major challenge in developing a full-wave model for PCB metallic traces, is to develop the adequate Green's Function (GF). The GF calculates the electric field at a certain observation point r due to an infinitesimal point source or dipole located at the position r'. Since any metallic trace in a PCB can be decomposed into smaller segments, which are effectively point sources, the GF represents the main component of the Method of Moments (MOM) full-wave electromagnetic solver. Over the past year, we developed an accurate and numerically efficient GF for PCBs. The GF contains Sommerfeld type integrals, which are extremely difficult to evaluate because they are semi-infinite integrals and in many cases they exhibit singularities within the integration range. We developed an efficient Green's Function solver by deforming the integration contour to avoid the singularities. This GF will be then incorporated into a full wave MOM electromagnetic solver that will be used to develop guidelines to minimize/maximize coupling to PCB metallic traces with a wide range of dielectric properties, sizes, and shape variations.

In parallel, we are using commercial electromagnetic solvers, until our fast and accurate solver is finalized, to simulate practical PCB scenarios with realistic dimensions and material properties. The Raspberry Pi and Arduino boards are two common single board computers that are used in many electronic systems. Fig. 9 shows the latest model of a Raspberry Pi with high-end computing power, which could reach operating speeds of up to 1.4 GHz. The highlighted areas in Fig. 9 shows various shapes and sizes of traces. Our motivation for studying this board is some recent experimental measurements performed by our collaborators, the group of Professor Daryl Beetner, at Missouri University of Science and Technology, which showed significant field to trace coupling to a Raspberry Pi at frequencies above 1.5 GHz. This coupling occurred even if no wires were attached to the Raspberry Pi, indicating that it occurred directly to the PCB. We used CMA to investigate the modes that are responsible for this coupling, understand the behavior of these modes, and use this behavior to maximize/minimize coupling to specific PCB traces at various locations on the Raspberry Pi.

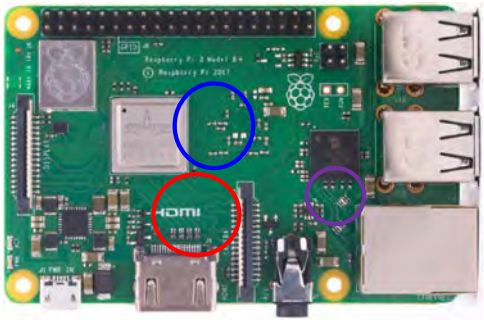

Fig. 9. The latest Raspberry Pi 3 b plus model with a Broadcom microprocessor at operating frequency of 1.4 GHz.

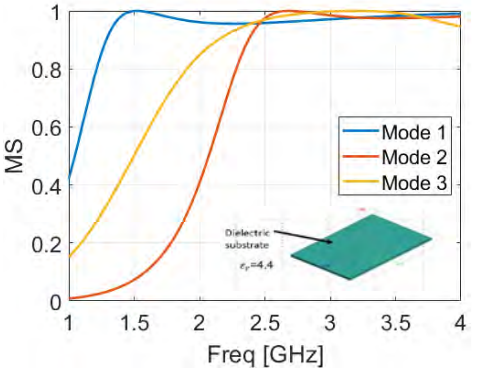

Fig. 10: Modal significance of simplified PCB composed of a ground plane + dielectric layer on top.

Modeling the Raspberry Pi with all of its components will require a large computational time. Therefore, we started by simulating a simplified model of the Raspberry Pi and we will progressively

increase the complexity of the structure by adding more features. We first considered only the ground plane of size 85.6 mm × 56 mm which matches the dimensions of the ground plane of a Raspberry Pi as described in [4]. Later, a dielectric layer was added on top of ground plane of the same lateral dimensions and with a thickness of 2 mm. The relative dielectric permittivity of the layer was set to $\varepsilon_r = 4.4$. The modal significance of the dielectric layer backed by the ground plane is shown in Fig. 10. It is important to note that, in spite of their simplicity, the model in Fig. 10 can help explain the coupling measurements from a broad range of practical PCBs with similar dimensions.

Fig. 10 corroborates the experimental measurements which showed that no direct coupling can occur to the Raspberry Pi at frequencies below 1.5 GHz which is the resonance frequency of Mode 1. This is because the modal significances of all of the modes in Fig. 10 are small below 1.5 GHz and, therefore, no efficient coupling pathways to the Raspberry Pi are available. Therefore, if the goal is to maximize direct coupling to a Raspberry Pi, CMA shows that the incident electromagnetic pulse should not have any energy below 1.5 GHz because these frequencies do not couple efficiently to the Raspberry Pi.

The current distributions of the modes of the simplified PCB structure are shown in Fig. 11. The current distribution of Mode 1 is predominantly parallel to x-axis, current distribution of Mode 2 is predominantly parallel to y-axis, and Mode 3 is a combination of Mode 1 and Mode 2 with currents oriented in both the *x* and *y* directions. To demonstrate how CMA can guide field to trace coupling in a practical PCB, we added a single trace of length (L) = 81 mm and width (W) = 3.854 mm to our structure with open circuit loads at both its the ends. In addition to the characteristic impedance and shape of trace, the location of trace on the board is equally important. Therefore, we placed a single trace at three different locations on the board: (a) top, (b) center, and (c) bottom as shown in Fig. 12. One way to excite these traces, is by using an incident electric field parallel to the traces in Fig. 12. Fig. 13 shows the coupled current to the three trace locations at 1.5 GHz which is the resonance frequency of Mode 1. A trace located at the edges (top edge or bottom edge) shows significantly higher current amplitudes than a trace located near or at the center. For example, the traces at the top and bottom edges of the board exhibited a maximum coupled current of 60 mA/m whereas the trace at the center of the board exhibited a maximum coupled current of only 30 mA/m. This can be justified because Mode 1 of the ground plane has hotspots at the edges as shown in Fig. 11. Therefore, traces located at the edges will be prone to a higher coupling currents at 1.5 GHz.

Therefore, in summary we showed in this section that CMA can be used to determine the frequency range where the modes have high modal significance and therefore will act as efficient pathways for field to trace coupling. Moreover, CMA provides the current distribution of each mode.

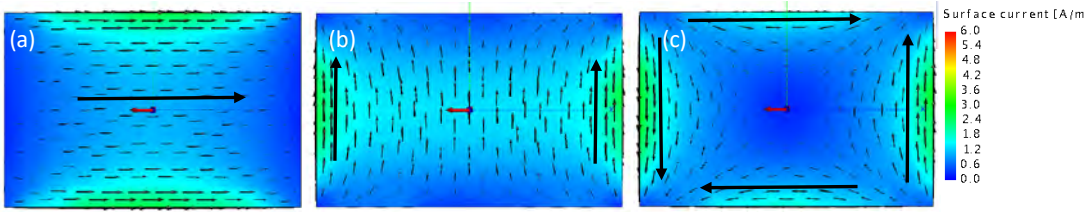

Fig. 11. Current Distribution of the first three modes of the simplified PCB composed of a dielectric layer backed by a perfectly conducting ground plane.

Therefore, if a specific trace on a PCB needs to be targeted we can calculate the optimum incident waveform that excites the modes with hot spots in the vicinity of these traces.

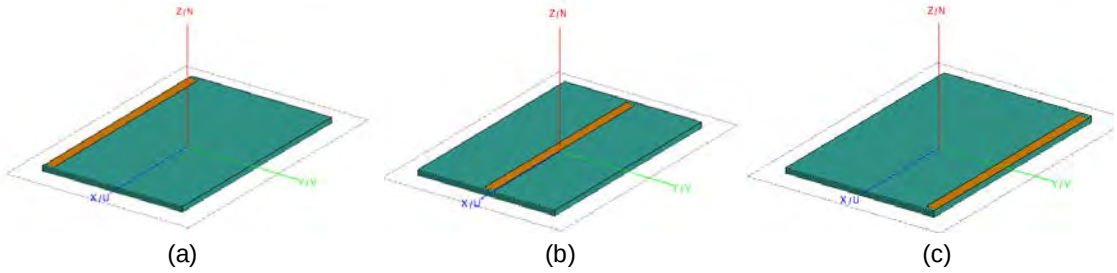

Fig. 12. Three different configurations (a) Trace located at the top edge, (b) Trace located at the center, and (c) Trace located at the bottom edge of the PCB board.

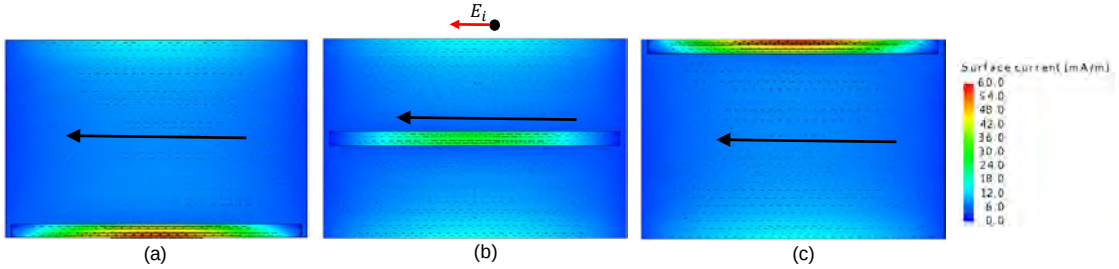

Fig. 13. Coupled currents at 1.5 GHz for trace at the (a) bottom, (b) center, and (c) top of the PCB board.

(4) As the number of wires and PCB traces increases, the computational expense of the CMA increases significantly. Therefore, we started to investigate multiple options to accelerate our CMA codes to be able to achieve our future goal of performing the CMA of hundreds of wires. A system with hundreds of wires will contain millions of unknowns generating Method of Moments impedance matrixes with millions of elements. Moreover, these matrices need to be calculated at every frequency, leading to terabytes of data, which creates a classical Big Data problem. Therefore, we are currently leveraging the well-established Big Data techniques for the acceleration of our CMA code. As CMA requires processing of complex numbers, we rewrote the code to use TensorFlow and Numpy libraries using Pyspark. Pyspark is a Python wrapper for Apache Spark. We read an input matrix of 50496 x 50496 complex numbers stored in HDFS and partitioned it into four equal sub matrices ZEE, ZEH, ZHE, and ZHH following the CMA algorithm for dielectric scatterers [5]. These submatrices arise only for dielectric scatterers where the MOM solution involves enforcing electric and magnetic surface currents on the surface of the scatterer. The size of these submatrices is only one fourth of the original MOM impedance matrix and therefore, they contain 25248 x 25248 elements. In the next step, we represented the magnetic currents in term of the electric currents and we computed the effective impedance matrix, Zeff, as Zeff = ZEE - ZEH*inv(ZHH)*ZHE. Finally, we computed the SVD of the real part of Zeff. The number of elements of the Zeff matrix is also 25248 x 25248 elements. The total process, took 45 minutes on a workstation with two Intel Xeon E5-2687W processors (20 cores / 40 threads in total) which is highly efficient given the size of the matrix. We are pursuing other Big Data techniques to further

optimize the CMA implementation and to adapt it for execution in parallel using a large number of processors.

3. Findings and Conclusions

Findings during FY17-18 are three-fold; (1) Non-straight crumpled wires experience larger field to wire coupling than straight wires of the same size, (2) Demonstrated how the CMA can be leveraged to excite a specific current profile to trigger the desired effect in a system of wires, and (3) Used several experimental measurements to validate these CMA predictions.

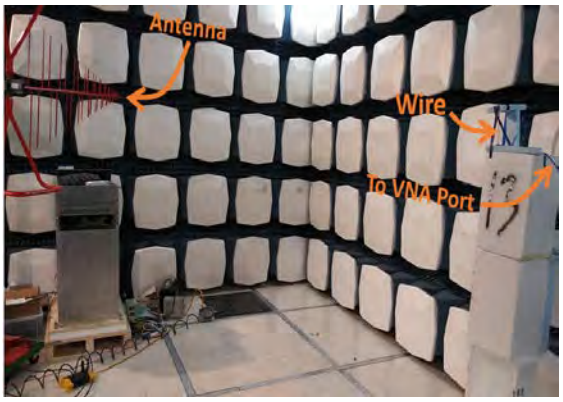

Fig. 14: Experimental Setup for measuring unterminated wire coupling in a semi-anechoic chamber, hybrid antenna.

Motivated by our CMA predictions, we collaborated with Professor Daryl Beetner's group at Missouri University of Science and Technology to collect experimental data to prove that, for the case of unterminated wires in free space, curved wires exhibit higher coupling current than perfectly straight wires. The experiment was conducted in the anechoic chamber shown in Fig. 14. A VNA was connected to a radiating antenna on Port 1 and a current clamp is connected to Port 2. The current clamp is attached to the center of the wire and is anchored by foam, as shown in Fig. 15, allowing it to measure the effect of Mode 1 which is highest in magnitude near the center of the wire. The wire is a semi-rigid coax which is 40 cm in length and 3.5 mm diameter.

The straight wire was placed vertically, parallel to E^i, to achieve maximum coupling to the straight wire. Then we repeated the measurements of the coupled currents at multiple orientations of the curved wires and calculated the averages. The ratio between the experimentally measured coupled current of a curved wire and that of a straight wire is shown in Fig. 16. The simulations result from the same configurations is also plotted in Fig 16 showing excellent agreement and hence validating both the experimental and simulation results. The experimental and simulation results show that the curved wire will exhibit coupling currents with larger magnitude than that of a straight wire which agrees with the CMA predictions.

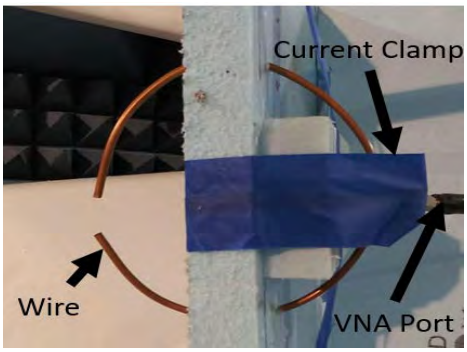

Fig. 15: Curved wire arc with the current clamp attached to the center of the wire.

In conclusion, the shape of a single wire has a significant effect on the coupled current. For a realistic wire system with many wires, we expect that the shapes and distribution of the wires will also have a significant effect on the coupling and the susceptibility of the wire system to interference and HPM. Therefore, CMA provides a useful tool for predicting and quantifying this shape and distribution effects.

Moreover, CMA allows the detection of the modes with the largest current amplitudes and the frequency where these modes have the highest model significance. These frequencies will be the optimum target frequencies to maximize the coupling current in a wireless system.

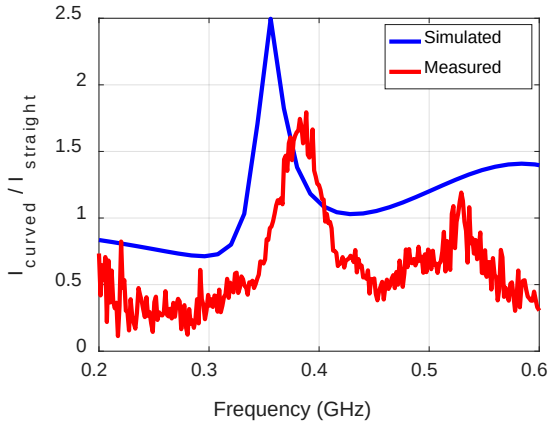

Fig. 16: Experimental/computational results showing the ratio between the currents coupled to a curved wire normalized with respect to the current coupled to a straight wire.

The CMA is not restricted to wires in free space. In this work, we showed how it can also be applicable to PCB traces and how CMA can guide the optimal location for trace placement on PCB to minimize the coupling current.

CMA can be used to predict the optimum excitation to generate a specific current pattern on a wire system. For example, consider two straight parallel wires, each 20 cm in length with a radius of 0.25 mm, as shown in Fig. 17. In this example, the goal is to develop the optimum excitation that excites a particular region in one of the wires and leave the second wire unexcited. This will be particularly beneficial for a differential two-conductor transmission line. The desired current pattern is shown in Fig. 17b.

From Fig. 18, we can see which modes are significant over the frequency of interest. Moreover, Fig. 18 shows the resonance frequencies where it will be most efficient to excite these modes. The wires will be then excited with 6 plane waves at these 6 frequencies to get the desired current pattern. Therefore, in total, six different plane waves at six different frequencies will be used to excite the wires in Fig. 17. The 6 waves will be assumed to propagate in the same direction (θ = 45°, φ = 45°) where θ is the polar angle measured from the z-axis and φ is the azimuthal angle. The optimization problem involves calculating the amplitude and phase of these six plane waves to achieve the desired current in Fig. 17b. At each frequency, multiple modes have high significance, and therefore each of the six plane waves will excite a mixture of modes with different weights. Using superposition, we add up the excited modes to get the total current. By equating the total current with the desired current in Fig 17b, a system of 6 equations in 6 unknowns can be formulated where the unknowns are the amplitudes/phase of the 6 plane waves. Calculating these amplitudes, the current in Fig. 19 is achieved which closely matches the desired current. This close agreement demonstrates the strength of the CMA in calculating the optimum excitation to generate

a desired current pattern on a system of wires. This optimization was performed at a very low computational cost without the need for a large number of trial and error iterations.

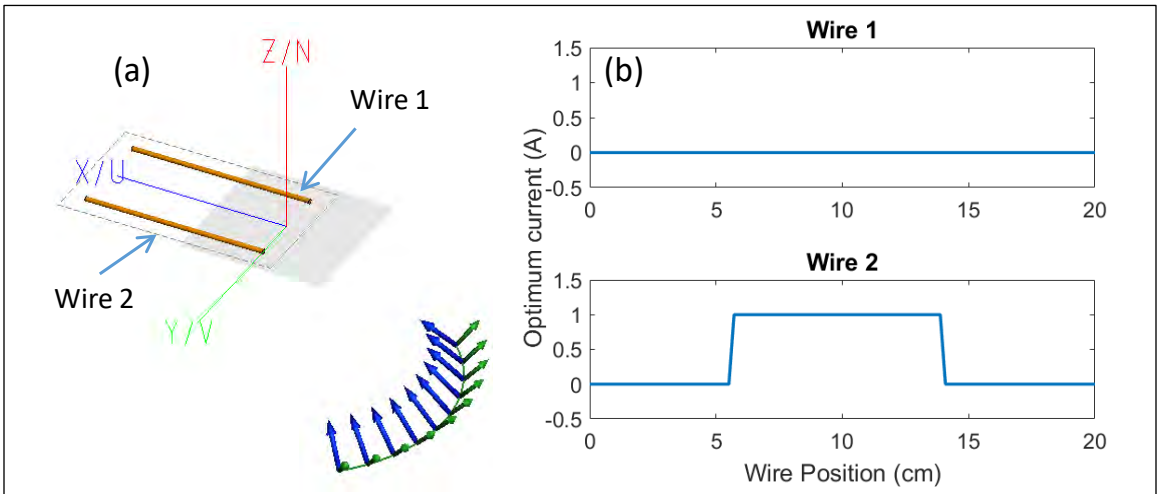

Fig. 17: (a) Two wire configuration with multiple incident excitations and (b) desired optimum current.

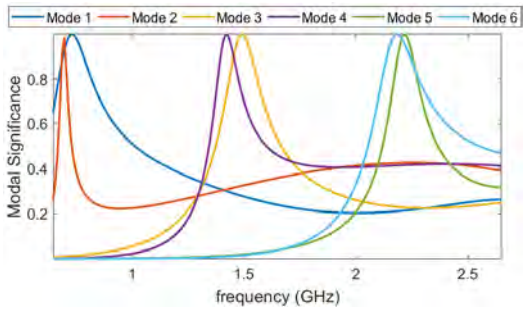

Fig. 18: Modal Significance of the first 6 modes of the two wire system in Fig. 1.

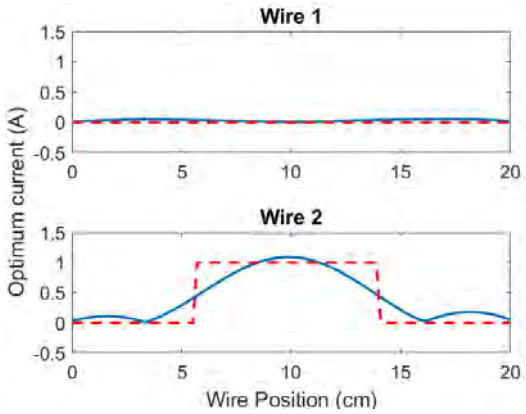

Fig. 19: The CMA optimized current excited (solid) on the wire system versus the desired current distribution (dashed).

References

[1] S. Herasati and L. Zhang, "A new method for characterizing and modeling the waviness and alignment of carbon nanotubes in composites," *Composites Science and Technology*, Vol. 100, Pages 136-142, 2014.

[2] A. Vukicevic, F. Rachidi, M. Rubinstein, and S. V. Tkachenko, "On the Evaluation of Antenna-Mode Currents Along Transmission Lines," *IEEE Trans. Electromagn. Compat.*, vol. 48, no. 4, pp. 693–700, Nov. 2006.

[3] A. M. Hassan, F. Vargas-Lara, J. F. Douglas, and E. J. Garboczi, “Electromagnetic Scattering From Multiple Single-Walled Carbon Nanotubes Having Tumbleweed Configurations,” *IEEE Trans. Antennas Propag.*, vol. 65, no. 6, pp. 3192–3202, Jun. 2017.
[4] https://www.raspberrypi.org/products/raspberry-pi-3-model-b-plus/
[5] Y. Chen and C.-F. Wang, “Surface integral equation based characteristic mode formulation for dielectric resonators,” *in 2014 IEEE Antennas and Propagation Society International Symposium (APSURSI), Memphis*, TN, USA, pp. 846–847, 2014.

4. Plans and Upcoming Events

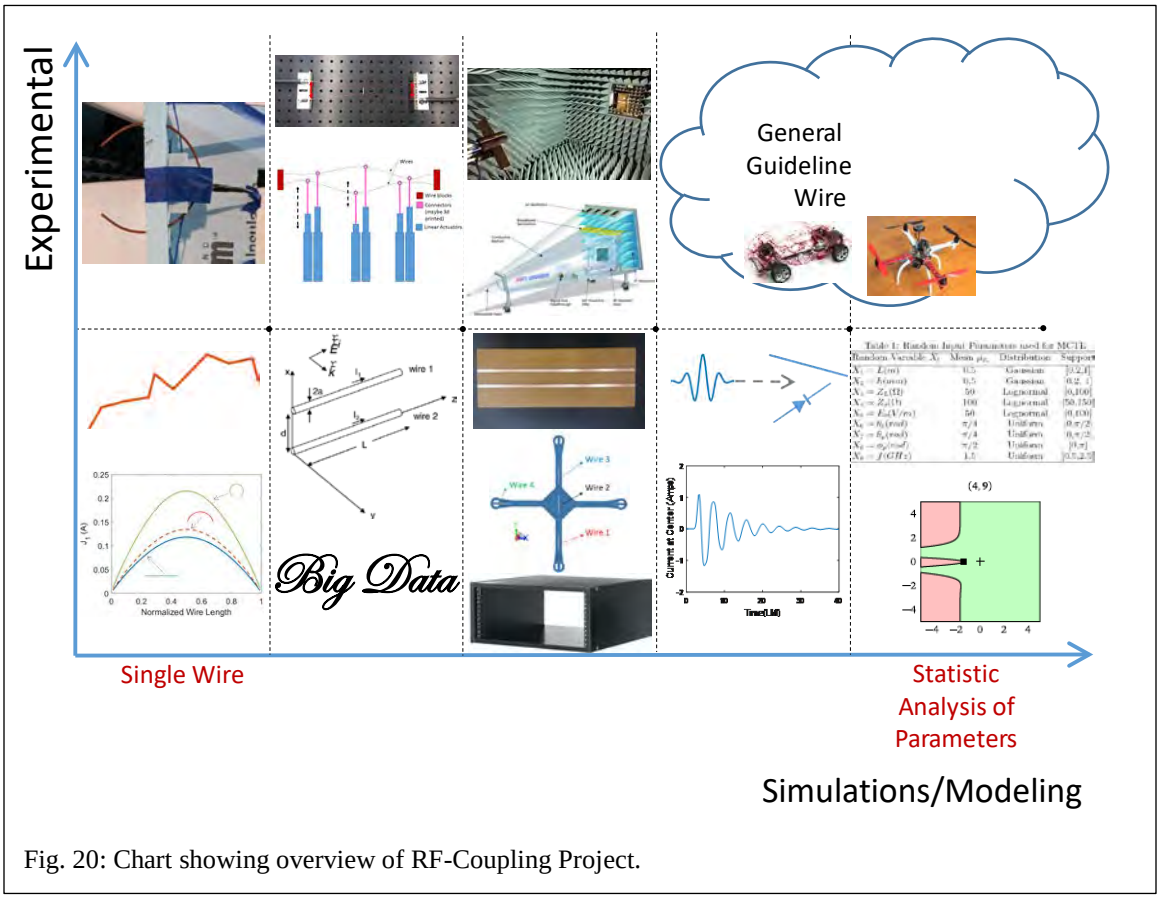

Fig. 20: Chart showing overview of RF-Coupling Project.

Fig. 20 shows a general overview of the main tasks of the project. The *x*-axis of the chart shows the simulations/modeling tasks and the *y*-axis shows the corresponding experimental validations highlighting our dual experimental/modeling approach. So far we finalized the “Single Wire” step and are currently working on the case of “Multiple Wires.” To facilitate the CMA analysis of a large number of wires, we will continue with exploring various Big Data and parallelization techniques to accelerate the CMA. This acceleration is vital for the simulations of a large number of configurations necessary to develop accurate crosstalk and coupling guidelines.

After finalizing the analysis of Multiple Wires in free space, we will expand the study to include "Wires in a Realistic Environment." For example, we will integrate the developed GF in this report with a full-wave efficient electromagnetic solver which will allow us to extend the CMA to PCB traces. We will also study wires in a perforated cavity or on top of the frame of an unmanned aerial vehicle (UAV). We plan to investigate the effect of nonlinear terminations on the coupling and crosstalk of wires and PCB traces. For nonlinear loads, time domain electromagnetic solvers will also be investigated as a more efficient alternative to frequency domain electromagnetic solvers. Finally, all of the conclusions achieved form the previous tasks will be integrated to achieve "General RF Coupling Guidelines to Practical Wire Systems."

Milestones:

Year 1

1- CMA of single wire.
2- CMA of few wires.

Year 2

1- CMA of practical wire systems.
2- Big Data acceleration of CMA.
3- CMA of wires in a realistic environment (e.g. PCB, perforated metallic cavities, in the vicinity of a UAV frame).

Year 3

1- Statistical analysis of multiple wire configurations.
2- Develop general RF coupling guidelines to practical wire systems.

5. Transitions and Impacts

The highly efficient CMA codes, accelerated using Big Data techniques, will be augmented with adequate Graphical User Interfaces (GUI) and documentations and presented for the general use of ONR and its defense contractors, e.g. Verus Research (http://www.verusresearch.net/). Moreover, the CMA conclusions and the statistical analysis will be used in FY2020 to prepare several monographs to act as accurate guidelines for RF coupling and interference mitigation and protection.

6. Collaborations

- Professor Daryl Beetner, Missouri University of Science and Technology, Electromagnetic Compatibility Lab
- Assistant Professor, Victor Khilkevich, Missouri University of Science and Technology, Electromagnetic Compatibility Lab
- Assistant Professor, Zhen Peng, Department of Electrical and Computer Engineering, University of New Mexico, Albuquerque.

7. Personnel

Principal investigator

Anthony N. Caruso, National Academy Member (Y/**N**)

Co-investigator or Co-PI

Ahmed Hassan, National Academy Member (Y/**N**)

Business Contact

Linda Daugherty

Team Members:

Deb Chatterjee, Praveen Rao, John Lancaster, Mohamed Hamdalla, Kalyan Durbhakula, Jesus Miguel Roacho-Valles, Waleed Al-Shaikhli, Khulud Alsultan, Khadimul Islam, Caylin Hartshorn, Clayton Kettlewell, National Academy Member (Y/**N**)

8. Students

Undergraduate Students: Caylin Hartshorn, Jesus Miguel Roacho-Valles, Clayton Kettlewell

Graduate Students: John Lancaster, Mohamed Hamdalla, Kalyan Durbhakula, Waleed Al-Shaikhli, Khulud Alsultan, Khadimul Islam

9. Technology Transfer

None

10. Products, Publications, Patents, License Agreements, etc.

Publications resulting from this project:

Archival Publications (publication reference information (article title, authors, journal, date, volume, issue) can be automatically entered using a DOI)

a. *Article Title:* Electromagnetic Coupling to Wires with Realistic Shapes: A Characteristic Mode Approach
b. *Journal*: IEEE Transactions on Electromagnetic Compatibility
c. *Authors*: M. Hamdalla, W. Al-Shaikhli, J. Lancaster, J. D. Hunter, L. Yuanzhuo, V. Khilkevich, D. G. Beetner, A. N. Caruso, A. M. Hassan
d. *Keywords*: Field-to-wire coupling, Characteristic Mode Analysis, Shapes, Full-wave analysis
e. *Distribution Statement*: Paper is still under preparation and has not been submitted. Authors will submit the paper for review and approval. However, authors believe paper can be Distribution A.
f. *Publication Status*: Under Preparation
g. *Publication Identifier Type*:
h. *Publication Identifier*:
i. *Publication Date*: 2019
j. *Volume*:
k. *Issue*:
l. *First Page Number*:
m. *Publication Location*: New Jersey, USA

n. *Acknowledgement of Federal Support?* Yes
o. *Peer Reviewed*? Yes

Conference Papers

1. K. Alsultan, P. Rao, A. N. Caruso, and Ahmed M. Hassan, "Scalable characteristic mode analysis using big data techniques," *Submitted to the International Symposium on Electromagnetic Theory (EMTS 2019)*, San Diego, CA, USA, May 27-31, 2019.
2. M. Z. M. Hamdalla, W. Al-Shaikhli, J. Lancaster, J. D. Hunter, L. Yuanzhuo, V. Khilkevich, D. G. Beetner, A. N. Caruso, and Ahmed M. Hassan, "Characteristic Mode Analysis of Electromagnetic Coupling to Wires with Realistic Shapes," *Submitted to the International Symposium on Electromagnetic Theory (EMTS 2019)*, San Diego, CA, USA, May 27-31, 2019.
3. C. Hartshorn, K. Durbhakula, D. Welty, D. Chatterjee, J. Lancaster, Ahmed M. Hassan, A. N. Caruso, "Crosstalk and Coupling to Printed Circuit Board Metallic Traces with Arbitrary Shapes," *Proceedings of the AMEREM 2018 Conference,* Aug 27-31, Santa Barbra, CA, 2018.
4. M. Hamdalla, J. Roacho-Valles, J. Hunter, D. Beetner, Ahmed M. Hassan, A. N. Caruso, "Electromagnetic Analysis of Unmanned Aerial Vehicles Using Characteristic Mode Analysis," *Proceedings of the AMEREM 2018 Conference*, Aug 27-31, Santa Barbra, CA, 2018.
5. C. Hartshorn, M. Hamdalla, J. Lancaster, Ahmed M. Hassan, A. N. Caruso, "Electromagnetic Vulnerability of Wires with Arbitrary Shape," *Proceedings of the AMEREM 2018 Conference*, Aug 27-31, Santa Barbra, CA, 2018.
6. M. Hamdalla, Ahmed M. Hassan, A. N. Caruso "Characteristic Mode Analysis of Unmanned Aerial Vehicles with Realistic Shapes and Material Composition," *IEEE International Symposium on Antennas and Propagation and USNC-URSI Radio Science Meeting at Boston*, MA, 2018.

11. Point of Contact in Navy

- Ryan Hoffman, ONR, ryan.hoffman@navy.mil, Date of Last Research Progress Meeting: 09/11/2018
- Matthew McQuage, Naval Surface Warfare Center Dahlgren, matthew.mcquage@navy.mil, Date of Last Research Progress Meeting: 09/11/2018

12. Acknowledgement/Disclaimer

This work was sponsored by the Office of Naval Research (ONR), under grant number N00014-17-1-2932. The views and conclusions contained herein are those of the authors only and should not be interpreted as representing those of ONR, the U.S. Navy or the U.S. Government.

Electrochemical Prime Power Supply for a Repetitively Operated High Power Marx Generator

Grant No. N00014-17-1-2847

First Annual Report for Fiscal Year 2018

Period of Performance: October 1, 2017 to September 30, 2018

Prepared by:

Professor David Wetz, Principal Investigator
Associate Professor Electrical Engineering Department
University of Texas at Arlington
Department of Electrical and Computer Engineering
416 Yates Street, Rm. 537
Arlington, TX 76019
Tel: (817) 272-0719
Email: wetz@uta.edu

This work was sponsored by the Office of Naval Research (ONR), under grant number N00014 - 17-1-2847. The views and conclusions contained herein are those of the authors only and should not be interpreted as representing those of ONR, the U.S. Navy or the U.S. Government.

Grant or Contract Number: N00014-17-1-2847
Date Prepared: 8/31/2018
Project Title: Electrochemical Prime Power Supply for a Repetitively Operated High Power Marx Generator
Annual Summary Report: September 1, 2017 to August 31, 2018
Principle Investigator: [PI David Wetz, 5127880848, wetz@uta.edu, University of Texas at Arlington (UTA), Arlington, Texas, 76019

Section I: Project Summary

1. Overview of Project

Abstract:
The US Navy has a number of active research projects that are aimed at bringing electrically powered weaponry to the fleet, typically referred to as directed energy weapon (DEW) systems. Though many technical advances are being made, most of these efforts are still in the research phase with many unanswered questions still to be answered before they will be deployed. Regardless of whether the DEW is deployed on a ship or on a smaller, more mobile, platform, it must have a reliable and resilient power source from which to draw its prime power. Such a prime power may be used to directly drive the DEW load or it may feed energy to some other intermediate energy storage device that eventually powers the load. A power supply that operates on its own or in some sort of hybrid fashion with the platform's existing power source is required. Energy storage in the form of ultracapacitors (UCs) and lithium-ion batteries (LIBs) hold a great deal of promise for use as a prime power source for DEWs but given that the power source must source high power while also being as compact as possible, there is still a great deal of research to be performed to understand how these devices will operate, age, and fail in such an application. The research performed over the past year has been focused on identifying UCs and LIBs that have potential for operation at high power and characterizing them under controlled conditions representative of how they will be used if they were to power a DEW load. Additionally, considerable time has been spent developing an electrochemical energy storage sizing tool that can be universally used to optimize the design of a prime power supply for DEW and other future Navy applications.

Objective:
The objective of this effort performed this past year was to study the present state of the art electrochemical ultracapacitors (UCs) and lithium-ion batteries (LIBs) to better understand how these types of devices will operate, age, and fail when used to supply high power under various environmental conditions. The knowledge gained is being used to advance ONR's understanding of these devices and towards the development of a universal energy storage sizing tool that can be used to optimize the design of prime power supplies in future Navy DEW applications.

Introduction:
Abbreviation List: DEW: Directed Energy Weapon, UC: Ultracapacitor, LIB: Lithium-ion Battery, COTS: Commercial-Off-the-Shelf, DE: Directed Energy, EDLC: Electric Double Layer Capacitor, LIC: Lithium-ion Capacitor, UTA: University of Texas at Arlington, PPEL: Pulsed Power and Energy Laboratory, and CC: Constant Current

Electrochemical energy storage is being studied across the US Navy to fulfill the electrical power requirements that have arisen in their effort to become a more electric fleet. Many different chemistries are available commercially off the shelf and each has very unique properties with respect to its voltage, power, energy, impedance, and size characteristics, among many others. This makes choosing the correct energy storage for any application difficult and unfortunately there is no one-size-fits-all approach that can be taken. Energy storage manufacturers often design cells specifically for an application when approached by a customer. Even though they are designed for a specific application, the manufacturer's often make them available commercially to other customers once fabricated, meaning that cells of countless geometries are available with very few industry standards available. This only increases the challenges faced when sizing energy storage for an application using COTS devices. When choosing a chemistry, there are many factors that should be considered. Those that are often considered first are the power density, energy density, impedance, and of course safety. Figure 1 presents a Ragone chart that demonstrates the range of power and energy density available from multiple energy storage chemistries.

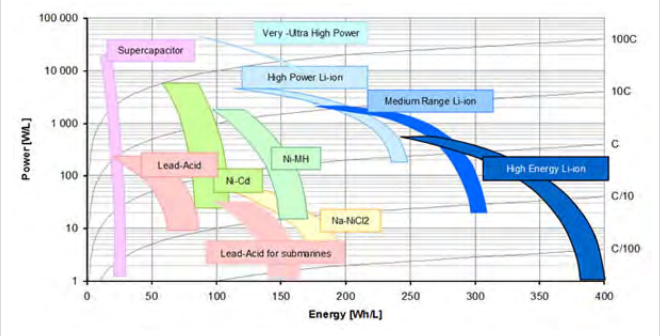

Figure 1. Ragone chart displaying the power and energy density (with respect to volume) for various energy storage chemistries [1 - 24]

In Figure 1, lithium-ion batteries (LIBs) and ultracapacitors (UCs) are especially of interest due to their high power density which makes them perfect for use in directed energy applications demanding a compact power supply that is able to supply high power transiently. Within the category of UCs, there are electric double layer capacitors (EDLCs) and lithium-ion capacitors. These technologies are perfect for applications that require a power supply with high power, long life, and high safety but not a significant amount of energy stored. When higher energy stored is required, a LIB may be a better choice but they come with many tradeoffs as well. Within the LIB category, there are many different chemistries to choose from, most of which have not been studied under high power operation. These vast choices make the design of a prime power supply for DE applications a non-trivial task. The intent of the research being performed here is to research the present state of the art UC and LIB technologies and assess their operation at high power. Because these technologies are rarely used at the power levels required by DE applications, little is understood about how they perform, age, fail, and how to properly size them for a particular application. In the first year of this three year effort, a market survey was performed to identify COTS cells that would be well suited for use in the prime power supply for a repetitive pulsed power supply known as a Marx generator. A Marx generator is essentially a voltage multiplier in which high voltage capacitors are charged in parallel and then switched in series to produce a high pulsed voltage to the load. Marx generators are typically low energy supplies that deliver a high peak to average power to the load. Energy storage with high power density and lower energy density, UCs, are best suited for this application. Two UC technologies were studied electrically

and characterized through 1000 cycles. The results of the market survey and the electrical experiments performed on two UCs have been used to develop a computer aided sizing tool that can be used to optimize the size of DE prime power supplies. The results obtained thus far will be presented here.

Background:
Since 2010, the University of Texas at Arlington's (UTA's) Pulsed Power and Energy Laboratory (PPEL) has been supporting the Office of Naval Research (ONR) in its study of electrochemical energy storage devices and systems. In the work performed here, the PPEL has conducted a market survey to assess the current state of the art COTS devices that are suitable as a prime power supply for a low energy, repetitively operated, 100 Hz, Marx generator. LIBs that have low capacity but high power density have been identified along with an LIC option, and two UC options, respectively. A Microsoft Excel based sizing tool that was first designed for an earlier PPEL/ONR effort, was significantly improved to study how each of the identified technologies compares with respect to power supply size and weight. Towards the end of the year, shortcomings were identified that could not be overcome using Excel and the sizing tool was redesigned using Matlab so that time based, iterative processing could be achieved. In order to ensure its accuracy, the sizing tools were developed using data that was experimentally collected at the high power rates required of a compact DE prime power supply. The power rates they were studied at are rarely published by the manufacturer making the work performed by the PPEL critical to understanding what is achievable using these COTS energy storage devices. Ultimately the need for very long shelf life, roughly thirty years, led to the down selection of two UCs that were ultimately experimentally studied in greater detail using programmable loads and power supplies. As will be shown in the accomplishments section, the two respective UC technologies were studied in a pulsed profile representative of the way they would be deployed in a DE Marx generator application. Measurements including conduction voltage, conduction current, temperature, capacity fade, and impedance were made to study the cells performance and cycle life under high rate operation.

2. Activities and Accomplishments

During this reporting period, three primary tasks were completed. The first was to perform a market survey of COTS UC, LIB, and LIC technologies to find ones that have lower energy density and high power density. The second was to improve a Microsoft Excel based energy storage sizing tool that can be used to accurately design a prime power supply for DE and other Navy applications. This task was completed but shortcomings of the Excel based software were identified, primarily the lack of iterative processing, that prompted the tool to be redesigned using Matlab. The final task was to experimentally characterize the electrical/thermal performance of two UC cells at high power using a pulsed profile representative of a DE application. Two cells of each respective type were studied, each in a different environmental condition. The four cells were periodically baselined and their impedance growth and capacity fade was measured.

With respect to Task 1, ten LIBs, two UCs, and one LIC were identified as viable candidates for use in low energy, high power applications. Their properties at the cell level are listed in Table 1 below. As the table indicates, the cells take on three main form factors being pouch, prismatic, and cylindrical respectively. Among the ten LIBs are four different chemistries, namely NCA, LTO, LFP, and NMC, respectively, each of which has vastly different capabilities when it comes to voltage, power density, energy density, impedance, and safety. The LFP and LTO chemistries are the safest of the four with NMC and NCA being a bit more volatile in the event of a thermal

runaway. Besides that, there is no reason why any one of the ten cells identified here would not work for such a DE application so the real choice comes down to which has the best size and weight to meet the DE repetitive rate and shot count requirements. One drawback to using LIBs is their limited shelf life. There are many DE applications that may have the requirement to sit idly for as long as 30 years. It is presently unclear what would happen to LIBs sitting for that long, even if they are maintained but it is safe to say that there would be significant calendar aging and electrolyte decomposition that would increase their impedance significantly. This would reduce their ability to supply enough power or energy to meet the power requirements and therefore are likely unable to be considered further unless that requirement is reduced considerably.

Table 1. LIB, UC, and LIC identified as viable low energy, high power technologies.

	Cell Name	Chemistry	Capacity (Ah)	Peak Power (W)
Lithium-ion Batteries	Kokam SLPB43671114H6 Pouch	NCA	1.30	156
	Toshiba 2.9 Ah SCiB™ Prismatic	LTO	2.90	360
	Saft SL2A Pouch	NCA	2.25	1170
	Navitas 20125040 Round Pouch	NMC	1.90	310
	K2 18650P Cylindrical	LFP	1.25	41
	K226650UP02 LFP Cylindrical	LFP	2.85	138
	A123 ANR26650m1B Pouch	LFP	2.50	159
	A123 18700m1 Cylindrical	LFP	0.80	753
	A123 26700m1 Cylindrical	NCA	2.20	760
	Saft VL3 Cylindrical	NCA	3.40	555
Ultracapacitors	Maxwell SuperCap Cylindrical	UC	0.22	263
	Skeleton SCA0500 Cylindrical	UC	0.23	1539
Lithium-ion Capacitors	JM Energy CLQ1500S1A Prismatic	LIC	0.67	1400

Two UC technologies were selected due to them already being considered for use by an ongoing ONR DE program. Unlike batteries, it is a bit more likely that they can be stored for a significant number of years without significant degradation. This makes them more promising and for that reason were the focus of this FY's experimental research activities. Part of that stems from their ability to be stored with no charge in them. The Maxwell UC is a standard capacitor offered by Maxwell based off their well-established UC technology. Skeleton is a new Estonian company offering cells with significantly lower impedance than any other UC company. They are able to

achieve the lower impedance through their use of rolled graphene electrodes and as a result are able to achieve significantly higher power densities than those available from Maxwell, Ioxus, or other domestic UC manufacturers. In Task 3, the Skeleton 500 F cell and the Maxwell 310 F were studied considerably and those experiments and their results will be discussed shortly.

Though multiple LIC companies have emerged recently, only the one cell from JM Energy, a Japanese company, was chosen for sizing in this particular study. The reason for that is that like LIBs, they must be stored with charge on them and may suffer degradation during long term storage. LICs are essentially a hybrid LIB/UC technology that leverages advantages from both to build what is essentially a UC with roughly four times a UC's energy density. This makes them attractive for consideration and therefore it was included in the sizing study.

With respect to Task 2, a sizing tool was developed using Microsoft Excel software. The sizing tool allows the user to enter datasheet or experimentally obtained properties at the cell level along with a generic constant power profile that the energy storage must supply. From those inputs, the sizing tool is able to estimate the number of cells that must be assembled in a series/parallel manner to meet the load requirements. It would be too large to show many details of the sizing tool here. However, a screen capture showing an abbreviated version of its output results are shown in Table 2 below.

Table 2. Excel Sizing Tool Results Summary

	Summary					
	Cell	650 F Maxwell SuperCap	JM Energy 1500 F Li-Ion Cap	A123 18700m1	SkelCap SCA0500	Saft SL2A
Battery Module Composition	Series Cells Per Module	1	1	1	1	1
	Parallel Strings Per Module	1	1	1	1	1
Number of Cells	Total Number of Cells	400	90	410	100	146
	Series Cells	100	90	82	100	73
	Parallel Strings	4	1	5	1	2
Physical Characteristics/ Cooling Estimates	Weight (Cells Only) (kg)	34.00	15.84	15.99	11.10	12.41
	Volume (Cells Only) (L)	60.79	9.00	7.30	7.90	10.40
	Estimated Total Weight (kg)	192	64	151	55	71
	Estimated Total Volume (L)	79	6	9	10	15
Capacity Usage	Percentage Capacity Used	19%	29%	11%	87%	4%
Total Battery Voltage Range	Maximum Voltage	285	342	287	300	307
	Nominal Voltage	263	270	271	270	270
	Minimum Voltage	240	198	164	240	197

The sizing tool optimizes the number of parallel/series cells required by assuming the energy storage is able to source as much current as it needs to, such that it does not exceed the manufacturer's ratings. It heavily relies upon experimentally collected data by UTA from each cell across their usable discharge rates (C rates) to more accurately estimate the conduction voltage as a function of the current the supply must be sourcing. These values are typically not given by the manufacturer at the upper end of the cell's rated values making sizing without that experimentally collected data very difficult. The results do not take into account any size and weight added by ancillary electronics, passive/active cooling, or the buss work needed to connect them into modular form. As shown the technology that has the least weight is not necessarily the one that takes up the least volume and vice versa. As shown the Skeleton 500 F capacitor would be lightest while the JM Energy LIC would take up the least volume. The JM Energy LIC would have the lowest combined size and weight but additional work would be needed to further validate its long term performance and aging.

Though the tool works well and has been validated in many cases, it has been found that that tool works much better for LIBs than it does for UCs and LICs. This stems from the fact that LIBs have

nearly flat conduction voltage as they are discharged whereas UCs and LICs have a conduction voltage that decays steeply as a function of supplied energy. The inability of Excel to iterate the voltage as a function of time severely reduces its accuracy in sizing UC and LIC power supplies. Therefore time has been spent in the latter half of the year to convert the sizing tool over to a Matlab/Simulink software so that iterative processing and simulation features can be built in. As of now a UC sizing tool is completed using Matlab/Simulink. The tool is able to take in cell data from the same Excel sheet used earlier, perform a mathematical sizing study, and even simulate the results for verification. Results obtained from a Skeleton 500 F cell are shown below in Figure 2 where they are over plotted with data collected experimentally from the same type of cell. As shown there is very good agreement between the modeled and experimental data. Presently the Matlab UC sizing tool takes in the user data from an Excel sheet, sizes and simulates an option for each type of cell in the sheet, and produces a table for the user that details the number of each type of cell that would be required in parallel/series to meet the load requirements. The LIB sizing tool is still being converted over and is expected to be completed in early Fall 2018.

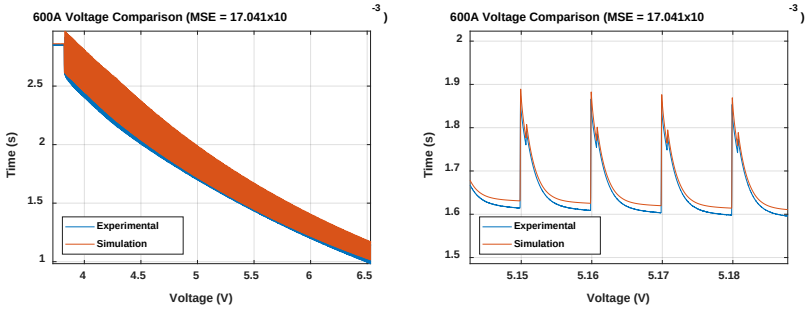

Figure 2. Model validation results for the Skeleton SCA500 ultracapacitor at 600 A. The model is accurate within 1% of the experimental data.

The third and final task presented is the one in which six UCs have been experimetally studied. Of the six cells, three are Maxwell 310 F cells while the other three are Skeleton 500 F cells. Two of the cells, one of each respective type, have only been characterized as new cells to obtain baseline capacity and impedance values. The other four cells were all repetitively discharged at the manufacturer's maximum rated values, 600 A for the Skeleton 500 F cell and 200 A for the Maxwell 310 F cell, under a 9 ms discharge / 1 ms rest pulsed profile. That profile repeats from 2.85 V, the peak charge voltage, down to 1 V and is representative of how the cells may be expected to perform in a DE application. Once discharged, each cell is recharged at a constant current (CC) of 10 A before being pulsed discharged again. Two Skeleton 500 F cells and two Maxwell 310 F cells, respectively, were cycled 1000 times each. One of each type of cell was cycled while stored in a 25ºC enviornmental chamber while the other of each type as cycled in a 70ºC enviornmental chamber, the peak temperature that may be expected aboard a DE mobile platform. A sample conduction voltage waveform obtained from each type of cell during a pulsed discharge are shown in Figure 3. In an effort to keep this discussion short the results of the experiments are as follows. Each cell is able to perform well over 1000 cycles under each respective test condition. As expected, the level of capacity fade is increased slightly when cycled at elevated temperatures but it is not significant as summarized in Figure 4. Though it will not be shown, impedance measurements made periodically along the way do not show significant impedance growth from either cell after 1000 cycles have been performed.

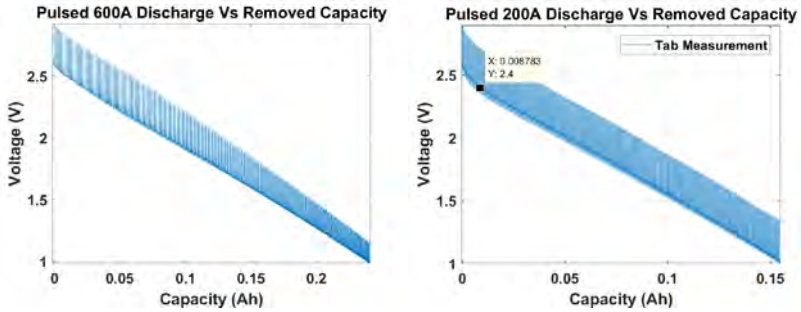

Figure 3. Conduction voltage as a function of capacity removed from a Skeleton 500 F cell at 600 A (left) and Maxwell 310 F cell at 200 A (right)

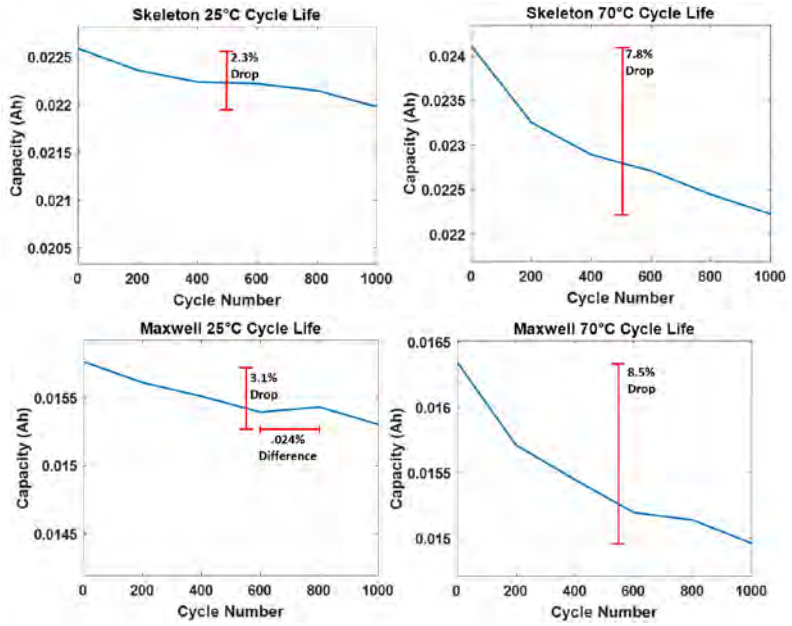

Figure 4. Capacity fade measured from the Skeleton 500 F cells cycled in a 25ºC environment (upper left) and 70ºC environment (upper right) and the Maxwell 310 F cells cycled in a 25ºC environment (lower left) and 70ºC environment (lower right), respectively.

3. Findings and Conclusions

In the work performed to date, an assessment of the current state-of-the-art energy storage devices that can be used to meet the low energy, high power demands of a high voltage Marx generator, used for DE applications, has been performed. A number of LIB, UC, and LIC technologies have been identified and studied experimentally under high pulsed load conditions. Using the data collected and the manufacturer data sheets, a sizing tool has been developed using both Excel and Matlab/Simulink software packages that can be used by DE engineers to optimize the size of their prime power energy storage system. The tool is still being improved upon and eventually will be able to size and simulate LIB, UC, and LIC technologies using only a few required parameters input by the user. Lastly, two different UC technologies have been experimentally cycled at high power using a pulsed discharge profile in both 25ºC and 70ºC environmental conditions, respectively. The results have shown that each respective UC technology is able to be cycled over

1000 times with less than 10% capacity fade, with slightly higher fade measured from the cells cycled in the higher temperature environment.

4. Plans and Upcoming Events

In the next FY, a few tasks are planned. The first involves the completion of the Matlab/Simulink sizing tool was begun during this past FY. It is anticipated that the tool can be completed by December 2018. The second will involve the experimental evaluation of the high voltage intermediate energy storage capacitors used in the construction of a high voltage Marx generator. To date there has been limited research performed to date studying how these capacitors perform and fail when they are repetitively cycled in higher temperature environments. UTA will work with researchers at Maxwell and Sandia National labs to facilitate this testing. The work performed will involve setting up the experiments, creating a design of experiments, performing the experiments, and finally analyzing and documenting the results. It is anticipated that these experiments will take up much of the next FY.

5. Transitions and Impacts

To date the knowledge gained can be transitioned on to any team performing work in the directed energy (DE) area Any groups interested in designing compact prime power systems utilizing electrochemical energy storage would benefit from the knowledge gained to date It is our understanding that many laser, high power microwave, and electromagnetic railgun programs are ongoing that are considering batteries as their prime power systems who may benefit.

6. Collaborations

We have collaborated with:

Jordan Chapparo – NSWC-DD, John Krile – NSWC-DD, Frank Hegeler – Naval Research Laboratories (NRL), Dale Coleman – Sandia National Laboratories, and Mark Schneider – General Atomics

7. Personnel

Principal investigator: Dr. David Wetz – 3 months (480 hours), National Academy Member (N)
Business Contact: Jeremy Forsberg, ogcs@uta.edu
Team Members: Listed as students below
Subs: None

8. Students

Blake Adame: EE Undergraduate Student, Alex Johnston: EE Undergraduate Student, Bradley Pipes: EE Undergraduate Student, David Dodson: EE PhD Candidate, Charles Nybeck: EE PhD Candidate, and Jacob Sanchez: EE PhD Candidate

9. Technology Transfer

None

10. Products, Publications, Patents, License Agreements, etc.

No publications have been published to date. One is in process of being written to document the results of the 1000 cycle experiments. Monthly reports were compiled and delivered to ONR. A

status brief was given in Albuquerque on November 16, 2017 and at the DE Program Review in Washington DC in April 2018.

11. Point of Contact in Navy

Ryan Hoffman – ONR PM (contacted September 2018, visited in August 2018)
Matthew McQuage – NSWC-DD (contacted September 2018, visited in August 2018)
Frank Hegeler - (contacted September 2018, visited in August 2018)
Yeong-Jer Chen - (contacted September 2018, visited in August 2018)
Jordan Chapparo - (contacted September 2018, visited in March 2018)
John Krile - (contacted May 2018, visited in March 2018)

12. Acknowledgement/Disclaimer

This work was sponsored by the Office of Naval Research (ONR), under grant number N00014-17-1-2847. The views and conclusions contained herein are those of the authors only and should not be interpreted as representing those of ONR, the U.S. Navy or the U.S. Government.

Efficient, Insulators for High Power Radio Frequency Devices

Grant No. N00014 -17-1-2848

First Annual Report for Fiscal year 2018

Period of Performance: September, 1, 2017 to August 31, 2020

Prepared by:

Professor Jane Lehr, Principal Investigator
University of New Mexico
Department of Electrical and Computer Engineering
MSC 01 1100
Albuquerque NM 87131-0001
Tel: (505) 277-1749
Fax: (505)277-1439
Email: jmlehr@unm.edu

This work was sponsored by the Office of Naval Research (ONR), under grant number N00014 -17-1-2848. The views and conclusions contained herein are those of the authors only and should not be interpreted as representing those of ONR, the U.S. Navy or the U.S. Government.

Grant Number:	N00014 -17-1-2848
Date Prepared:	30 November 2018
Project Title:	Efficient, Insulators for High Power Radio Frequency Devices
Annual Summ Report:	FY2018
Principle Investigator:	Jane Lehr

(505) 277 1749
jmlehr@unm.edu
University of New Mexico
Electrical and Computer Engineering Department
MSC01 1100 1 University of New Mexico
Albuquerque NM 87131-0001

This work was sponsored by the Office of Naval Research (ONR), under grant number N00014 -17-1-2848. The views and conclusions contained herein are those of the authors only and should not be interpreted as representing those of ONR, the U.S. Navy or the U.S. Government.

Section I: Project Summary

1. Overview of Project

Abstract: In the design of directed energy and high power radio frequency (HPRF) sources, high power electrical pulses are generated in a volume filled with high dielectric strength fluids while the directed energy source typically operates in vacuum. The two sections, then, require an insulating barrier that is subject to very high electric fields and susceptible to electrical breakdown. This insulating barrier is, by far, the most likely component to fail within the system. Electrical breakdown is overwhelmingly more likely to occur along a solid immersed in the fluid (called a surface flashover) and the mechanism of its development remains only marginally understood. The system implications of failure of this barrier is critical: not only does the flashover prevent power flow to the directed energy load, but the reflected power results in a large, repetitive voltage reversal which either degrades or destroys the pulsed power driver resulting in complete system failure.

This research effort is intent on improving the voltage withstand capability of an insulating barrier efficiently – that is, without introducing new reactances. This is accomplished by utilizing a high gradient insulator geometry, surface contouring to control the electric field components driving the discharge and investigating the origins of surface flashover in vacuum through coupled modeling and experiment.

Objective: Our objective is to experimentally demonstrate an insulating barrier in vacuum with a factor of two improvement in withstand capability over the current state-of-the-art, preferably with a vacuum compatible material. To accomplish this goal, the relative importance of secondary electron emission material properties, triple points, surface shape, insulator length and high gradient insulator design will be investigated.

Introduction: Generally, for HPRF vacuum electronics, the insulator separating the pulsed power driver from the directed energy source is in an axial stack as shown below. The geometry adds significant inductance and size to the device. Using high gradient insulators, UNM has designed a radial insulating stack to hold off voltages on the order of 750 kV in a 10cm diameter tube in

vacuum, resulting in great savings of space and inductance. UNM's insulating stack converts the logarithmic dependence of the electric field in concentric cylinders to be both uniform and close to the mean electric using high gradient insulators.

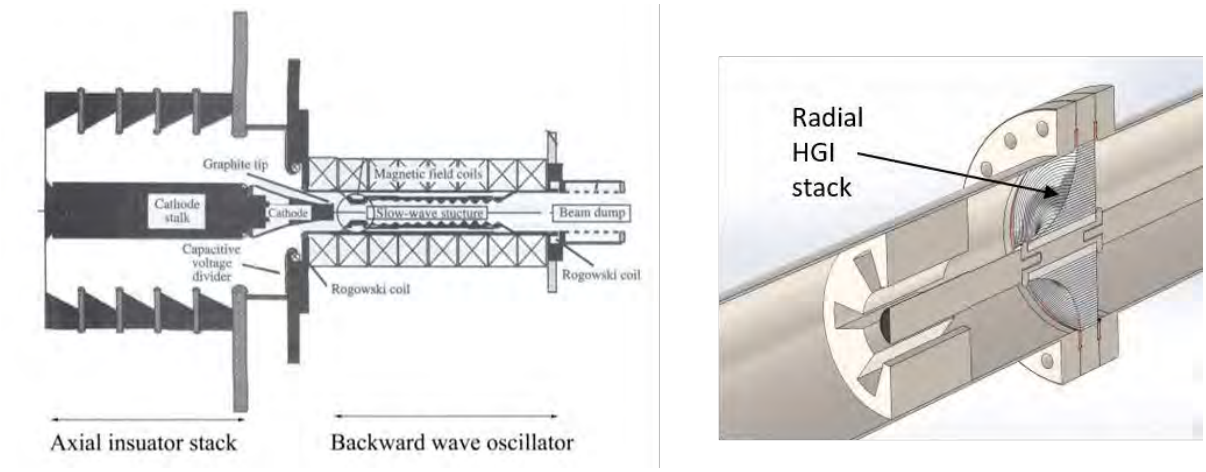

Figure 1 A conventional axial insulating stack for high power vacuum electronics and the radial high gradient insulating stack being developed.

The goal of our current research into surface flashover in vacuum is to demonstrate these novel insulating geometries have an enhanced voltage holdoff capability. It is widely acknowledged that electrical failures are more likely near surfaces. We are pursuing the high gradient insulator (HGI) geometry where walls and insulating posts can be made to withstand higher voltages by alternating thickness of insulators and conductors. In the early 1980s, Gray [1] conceived a "microstack" from the observation that the threshold electric field strength for surface flashover *increases* with *decreased insulator length*. Thus, by breaking up the total insulator length into small segments, the vacuum surface flashover initiation value increases compared to conventional insulators of the same length. The "microstack" moniker is a derivative of the "vacuum stack" used in large accelerator designs where the vacuum load is typically located in the center of a radial transmission line. Gray's microstack was made by pressing alternating layers of Mylar and conductor together to build up the "stack". The results were promising with increases ~ 1.5 in initiation voltage. Microstacks, or High Gradient Insulators, have shown significant progress but the theory of operation is still not well understood.

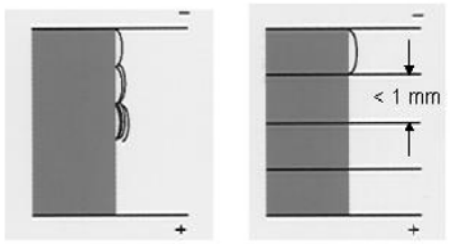

Figure 2 Conventional monolithic insulator and the high gradient geometry (right).

Background: Central to the Saturated Secondary Electron Emission Avalanche (SSEEA) model is the emission of secondary electrons from the dielectric surface resulting from the impact of an electron. In this model, the initial electrons are emitted from the cathode triple point - the intersection of the insulator, the vacuum, and the cathode. The yield of secondary electrons per impacting electron, given by the secondary electron emission (SEE) coefficient, δ, depends on the energy of the impacting electron and the characteristic of the insulator. Figure 4 shows a generic SEE yield curve, which is typical for many dielectric materials.

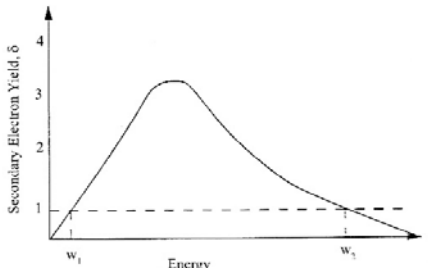

Figure 3 A generic secondary electron emission curve for an insulator. For an electron with δ=1 indicates that one secondary electron is produced upon impact.

There are two energies of the impacting electron (w_1 and w_2) at which the secondary electron yield is unity. The surface charging resulting from the impact of the electrons is, in essence, a negative feedback process that drives the energies of the impacting electrons back to w_1 . Assume that an electron emitted from the triple point under the influence of an electric field applied parallel to the insulator surface and impacts the surface with an energy greater than w_1 . Since $\delta > 1$ for this case, the negative charge leaving the point of impact (in the form of secondary electrons) will be greater than the negative charge arriving at the point of impact (the impacting electron), and thus the insulator surface will attain a *net positive charge*. A successive electron will be attracted by this positive charge and spend less time in the applied electric field, therefore gaining less energy from the field and driving the operating point back toward w_1 . Now assume that an electron strikes the surface with an energy less than w_1 . This will produce a net negative charge on the surface that will repel a successive electron. This electron will then gain more energy from the applied field, and the operating point will again tend toward w_1. After a period of time (on the order of nanoseconds) the energies of all of the impacting electrons will converge to w_1 . This convergence is referred to as the ***saturated secondary electron avalanche condition***.

Starting with the SSEEA model, Pillai and Hakam coded the breakdown criterion for surface flashover in vacuum and included electron-stimulated desorption of gas from the insulator surface as described by Anderson and Brainard. The electrons impacting the surface, after saturation of the avalanche, constitute a current density perpendicular to the insulator surface, with the amount of gas desorbed assumed to be proportional to this current density. The electrons in the avalanche undergo ionizing collisions with the desorbed gas, and Paschen breakdown then occurs when the density of the desorbed gas reaches a critical value.

However, upon examination of the mechanism proposed by Pillai-Hackam, where outgassing plays the predominant role, an accounting for the SSEEA model indicating the saturation condition $\delta \rightarrow 1$ is inevitable. That is, the Pillai-Hackam model implies that the material response to electron bombardment is irrelevant in the development of a surface flashover and, instead, the desorbed gas from electron bombardment plays the crucial role. Thus, the nuanced research question is ***should materials be selected (or developed) for a low outgassing or a low SEY property for high voltage vacuum applications?***

2. Activities and Accomplishments

HGIs were originally proposed to take advantage of the observation from the SSEEA theory that shorter insulators were able to withstand higher electric field gradients. By creating an insulating structure composed of alternating metal and dielectric layers, a large distance can be spanned by what is effectively a large number of short insulators. Later efforts worked under the assumption that the HGI metal layers functioned to physically intercept the avalanche generally believed to precede vacuum surface flashover. This assumption led to HGIs with metal layers much thinner than the intervening dielectric. Later work modeled the electron trajectories and showed that

thicker metal layers may have advantages. The ratio of dielectric to metal layers continues to be a subject of debate. Deep understanding of the operation of HGIs is lacking.

Figure 4 Two variations with approximately equal performance with the HGI on the right after Leopold.

The experimental fixture for testing insulator flashover in vacuum and various geometries of HGI is shown below. It consists of a Marx generator capable of delivering 300 kV into a vacuum vessel with a sample holder. Calibrated diagnostics measure the electrical signals.

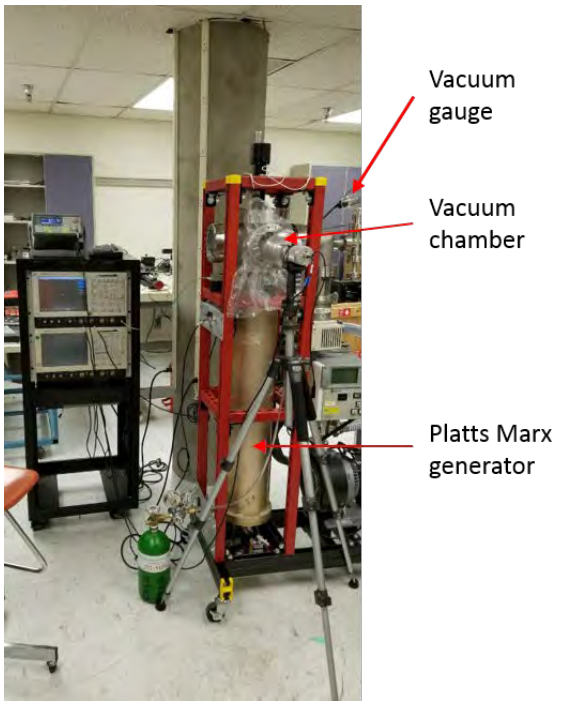

Figure 5 The experimental fixture for surface flashover in vacuum.

To date, a large number of aluminum nitride (AlN) HGIs, in cylindrical form, have been tested with a variety of results. Initial testing was dedicated to determining if the many layers of alternating insulator and metal performed better than the large bands of metal (HGI on the right). It appeared that the large bands did indeed work better. The large metal bands are inappropriate for the barrier in the HPRF device since it would also block power flow. Putting that result aside, we focused on determining if the material had an effect. One of the many features of AlN is that it can be made in many polycrystalline varieties and the manufacturer, Sienna, has had the secondary electron emission (SEE) curves measured. We have now determined that the lowest SEE AlN material does indeed have the highest breakdown strength. Moreover, a HGI with a large numbers of layers has worked to field gradient levels of 150 kV/cm. This field gradient allows radial HGI geometries to be considered for coaxial vacuum electronics.

To date, our best HGI sample has been obtained using the ST100 formulation of AlN with an I/M ratio of 13. The insulator length is 0.5mm with 22 layers. The voltage holdoff was 168kV/cm over a significant number of shots.

HS-768-1

22 layers AlN/ length = 0.5 mm

AlN type: ST 200

21 layers Cu/ length= 0.04mm

Diameter: 25.9 mm

Height: 11.9 mm

I/M ratio: 13

E-field: 168 kV/cm

These shots were taken while the Marx was charged to 9kV/stage. The sample was able to hold off approximately 200kV.

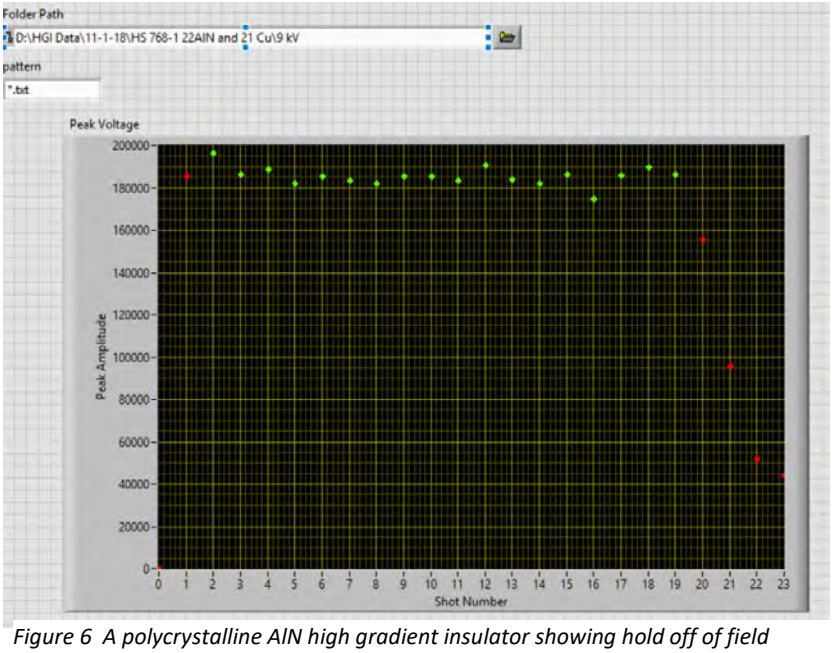

Figure 6 A polycrystalline AlN high gradient insulator showing hold off of field gradients of 168 kV/cm. The red dots shows sample failure and the green is hold off.

In our modeling work, we starting to look at particle trajectories to aid in the design of HGIs. There are two approaches that have been identified. The initial work by Tetra Corp, and advanced by Lawrence Livermore National Laboratories, used many thin layers of alternating metal and insulator. The work of Leopold used particle tracking to show that thick metallic layers repelled electrons away from the surface. Both approaches seemed to yield positive results. That is, the theory of operation of each group was supported by their own data.

In this effort, we are focused on using a polycrystalline form of the ceramic aluminum nitride (AlN) as the insulator for its many attractive properties. We started using the Particle Tracker package in the commercial electrodynamic solver CST to aid in down-selecting the most appropriate geometries. Starting with the monolithic case, we found that subsequent to a number of surface bombardments, the electrons lift off the surface and gain energy in the electric field until reaching the anode. This is reasonable in that the electrons lose energy to the surface but gain energy once the interactions stop. Also, the electric field that drives the electrons into the surface could be expected to saturate.

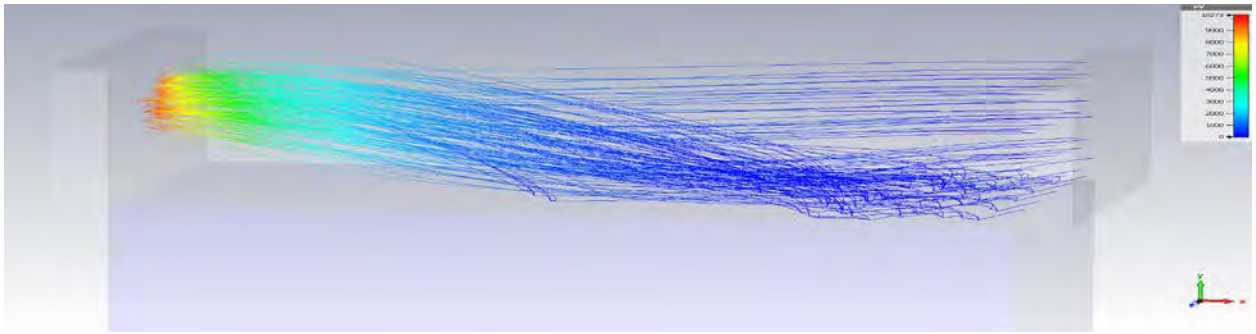

Figure 7 The electron trajectories from the CST Particle Simulator shows the electrons impact the surface and then lift off the surface when the saturation condition (δ=1) is reached. This is in stark contrast to the conventional picture shown in Figure 7 yet looks like the depiction of the experimental results of Figure 8.

Figure 8 The conventional view of electron bombardment of a surface where the surface charge creates a normal electric field that drives the electrons into the surface.

This is in stark difference to the conventional picture of avalanche development where the electron impacts the surface continually across the surface. The particle trajectory images are interesting because it is strongly reminiscent of observations from experimental data. That is the discharge has weak luminosity and then takes on a bright volumetric shape. In the Pillai-Hackam model, this is attributed to a critical pressure from outgassing so that breakdown occurs in the gas by Paschen breakdown.

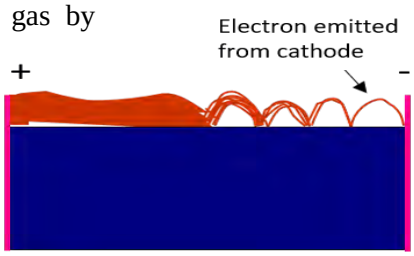

Figure 9 An illustration of the evolution of surface discharge where electrons sourced from the cathode desorb sufficient gas that Paschen breakdown occurs due to outgassing (Pillai-Hackam).

This observation may be key to advancing our knowledge of the physical processes inherent in surface breakdown, but in our present circumstance, the interest is more pragmatic: due to the intensive fabrication process, modeling is needed to guide the design.

3. Findings and Conclusions

The end result of this effort will be to determine the feasibility of a radial high gradient insulator for directed energy applications. Current technology limits the system performance by adding size and reactance. Moreover, the fear of catastrophic failure forces a tradeoff between size, weight and power (SWaP) and system reliability.

UNM used the commercial electromagnetics simulation software CST to do a notional design for a radial insulator to hold off 750kV in a 10cm radius HPRF tube. In addition to the metallic layers

in the radial direction, the vacuum side surface is contoured to control the electric fields. This modeling indicates that tangential electric fields of 80 kV/cm are adequate to accomplish this goal. The radial geometry is enabled by using our material of choice, a polycrystalline form of aluminum nitride (AlN). Previous high gradient insulator geometries were manufactured by pressing polymers and could only be fabricated in compatible geometries such as slabs and cylinders. AlN can be tape wound and formed around a cylinder (the cathode) leading to an efficient use of insulation. AlN, a ceramic material not found in nature, has low outgassing and high breakdown strength properties which make it vacuum compatible and suitable for sealed tube technology.

UNM has concluded this year that of the various formulations tested, the AlN ST200 is has yielded the best results. This is not surprising since it was specially formulated to have a low secondary electron emission yield. UNM tested the electrical breakdown strength of the ST200 to the ASTM standard and found the bulk breakdown strength to exceed 900kV/cm – far in excess of the gradient between layers. We are currently pursuing the optimal number and thickness of layers which is proving tricky. Our most promising results has 22 layers of insulation of thickness 0.5mm each and holds off 168kV/cm. Contrast this with the researchers from the National University of Defense Technology (NUDT) in Changsha China whose ceramic insulator has a field gradient of 60 kV/cm.

The optimization of the geometry is being pursued through modeling of both electrostatics and particle trajectories. The particle trajectory model was implemented to explore the benefits of using the conductor lengths to deflect electrons away from the surface and thus raising the flashover electric field. As a baseline, a monolithic insulator was modeled and it appeared that the discharge lifts off the surface prior to reaching the anode. We note that this looks very much like experimental results where the discharge is thought to initiate along the surface and then breakdown when the outgas products reach a certain number density to sustain breakdown via a Paschen-like mechanism. From our modeling results, it appears that the liftoff occurs when the surface charge density is sufficiently high that the electrons are no longer attracted to the surface. This corresponds to the saturation condition. We are presently doing surface simulations in Aleph, a custom Monte Carlo Particle in Cell code, to investigate further. A focus has become to tease out the relative importance of the SEE versus the outgassing properties of the material on the flashover potential as an aid for material selection. Both of these properties have clear implications for the widely accepted SSEEA theory.

4. Plans and Upcoming Events

We are intent on proving the HGI technique can be fabricated in a radial configuration. An auxiliary series of tests are planned to determine the effectiveness of using “grooves” in the insulator to inhibit flashover.

An invited conference talk at the next conference season is anticipated. Results suitable for a journal article are being obtained – with the conclusion that the material properties are important. I have a seminar-length talk in preparation on surface flashover/high gradient.

In the next year, we must sort through the modeling and identify whether the saturation condition caused the discharge to lift off the surface. This is interesting because the observed phenomena has been attributed to a critical outgassing rate. We intend to address this with modeling. Modeling should also aid in understanding the length dependence of the HGI structure.

5. Transitions and Impacts

The Air Force Research Laboratory's Directed Energy Directorate (POC Dr. Brad Hoff) has provided a small contract to design standoff pins for a cathode in a high power microwave source. The standoffs are located in a high electric field region and are in shear stress.

Student J. Cameron Pouncey is a Smart Scholar slated for NSWC Dahlgren and spends summers in Virginia working on HPRF systems for Jacob Walker. He will aid in transitioning the results of this research into their devices.

Student Leonardo Rossetti who worked on the experimental setup and data acquisition system is in discussions regarding employment at the Naval Research Laboratory's Electromagnetic Effects Section with POC Zachary Drikas (202-767-6629 / zachary.drikas@nrl.navy.mil).

6. Collaborations

We continue to have technical discussions with Dr. John Harris from the Air Force Research Laboratory who has previously worked on high gradient insulators at Lawrence Livermore National Laboratory for applications in the development of the dielectric wall accelerator. Dr. Harris, noting that two sets of researchers have vastly different designs, has impressed on us the need to determine the theory of operation of the high gradient insulating structure.

7. Personnel

Principal investigator	Prof. Jane Lehr/ 0.5 person month/ National Academy: N
Co-investigator	N/A
Business Contact	N/A
Team Members	Dr. Lisa Fisher/ 3 person months/ National Academy: N
Subs	Dr. Ender Savrun/ / 0.25 person months/ National Academy: N

8. Students

Graduate Students: (4) J. Cameron Pouncey, Cameron Harjes, Leonardo Rossetti, Abee Alazzwi

Undergraduate students: (4) Jonathan Pound-Espericueta (graduated December 2017, Raytheon Boston, MA), Naveed Jafari (graduated December 2017, Raytheon Tucson, AZ), Brad Maynard (super-junior, current), Isaac Garcia (first semester freshman, current)

High School students: (3) Jack Brown, Connor Nellis and Levi Barela

9. Technology Transfer

The Air Force Research Laboratory' Directed Energy Directorate (researcher Brad Hoff) has provided a small contract to design standoff pins for a cathode in a high power microwave source. The standoffs are located in a high electric field region and are in shear stress.

10. Products, Publications, Patents, License Agreements, etc.

Publications resulting from this project:

Archival Publications (publication reference information (article title, authors, journal, date, volume, issue) can be automatically entered using a DOI)

a. Article Title: Erection of Compact Marx Generators
b. Journal: IEEE Transactions on Plasma Science
c. Authors Jon C. Pouncey, Jane M. Lehr and David V. Giri
d. Keywords stray capacitance, efficient erection, high voltage
e. Distribution Statement: A: Unrestricted
f. Publication Status accepted
g. Publication Identifier Type: DOI
h. Publication Identifier: N/A
i. Publication Date N/A
j. Volume N/A
k. Issue N/A
l. First Page Number N/A
m. Publication Location: Piscataway, NJ, USA
n. Acknowledgement of Federal Support? Yes
o. Peer Reviewed? Yes

a. Article Title: A Parametric SPICE model for the Simulation of Spark Gap Switches
b. Journal: Review of Scientific Instruments
c. Authors Jon C. Pouncey and Jane M. Lehr
d. Keywords: spark gap, modeling, experimental verification, dynamic resistance
e. Distribution Statement: A: Unrestricted
f. Publication Status submitted
g. Publication Identifier Type: DOI
h. Publication Identifier: N/A
i. Publication Date N/A
j. Volume N/A
k. Issue N/A
l. First Page Number N/A
m. Publication Location: Piscataway, NJ, USA
n. Acknowledgement of Federal Support? Yes
o. Peer Reviewed? Yes

Conference Papers

a. Title: Triggering of Compact Marx Generators
b. Authors: Jon C. Pouncey, Jane M. Lehr and David V. Giri

c. Conference Name: American Electromagnetics (AmerEM) Conference
d. Conference Date: August 26-31, 2018
e. Conference Location: Santa Barbara, CA, USA
f. Publication Status: submitted for Student Paper Contest
g. Publication Date: N/A
h. Publication Identifier Type N/A
i. Publication Identifier N/A
j. Acknowledgement of Federal Support? Yes

a. Title: A High Voltage, Self-Matching, Nanosecond Pulser for Calibration and Experimentation
b. Authors: Cameron Harjes, Jon Cameron Pouncey and Jane M. Lehr
c. Conference Name: IEEE Power Modulator Conference
d. Conference Date: June 2018
e. Conference Location: Jackson Hole, WY, USA
f. Publication Status: submitted
g. Publication Date: N/A
h. Publication Identifier Type N/A
i. Publication Identifier N/A
j. Acknowledgement of Federal Support? Yes

Books

a. Title: Foundations of Pulsed Power Technology,
b. Authors: Jane Lehr and Pralhad Ron,
c. Edition: 1
d. Volume: N/A
e. Publisher IEEE Wiley
f. Publication Year 2017
g. Publication Location: Hoboken, NJ and simultaneously in Canada.
h. Publication Status: published
i. Publication Identifier Type ISBN
j. Publication Identifier ISBN 978-1-118-62839-3
k. Acknowledgement of Federal Support? Yes

Book Chapter N/A

Theses N/A

Websites N/A

Patents N/A

Other Products: Identify any other significant products that were developed under this project. Describe the product and how it is being shared.

a. Tracking demonstration and mitigation techniques using high gradient insulator approach combined with geometry for aids for UNM ECE 557 Pulsed Power and Charged Particle Beams
b. Product Type: Educational Aid

11. Point of Contact in Navy

Yeong-Jer (Jack) Chen
NSWCDD, E13
yeongjer.chen@navy.mil
Date of last contact: July 12,2018

Jordan Chaparro
NSWCDD, E12
jordan.chaparro@navy.mil
Date of last contact: October 24,2018

12. Acknowledgement/Disclaimer

This work was sponsored by the Office of Naval Research (ONR), under grant number N00014 - 17-1-2848. The views and conclusions contained herein are those of the authors only and should not be interpreted as representing those of ONR, the U.S. Navy or the U.S. Government.

Fundamental Studies for Nanoscale Vacuum Electronic Emission Devices

Grant No. N00014-18-1-2382

First Annual Report for Fiscal year 2018

Period of Performance: July, 1, 2018 to September 30, 2018

Prepared by:

Professor Ravi P Joshi, Principal Investigator
Texas Tech University
Department of Electrical and Computer Engineering
2500 Broadway MS 3102/Campus
Lubbock TX 79424
Tel: 806-834-7979
Email: ravi.joshi@ttu.edu

This work was sponsored by the Office of Naval Research (ONR), under grant number N00014 - 18-1-2382. The views and conclusions contained herein are those of the authors only and should not be interpreted as representing those of ONR, the U.S. Navy or the U.S. Government.

Section I: Project Summary

1. Overview of Project

Abstract: The goals and objectives of this research are focused on theoretical studies, simulations and basic research on electron emission from nanostructures for vacuum electronics and other high power applications. This includes not just electrons, but also outgassing of desorbates that can potentially alter the space-charge of high power microwave (HPM) systems in the vicinity of emitting electrodes. Such evaluations are important to advance the fundamental physics-based understanding of vacuum field emission in nanoscale emitters and their photoemission characteristics, analyze surface physics including effects due to incident ion impact, and probe the role of proximity effects in nanoemitter arrays with regards to screening, field enhancements and safe operating ranges.

Objectives: Cathode emitters are important components contributing to the overall successful development of high power microwave devices. For example in the magnetically insulated transmission line oscillators (MILOs), use of cathode arrays or field shaper cathodes have been demonstrated to affect the beam quality (i.e., the uniformity, stability, the cathode plasma expansion velocity, etc.) and thus, influence the performance. Given that there is interest in MILO development both at Texas Tech University (TTU) and the Navy, this proposed effort would also help MILO work with regards to: (a) enhancing reliability and lifetime, (b) achieving better electric field uniformity on the cathode surfaces for suppressing potential cathode flare formation, (c) focusing on emitter arrays for scalable increases in current and design of optimal spacing for increased emission output, and (d) in evaluating the efficiency of HPM systems driven by electron emissions.

Introduction: The project has begun analyses for electron emission, atomic ejection and is also moving towards evaluation of outgassing for HPM in systems characterized by low pressure. This includes evaluation of electric field enhancements at nanoemitters, with subsequent generalization to arrays. Collaborative efforts with Drs. John Kuginsland (Confluentsciences) and Drs. A. Garner (Purdue University) and J. Mankowski (TTU) will bring synergies. Details of the effort so far and the tasks planned in the near future, are given next.

Background: Study of emission from cathodes is important and is being studied at the multiple levels: (a) Electron emission from surface emitters based on self-consistent calculations of quantum tunneling that include interface barriers and wavefunctions modified by electric fields and photoexcitation, (b) Local heating due to incident photons and/or energetic charged particles that modify the surface temperature and create nonequilibrium distributions, (c) Out-gassing driven by temperature-dependent increases in diffusion that can affect space-charge in HPM systems above the emitting surface, with supporting Molecular Dynamics (MD) analysis (d) Modifications in electric fields due to proximity and screening effects based on both three-dimensional simulations based on software tools (e.g., CST Microwave Studio) and Linear Charge Models (LCMs). Some of the results (e.g., outgassing rates) will be fed as input parameters to PIC codes that are already capable of HPM analysis (e.g., Dr. John Luginsland efforts at Confluentsciences).

2. Activities and Accomplishments

(i) Probing Electron Emission from Laser Excitation in Presence of DC Field

The photon-assisted electron emission current calculations were developed, due to the superposition of both a DC field and an RF external signal (presumably a high intensity laser). The electron distribution function needed for the current density calculation was computed based on energy balance, taking account of: (i) the incident radiation which deposits energy in the metal, (ii) losses through electron-phonon interactions (a relaxation process). This provided a time-dependent lattice temperature $T_e(t)$, and modeled using rate equations as follows:

$$P_{abs} - G\,[\,T_e(t) - T_L(t)\,] = C_e\, dT_e(t)/dt \quad , \qquad (1a)$$

$$\text{and,}\quad G\,[\,T_e(t) - T_L(t)\,] = C_L\,[\,dT_L(t)/dt + \{T_L(t)-T_0\}/\Gamma_{ph}\,] \quad , \qquad (1b)$$

where G is the electron-phonon coupling constant (taken to be $4\text{x}10^{16}$ W/m^3/K as a typical value for copper), C_e and C_L are the electronic and lattice heat capacities (taken here to be: C_e = 71.5 J/m^3/K^2 T_e, and $C_L = 3.5\text{x}10^6$ J/m^3/K). Also, $T_e(t)$ and $T_L(t)$ are the effective temperatures of the electrons and the host (copper) lattice, "t" denotes the time, and P_{abs} is the power density (in Watts/m^3). Finally, T_0 denotes the ambient lattice temperature, while Γ_{ph} is the phonon lifetime of 7 ps due to anharmonic decay. The two terms on the left of equation (1a) represent the power input from the laser into the electron system and the power dissipated into the copper lattice, while the left term of equation (1b) denotes the power absorbed by the copper from the electrons. Thus, a two-temperature model was used to describe the electron and lattice sub-systems, with $T_e(t)$ and $T_L(t)$ denoting the time-dependent electron and lattice temperatures, respectively.

For the electron system, the distribution function $f_e(t)$ was taken to comprise of two parts given as:

$$f_e(T_e,\, t) = f_{e\text{-}NT}(t) + f_{e\text{-}T}(T_e,t) \, , \qquad (2)$$

where $f_{e\text{-}NT}(t)$ and $f_{e\text{-}NT}(t)$ denote the non-thermal and thermal components. The thermal part of the electron distribution was taken to be the usual Fermi-Dirac, but at an elevated, time-dependent temperature $T_e(t)$ as:

$$f_{e\text{-}T}(t) = 1/\{\exp[(E-E_f)/(kT_e(t))] + 1\} \quad , \qquad (3a)$$

where represents the fermi level of the metal (typically 5.53 eV for copper). The non-thermal part of the distribution $f_{e\text{-}NT}(t)$, was obtained at each time step based on the following relation:

$$f_{e\text{-}NT}(E,t+dt) = f_{e\text{-}NT}(E,t) - f_{e\text{-}NT}(E,t)\,\{[E - E_f]/E_f\}^2\, dt/T_0 +$$
$$+ [P_{abs}\, dt/(\hbar\omega)]\,[(E-\hbar\omega)/E]^{1/2}\,\{\exp[(E-\hbar\omega-E_f)/(kT_e(t))]+1\}^{-1} / T \, , \qquad (3b)$$
$$\text{with}\quad T = \int_{E_f-\hbar\omega}^{E_f} [E^{1/2}\, dE / \{\exp[(E-E_f)/(kT_e(t))] + 1]\} \, . \qquad (3c).$$

The time-dependent, nonequilibrium electron distribution function was next used to obtain the emission current due the incident RF signal with the superimposed external DC field. This current density (as discussed in detail in the monthly reports) are given as:

$$J_{tran} = \iiint q\, v_z\, D(k_z)\, [1/(2\pi)]\, 2\, k_{//}\, dk_{//}\, d\theta\, dk_z\, f(k_{//},k_z) \ , \qquad (4a)$$

$$\rightarrow \ J_{tran} = (qm)/(2\pi^2\hbar^3) \iint D(E_z)\, dE_{//}\, dE_z\, f(E_{//},E_z) \ , \qquad (4b)$$

where $f(k_{//},k_z)$ denotes the equilibrium probability function for the occupancy of state k_z, and $D(E_z)$ the transmission coefficient at energy E_z. *This function denotes a nonequilibrium, time-dependent distribution.* Letting $f_e(E,t) \equiv f_e(E_{//} + E_z, t)$, the symbolic expression for the transmitted electron current density, J_{tran}, becomes:

$$J_{tran} = (qm)/(2\pi^2\hbar^3) \int_0^\infty D(E_z)\, dE_z \int_0^\infty f(E_{//},E_z)\ dE_{//} \ . \qquad (5)$$

Evaluations of the electron distribution function and its evolution in response to an external RF field incident on a copper emitting surface were carried out based on the above theory. The time-dependent evolution of the electron temperature obtained in response to an incident power input from the RF source is shown in Figure 1. A sharp rise to about 50,000 ˚K is predicted within about 1.5 ps, followed by a more gentle rise. This heating of the electrons affects the overall distribution. The combined distribution $f_e(T_e, t)$, which equals $f_{e\text{-}NT}(t) + f_{e\text{-}T}(T_e,t)$, is shown in Figure 2. Due to the non-thermal part, a relative "shoulder" can be seen in the result. Since the laser was always assumed to be turned on, the distribution function here is predicted to monotonically increase in both the magnitude and the energy spread.

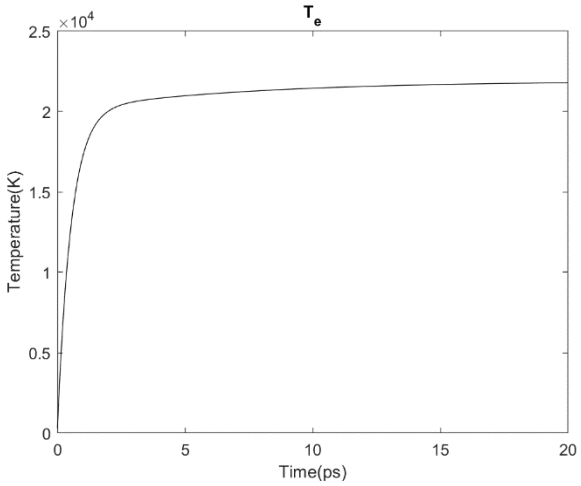

Figure 1. Electron temperature as a function of time following incident power from an RF source.

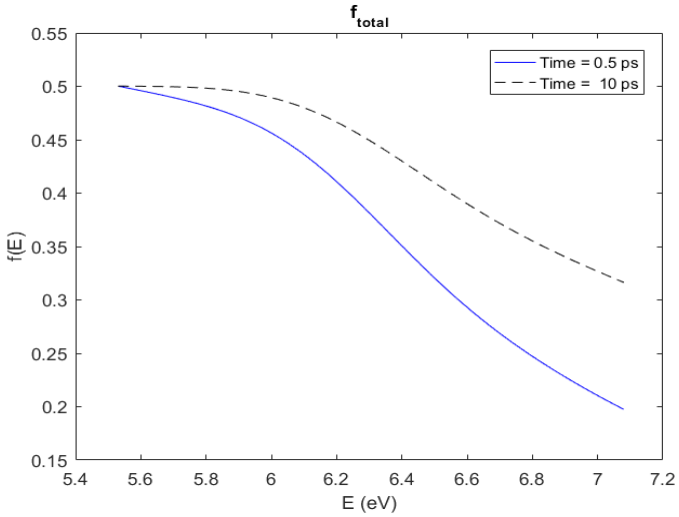

Figure 2. The overall combined distribution function $f_e(T_e, t)$ as a function of electron energy shown at two time instants of 0.5 ps and 10 ps. A shift to higher levels with a slight ″shoulder″ and a large spread are evident, especially at the longer times.

Since the distribution function is required for the current density calculation J_{tran} as given in eqn. *(5)*, expressions for the overall distribution $f_e(T_e, t)$ were obtained from a curve-fit.

For completeness, the response of the electron temperature [$=T_e(t)$] and that of the phonon bath [$=T_l(t)$] to a rectangular pulse, are shown in Figure 3. As might be expected, the electron temperature increases very rapidly during the initial phase when the laser is ON. An electron effective temperature on the order of 21,000 ˚K is predicted to be reached over the first 5 picoseconds. The temperature of the phonon bath also increases, but at a much slower pace. Once the laser is turned OFF at 10 ps, the system begins to relax back to equilibrium. The electron and phonon temperatures approach each other, and are predicted to relax back to 300 ˚K in less than 30 ps.

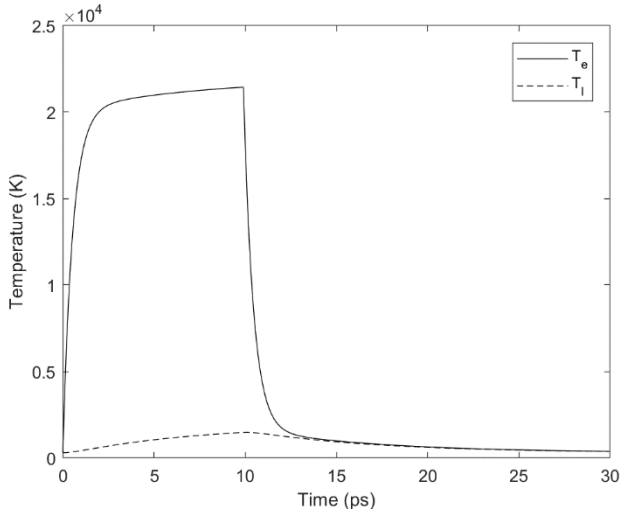

Figure 3. The predicted electron temperature $T_e(t)$ and that of the phonon bath $T_l(t)$ as a function of time, in response to a laser input pule of 10 ps duration. The ambient temperature was taken to be 300 ˚K.

Finally, the distribution functions obtained were used for predictions of the electron emission current density from the copper surface. Equation (5) was used, and the incident power density on the copper surface was assumed to be $8x10^{20}$ W/m^3. Results obtained are shown in Figure 4 for a range of external DC electric fields for two cases.

The plot of Fig. 4 shows the current densities for the time-dependent non-equilibrium case to be much higher than that of the standard Fowler-Nordheim prediction. Also, the threshold fields for the start of non-negligible currents are also seen to much lower than for the conventional case. Though not shown here, the current density with the time-varying distribution function $f_{e\text{-}NT}(E,t)$ can easily be obtained, and would lead to a three-dimensional surface for $J_{tran}(F,t)$.

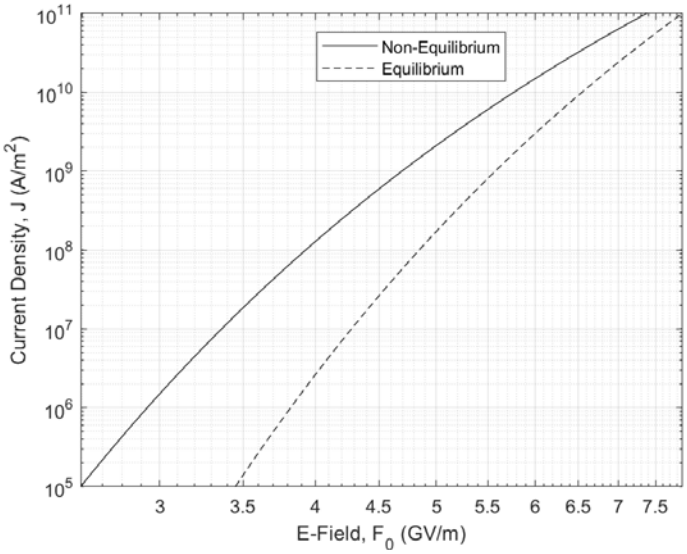

Figure 4. Emitted electron current density as a function of the externally applied electric field. The plots correspond to calculations based on an equilibrium and a nonequilibrium functions with time-dependent electron temperatures.

(ii) Study of Outgassing from Incidence of Energetic Particles on Electrode Surface

Electrode surfaces of HPM systems, including magnetically insulated transmission line oscillator (MILO) devices are subject to bombardment of high energy particles including electrons and ions that are routinely accelerated in the system. This leads to three consequences: (a) Potential damage at the surface, including disruption and ejection, (b) Local heating at the surface, and (c) Enhanced diffusion and outgassing of adsorbed species. The latter can potentially change the pressure in the HPM system, and be the source of space-charge creation through ionizations. Hence, it is important to probe and understand such surface effects mediated by incident particles.

Towards this end, Molecular Dynamic (MD) simulations were carried out. Graphene coating of copper electrodes were used as a test composite surface, since graphene is a durable and mechanically strong material. Impingement of carbon atoms at different energies were probed. The nanoscale coating of metal electrodes by graphene was shown to be a useful approach for suppressing the secondary electron yield. The resistance to possible degradation of this structure, in response to incoming atomic projectiles, was gauged. Our results for surface irradiation by

carbon atoms (as an example) on nanoscale graphene coatings indicated a defect threshold of about 35 eV, lower surface damage for thicker layers, negligible sputtering, and defects less than 6 A˚ in dimension for energies up to 300 eV. The electrode structure was thus shown to be robust with better resistance to damage than metal alone.

The sputtering probabilities given in Fig. 5 show that for energies around 300 eV, the sputtering yield for graphene coated copper is about 50%. The largest yield is predicted to occur for a one-layer graphene structure, while increasing the number of sheets leads to a protective shielding effect. Thus, thicker coatings with at least three or more monolayers would appear to be a more useful strategy to reduce damage to the topmost layer. This aspect of thicker layers is discussed subsequently. More interestingly, the sputtering yield for the copper material alone, without any graphene coatings, is predicted to be the highest. This is a clear implication then that graphene coatings, in addition to providing the benefit of reduced secondary electron emissions, would also offer a more stable and durable system against degradation.. A pertinent parameter is the damage caused by the incoming particles. The MD simulation result of Fig. 6 shows the average damage size (in $A^{\circ 2}$). Essentially, defects are created via primary knock-on, which can potentially lead to cascades if the incident energies are high. The results of Fig. 6 roughly follow the trend first discussed by Robinson [M. T. Robinson, in Defects and Radiation Damage in Metals (Cambridge University Press, Cambridge, 1969]. Not much damage was predicted in the copper.

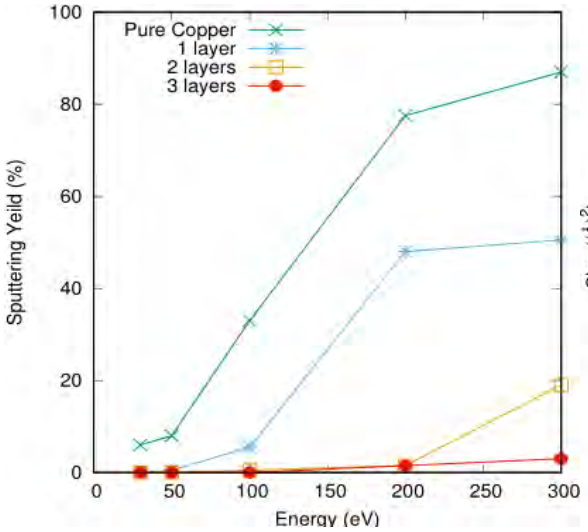

Figure 5. Simulations of sputtering yield on incident energy.

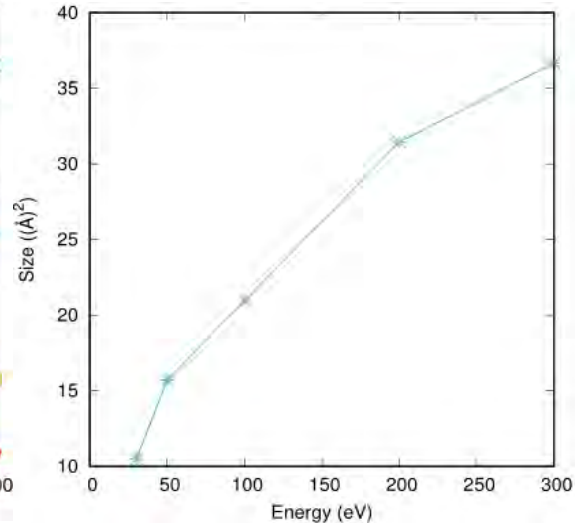

Figure 6. MD results for damage size as function of incident energy.

3. Findings and Conclusions

Two sets of results were obtained during the brief six-month duration that the start of the project in July 2018. These were as given below.

(i) Model development along with supporting calculations for photoemission in the presence of an externally applied electric field. The total driving force for electron emission was thus a combination of both a DC field and the RF excitation of the incident laser; together with the photon energy input for transcending the workfunction barrier at the surface. Such photoemission is an important source for high density electron emitters.

(ii) Carrying out Molecular Dynamics (MD) simulations of outgassing from electrodes. Though there are many applications of interest to the Navy, one specific area that such calculation will support and aid is in the assessment of the design of cathodes for the magnetically insulated transmission line oscillator (MILO) devices. For example, recent research on this topic (e.g., M. D. Haworth, K. L. Cartwright, J. W. Luginsland, D. A. Shiffler, and R. J. Umstattd, IEEE Trans. Plasma Sci. **30**, pp. 992-997, 2002) based on particle-in-Cell (PIC) codes for MILO systems have assumed some level of gas. However, the specific role of outgassing, the resulting inhomogeneities in the concentration, and release rates have not been assessed. Hence, the evaluations of the system efficiency and perturbations in space-charge could change if more realistic and physically-based input to the PIC formulation was made available. The MD simulations are a step in the direction towards including outgassing from surface adsorbates.

Both of the above aspects are very germane and relevant to electron emitters for various high density electron sources and other applications, to the Navy.

4. Plans and Upcoming Events

Plan to develop and run simulations for nanoemitter arrays, and compare with any data emerging from the group at Texas Tech University.

Plan to perform simulations for out-gassing upon energetic electron impact. These will be Molecular Dynamics results aimed at treating two routes to outgassing. (i) The dislodging of adsorbed gases at the surfaces due to the impact of high energy electrons, leading to their release from the anode material, and (ii) The local increases in temperature due to inelastic energy exchanges between the incident electrons and the host lattice. This would enhance the diffusion and lead to out-diffusion driven by local heating.

In addition, energy threshold should also become available. The results will be shared with Dr. John Luginsland at Confluentsciences, and the used as input into his Particle in Cell (LIC) codes for analyses of the design of cathodes for the magnetically insulated transmission line oscillator (MILO) devices.

Plan to attend the joint International Vacuum Nanoelectronics Conference (IVNC) and the International Vacuum Electron Sources (IVESC) Conference at Cincinnati, July 22-26, 2019.

5. Transitions and Impacts

None.

6. Collaborations

Dr. John Luginsland, Confluentsciences
Prof. John Verboncoeur, Michigan State University
Dr. Allen Garner, Purdue University

7. Personnel

Principal investigator	Ravindra P. Joshi
Co-investigator or Co-PI	Andreas Neuber, John Mankowski, James Dickens
Business Contact	Kathleen Harris, TTU Associate Vice-President for Research
Team Members	None others
Subs	None

8. Students

Sayeed Sami – PhD student
Lily Qiu – PhD student

9. Technology Transfer

None.

10. Products, Publications, Patents, License Agreements, etc.

Archival Publications

a. Article Title: Model Evaluations of Surface Modification by Energetic Incident Carbon Atoms on Graphene Coated Copper Electrodes
b. Journal: Physics of Plasmas
c. Authors: X. Qiu, J. Mankowski, J. C. Dickens, A. A. Neuber, and R. P. Joshi
d. Keywords: Incident Atoms, Surface Modification, Damage, Electrodes
e. Distribution Statement: Unrestricted distribution
f. Publication Status: Published
g. Publication Identifier Type: https://doi.org/10.1063/1.5056766
h. Publication Identifier: https://doi.org/10.1063/1.5056766
i. Publication Date: January 2019
j. Volume: 26
k. Issue: 1
l. First Page Number: 013501-1
m. Publication Location: New York, USA
n. Acknowledgement of Federal Support? (Yes/No): Yes
o. Peer Reviewed? (Yes/No): Yes

11. Point of Contact in the Navy

Dr. Ryan Hoffman, Program Officer, Office of Naval Research

12. Acknowledgement/Disclaimer

This work was sponsored by the Office of Naval Research (ONR), under grant number N00014-18-1-2382. The views and conclusions contained herein are those of the authors only and should not be interpreted as representing those of ONR, the U.S. Navy or the U.S. Government.

A High Repetition Rate, Long Lifetime Magnetically Insulated Line Oscillator (MILO)

Grant No. N00014-18-1-2384

Period of Performance: April 15, 2018 to September 30, 2018

Prepared by:

Dr. John Mankowski, Principal Investigator
Center for Pulsed Power and Power Electronics (P3E)
Texas Tech University
Department of Electrical and Computer Engineering
2500 Broadway, MS3102
Lubbock, TX 79409-3102
Tel: (806) 834-3168
Email: john.mankowski@ttu.edu

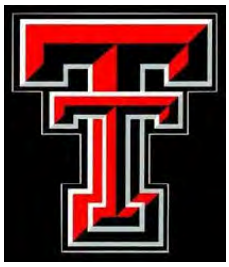

This work was sponsored by the Office of Naval Research (ONR), under grant number N00014 - 18-1-2384. The views and conclusions contained herein are those of the authors only and should not be interpreted as representing those of ONR, the U.S. Navy or the U.S. Government.

Grant or Contract Number: N00014-18-1-2384
Date Prepared: 12/15/2018
Project Title: A High Repetition Rate, Long Lifetime Magnetically Insulated Line Oscillator (MILO)
Annual Summary Report: CY2018
Principle Investigator:

Texas Tech University (TTU)
Center for Pulsed Power and Power Electronics (P3E)
Dr. John Mankowski
john.mankowski@ttu.edu

Co- Principle Investigators:

Texas Tech University (TTU)

Dr. James Dickens
james.dickens@ttu.edu

Dr. Andreas Neuber
andreas.neuber@ttu.edu

Dr. Ravi Joshi
ravi.joshi@ttu.edu

Financial POC:

Texas Tech University (TTU)
Office of Research Service
Ms. Amy Cook
amy.cook@ttu.edu

Section I: Project Summary

1. Overview of Project

The overall goals of this project are to design, fabricate and test a 1 GW class magnetically insulated line oscillator (MILO) capable of high repetition rates. The MILO source will be a hardtube design with advanced materials for high rep-rate operation. To that end, we are using particle in cell (PIC) simulation code to model the MILO source structure and materials for a prediction of output RF power and efficiency. In conjunction with the MILO development, we are constructing a low impedance (~10 Ω) Marx generator to drive the MILO and test in single shot mode. Since the project is 9 months into a 3-year program, the bulk of this report discusses the MILO PIC simulations and Marx generator development.
The fundamental objective of this applied research is to develop an enabling technology for future pre-detonation Counter Improvised Explosive Device (CIED) systems. HPRF system power

requirements are primarily driven by range (stand-off), and the pulse repetition frequency correlates to the desired speed of the USMC tactical vehicle. Current conventional microwave tube technology used for such systems is limited by output power to single digit MW and total system weight can exceed 20,000 lbs. By comparison, relativistic High Power Microwave (HPM) sources such as Relativistic Magnetrons (RelMags) and Magnetically Insulated Line Oscillators can be driven by short pulse Marx generator pulsed power devices and produced with total weights on the order of 2,000 lbs or less in compact form factors. This reduction in weight by an order of magnitude has potential to enable integration into a wide variety of Marine Corps tactical vehicles to include Mine Resistant Ambush Protected (MRAP) and HMMWV. If the size and weight can be further reduced, there is even potential to employ this counter IED technology on small unmanned ground vehicles with on board power. Additionally, there is potential to utilize this emerging technology for countering emerging Unmanned Aerial System threats. RelMags and MILO tube designs offer potential for achieving substantial increases in peak output RF power compared to existing commercial-off-the-shelf (COTS) magnetron and klystron tubes, but at the expense of efficiency. The inherent shortcoming of these relativistic tubes is pulse shortening which is an important factor when operating in the relativistic regime. Additionally, the lifetime of these novel tube design geometries has not been characterized.

Abstract:

This report details the development of a hardtube Magnetically Insulated Line Oscillator for testing in the high repetition rate regime. A brief background of the project is first discussed. The narrative portion of activities and accomplishments are divided into two segments. The first part details research performed on the MILO design conducted primarily with PIC code simulation. The second part reports on the design and development of a low inductance Marx generator which will drive the MILO. Finally, findings and plans are presented for the upcoming year.

Objective:

The objective of this research is to develop a 1 GW class, hardtube MILO that will be capable of high repetition rate operation.

List of Figures

Background:

The program objective is to design and construct a high-power microwave source capable of high RF power (> 1 GW) and high repetition rate. To this end we are proposing the development of a hard tube magnetically insulated line oscillator. This type of performance can be achieved by fabrication using advanced materials and sealed tube technology as well as design optimization through PIC code simulation. The high diode peak power will induce extreme temperatures within tube components. Advanced materials such as pyrolitic graphite can withstand these conditions which will result in shot lifetimes many orders of magnitude greater than traditionally used materials. These operating conditions will also create plasma within the AK gap which can result in pulse shortening. Sealed tube technology has been shown to reduce plasma generation as well as decrease plasma lifetime. Finally, PIC code simulation will be used to optimize MILO performance resulting in higher power efficiency and lower losses.

2. Activities and Accomplishments

MILO Source Development

The first and primary part of the activities and accomplishments reported upon is the MILO source design through PIC simulation. The initial focus was placed upon successfully simulating a MILO based upon the parameters published in literature, in particular work reported by Dixit et al, shown in Figure 1. The focus of the paper was the optimization of the cathode extension into the beam dump of a L-Band MILO to maximize the theoretical microwave power with CST Studio Suite as the simulation package. The provided parameters and design equations provided a starting point to model and simulate the MILO within CST Studio Suite and provided results for comparison. After solving a few issues caused by factors unspecified within the paper a matching simulation was completed. A side by side comparison of RF output power is shown in Figure 2.

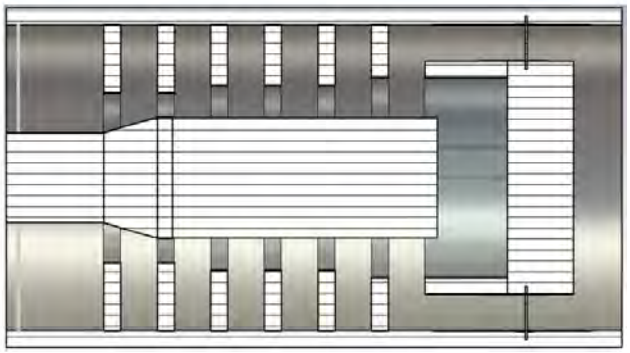

Particulars	Specifications
Voltage	600 kV
Current	52 kA
Cathode radius (r_c)	28 mm
Anode radius (r_a)	85 mm
SWS vane radius	45 mm
Extractor vane radius	54 mm
Choke vane radius	42 mm
Vane thickness (T)	4 mm
Periodicity (L)	19 mm
Beam dump outer radius	54 mm
Beam dump inner radius	52 mm

Figure 8. The three-dimensional model as seen within CST Studio Suite with accompanying design parameters.

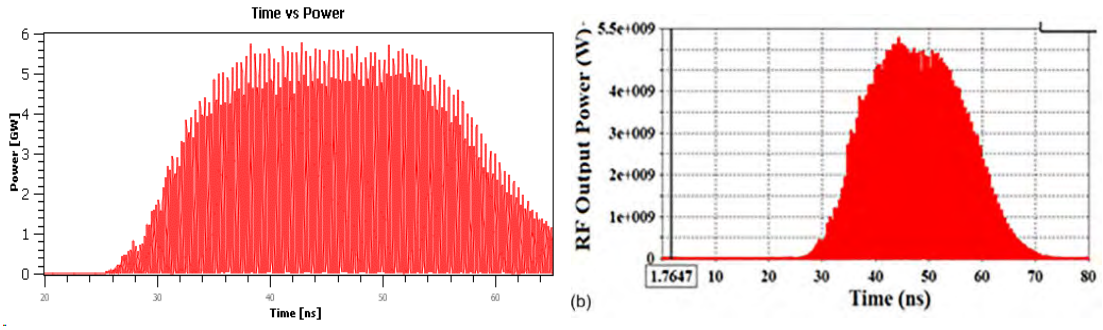

Figure 9. A side-by-side comparison of the results from our simulation, left, and the results stated in Dixit.

Once this successful simulation was achieved, a set of goals was defined for the project as well as operating parameters of the MILO. In particular, the operating frequency of the MILO was chosen as S-band for two primary reasons. First, the S-band MILO has a higher input impedance than the L-band which makes design and fabrication of the Marx generator easier. Second, the S-band source is smaller than the L-band resulting in higher power densities which would put higher thermal stresses on components during rep-rate operation making it easier to experimentally determine operational limits. Design equations used in the initial MILO design were employed on the S-band design. These parameters were then transferred to the three-dimensional model, shown in Figure 3, within CST Studio Suite, where an idealized rectangular pulse was applied during simulation, shown in Figure 4. Additional simulation results shown in Figure 4 include RF frequency output of 2.5 GHz and peak power ~ 4 GW which corresponds to an efficiency of the MILO RF power output to input pulse of approximately 10%.

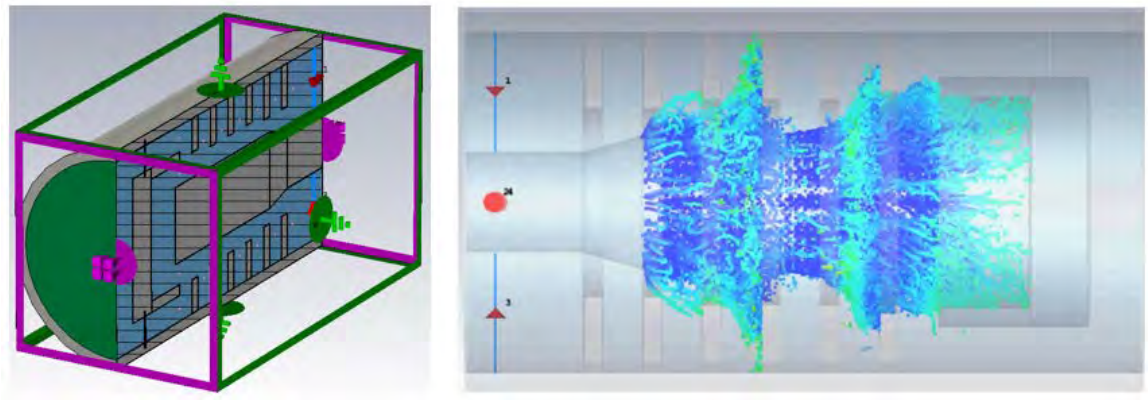

Figure 10. The isotropic view of the S-Band MILO design with a demonstration of pi-mode electron motion captured after simulation of the device.

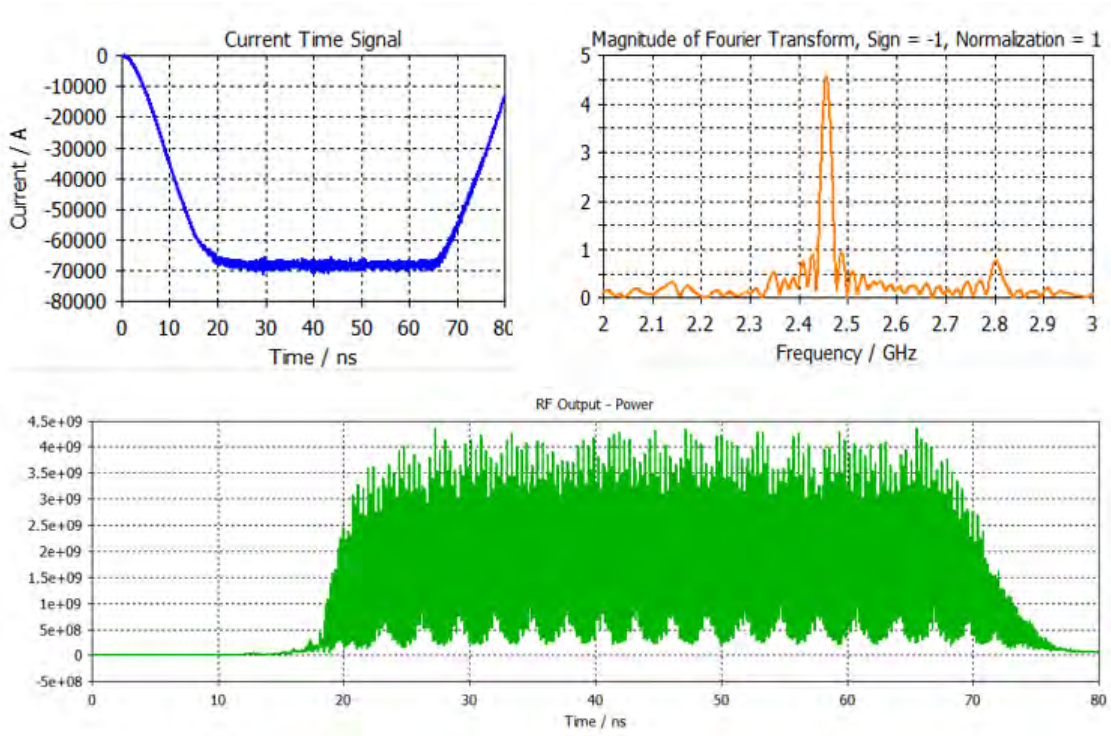

Figure 11. Simulation results of the S-Band MILO based upon the design equations presented in the Dixit paper. (Top Left) The calculated input current for a 600 kV rectangular pulse. (Top Right) The Fourier Analysis of the RF Output Power, approximately 2.45 GHz for a designed 3 GHz target still within S-Band. (Bottom) The magnitude of the output RF power from the MILO, a maximum of approximately 4.2 GW.

The next steps were to simulate with the actual material properties applied to the MILO components. Due to the expected thermal requirements applied to the MILO's fin structure we simulated with pyrolytic graphite for the fins. Pyrolytic graphite offers a high thermal conductivity along the AB plane though it has a low electrical conductivity. Graphite was used for the cathode material and all other components were simulated with stainless steel as their material. The MILO 3D structure with material properties is shown in Figure 5. After simulation with the applied materials the efficiency of the input power dropped drastically to about 2% as indicated by the RF output power waveform in Figure 6.

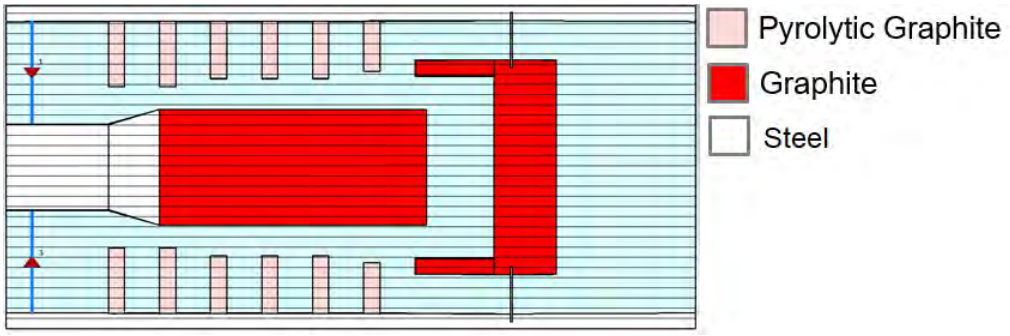

Figure 12. The MILO Model with color representing the material type of each of the components within the simulation. The fins, light pink, are set to be pyrolytic graphite while the cathode and beam dump are constructed from normal graphite. The remainder of the structure is simulated as stainless steel.

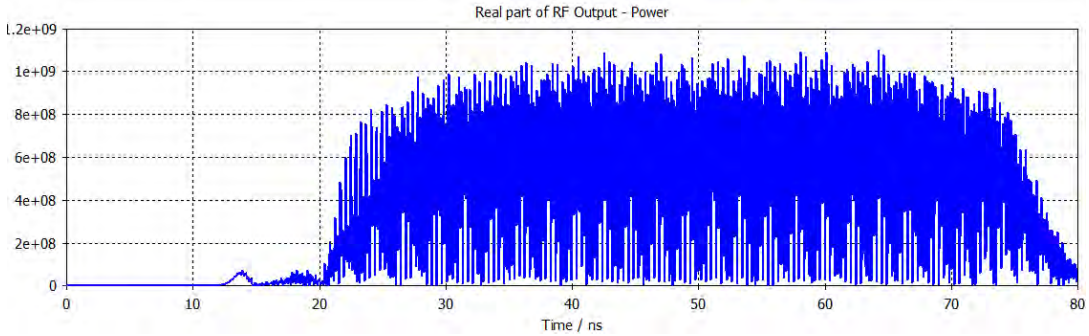

Figure 13. The RF output power measured for the MILO with simulated materials. The output power dropped drastically from an approximate maximum output power of 4.2 GW to 1 .1 GW reducing the power efficiency to near 2%.

To better predict MILO performance, the MILO simulation was driven with a lumped element pulsed power driver instead of the ideal square wave HV input pulse. CST contains a lumped element model SPICE simulation which can perform a co-simulation of the lumped elements which feeds the input of the PIC simulation of the MILO. This lumped element circuit, shown in Figure 7, modeled the performance of the Marx generator as detailed in the next section of this report. This presented a few challenges as some features are not currently supported by CST in co-simulation. Primarily, the measurement of the output power needed to be calculated by the integration of the power flow instead of the built-in waveguide port. The output waveform of the Marx from the co-simulation, shown in Figure 8, matched the expected waveforms closely enough to confirm our ability to successfully simulate the Marx and MILO as a combined unit to generate more realistic output expectations from the MILO. MILO RF output power is shown in Figure 9.

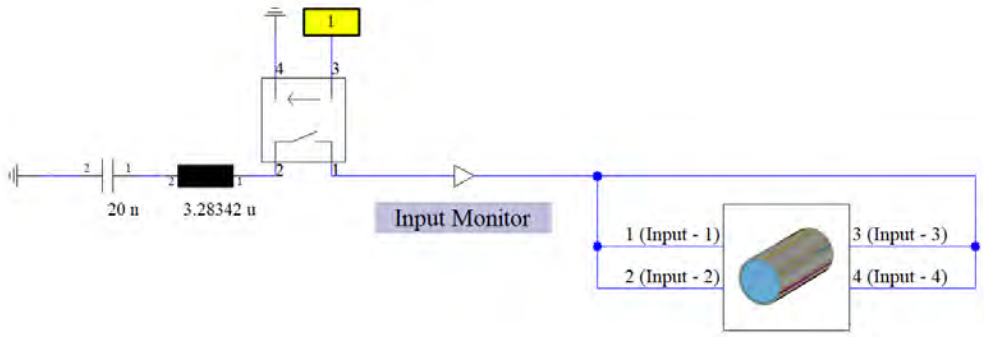

Figure 14. The lumped element setup within CST Studio Suite modeling the idealized Marx generator connected to the four discrete ports within the MILO model. The capacitor is initially charged with 1.1 MV. The switch is required by CST's SPICE implementation for proper excitation of the MILO.

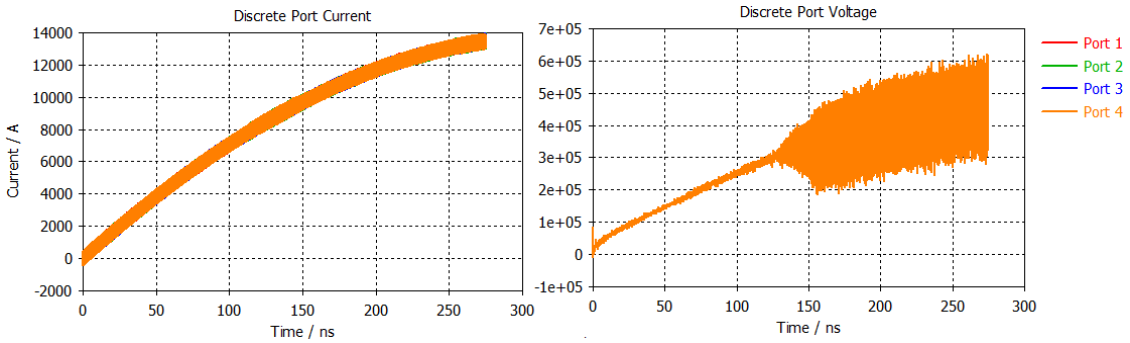

Figure 15. The discrete port results of the CST Co-transient simulation of the lumped element Marx as a source for the MILO. The discrete ports are in parallel with each other, thus the actual input current into the MILO is 4 times the magnitude of that on any one port.

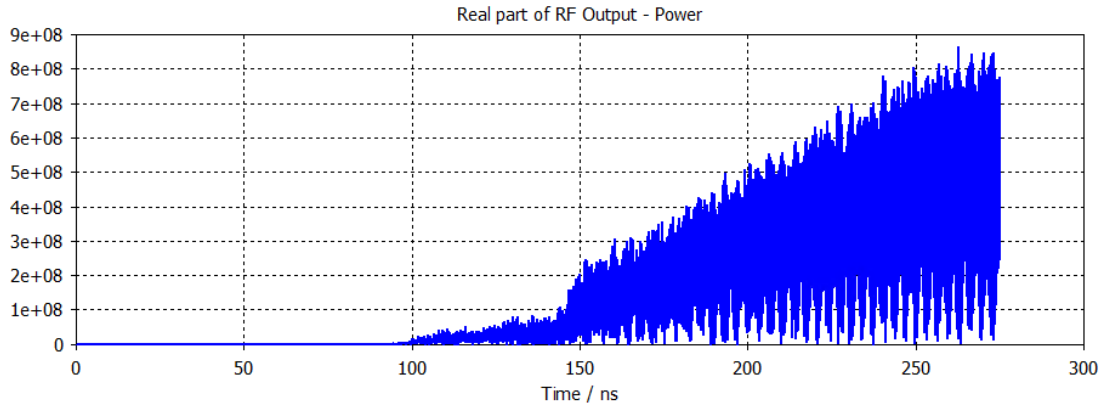

Figure 16. The resulting magnitude of the RF output power as a result of the co-transient simulation. Comparing with the input voltage wave form of the discrete ports, in figure 8, the RF output power rises after the applied voltage exceeds the minimal threshold for magnetic insultation to occur within the device.

Marx Generator Development

In order to effectively drive the low impedance of the MILO, a high current Marx generator needs to be designed and fabricate. The performance goals of the Marx are an output voltage of >500 kV, output current > 40 kA, risetime < 150 nsec, and pulsewidth >100 nsec. These performance goals were determined from PIC simulation of the MILO such that an RF efficiency (>10%) and RF peak power (> 1 GW) can be achieved.

Employing the General Atomics 31160 capacitor, tests were conducted on a small 3 and 4 stage Marx. These tests allowed us to experimentally determine the parasitic stage inductance of the basic design. Images of a CAD drawing and setup of the small Marx are shown in Figure 10. From the output current waveform of this setup the per stage inductance is calculated to be ~ 120 nH.

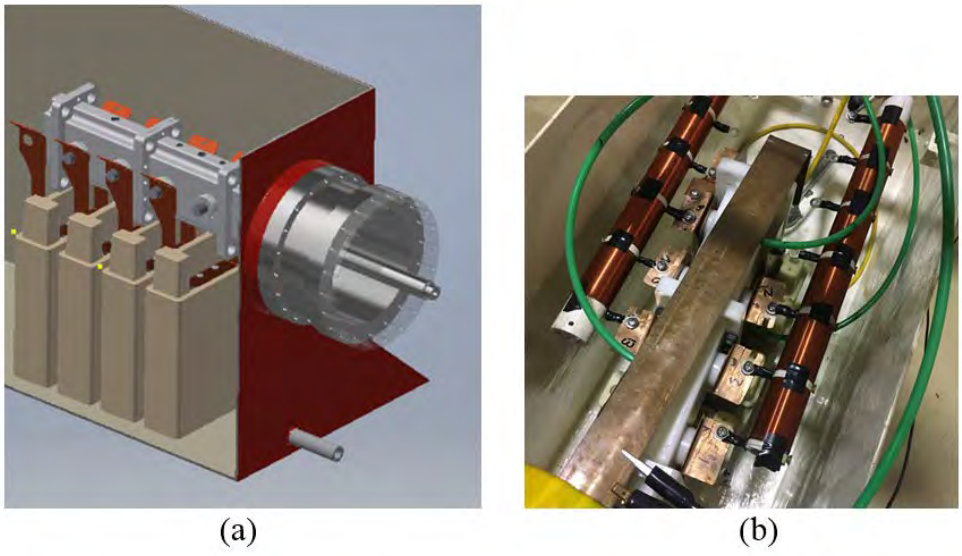

Figure 17. Small Marx (a) drawing and (b) experimental setup.

Using the experimentally derived per stage inductance several Marx configurations were simulated to determine the optimum design for achieving the performance parameters. An 18-stage with 2 capacitors per stage was determined to be the optimum design. The circuit schematic and output into a 12 ohm load of this Marx generator are shown in Figure 11 and 12, respectively. Peak voltage and current are 570 kV and 48 kA, respectively. Pulse risetime and pulsewidth are 170 nsec and 540 nsec, respectively.

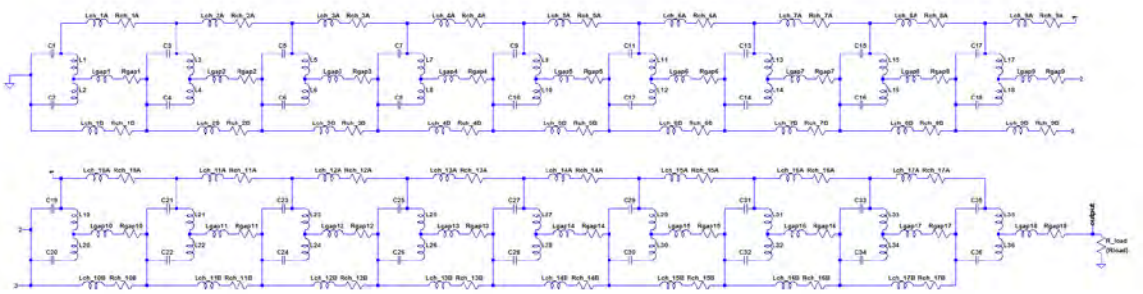

Figure 18. An 18-stage Marx generator with two capacitors per stage. Capacitors are initially charged to 50 kV and output is a 12 ohm resistive load.

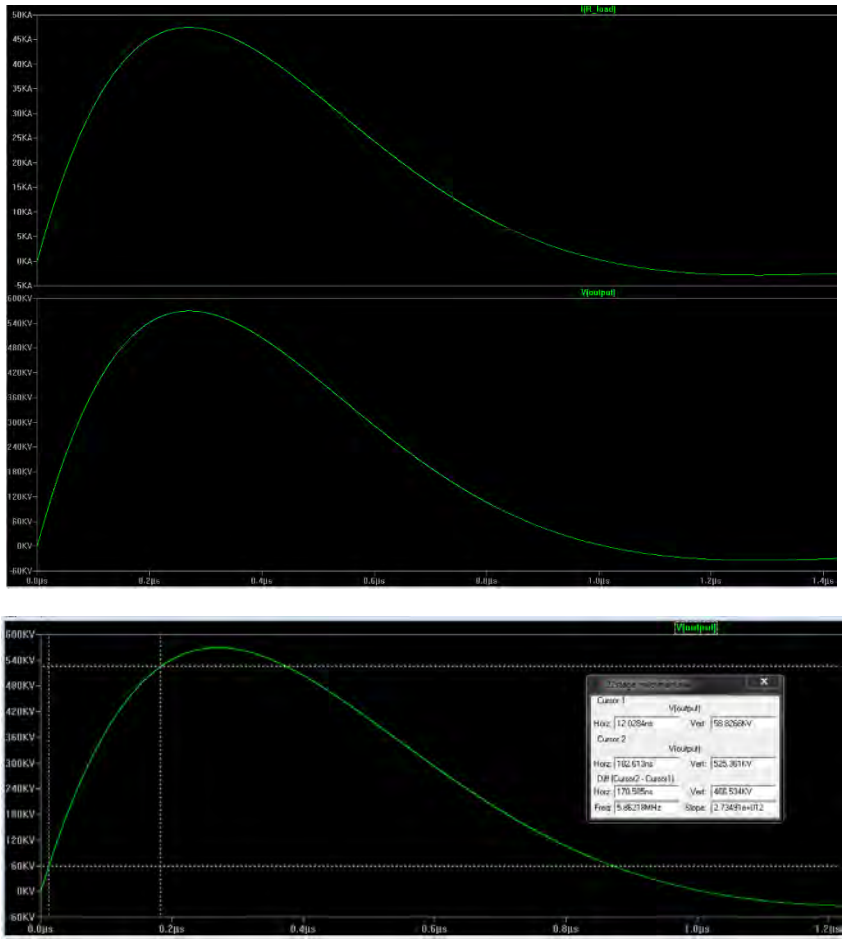

Figure 19. Simulation output indicating output voltage (top), current (middle), and pulse risetime (bottom).

Most of the Marx components have been designed. CAD drawings of several of the key components are shown in Figure 13. These include the sparkgap tube modules, output feed, and capacitor brackets. The overall assembly drawing of the Marx contained in an insulated support

structure is shown in Figure 14. The aluminum top plate of the support structure includes wire feedthrough for charging, gas line feedthrough for high pressure air flow, and eye bolts for lifting. This assembly will sit inside of an oil filled tank which has already been fabricated.

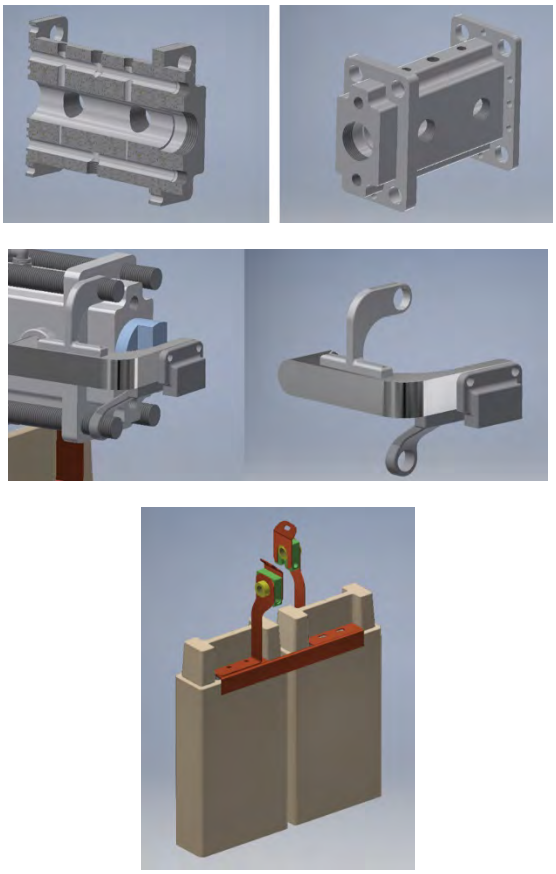

Figure 20. Key components of the large Marx generator including the sparkgap tube modules (Top), output feed bracket (Middle), and capacitor brackets (Bottom).

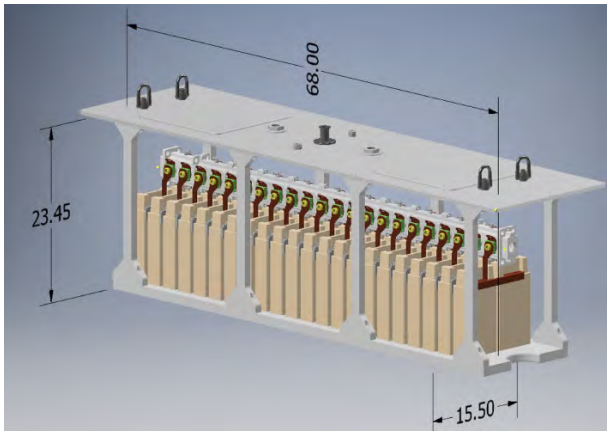

Figure 21. Full assembly drawing of the large Marx contained within an insulated support structure. Size dimensions in inches are shown.

3. Findings and Conclusions

There are several initial findings 7 months into this 3-year program. First, that the CST PIC code simulation of the MILO source is a plausible tool for source design. Second, simulations have predicted > 1 GW output RF power from the MILO driven by a "compact" Marx generator with the correctly designed impedance and with minimum inductance. Third, PIC simulations with pyrolitic graphite materials predict a significant reduction in RF output power and efficiency. This issue will be further examined in upcoming work.

4. Plans and Upcoming Events

Immediate plans for the MILO design are to re-examine the PIC simulations employing realistic material properties. Initial results showed a significant drop in RF power, however, this may have been a result of changes in meshing and not due to real RF losses due to material properties. If these RF power losses are real, we will minimize the use of pyrolitic graphite in the MILO structure design. Additionally, we will use optimization methods in the CST PIC code to increase efficiency and output power. These results will be employed as we start the MILO CAD design.

Now that the Marx generator is designed, fabrication and assembly is now beginning. Once constructed, the Marx will be tested into a dummy load to confirm impedance, risetime, and pulsewidth parameters. Additionally, the Marx will be used to test the HV feedthrough section between the Marx output and the MILO input.

5. Transitions and Impacts

None

6. Collaborations

We have had discussions with Sterling Beeson at AFRL regarding their development of a low-cost technique of bonding commercially available carbon fiber fabric, such as that used in hydrogen fuel cell manufacturing, to graphite. This would be a method we would like to employ in the fabrication of the MILO cathode.

7. Personnel

Principal investigator: John Mankowski,1 month effort

Business Contact:

Amy Cook
Texas Tech University
Office of Research Services
2625 Memorial Circle
Lubbock, TX 79409
Ph 806-742-3884
Fax 806-742-3892
Email: amy.cook@ttu.edu

Team Members: Senior Research Associate, David Barnett, 1 month effort

8. Students

2 PhD students, 1 Master's student, 1 undergraduate assistant

9. Technology Transfer

None at this time.

10. Products, Publications, Patents, License Agreements, etc.

Publications resulting from this project: None submitted during this initial report.

11. Point of Contact in Navy

Contact: Matt Mcquage, NSWCDD, E05

Contact information: matthew.mcquage@navy.mil

Date of last contact: Kickoff meeting on 7/31/2018

12. Acknowledgement/Disclaimer

This work was sponsored by the Office of Naval Research (ONR), under grant number N00014-18-1-2384. The views and conclusions contained herein are those of the authors only and should not be interpreted as representing those of ONR, the U.S. Navy or the U.S. Government.

Novel High Power Microwave System Designs Using Nonlinear Transmission Lines

Grant No. N000014-18-1-2341

Period of Performance: April 15, 2018 to September 30, 2018

Prepared by:

Dr. Allen L. Garner, Principal Investigator
Assistant Professor, School of Nuclear Engineering
Purdue University
400 Central Drive
West Lafayette, IN 47907-2017
Tel: (765) 494-0618
Email: algarner@purdue.edu

This work was sponsored by the Office of Naval Research (ONR), under grant number N00014 - 18-1-2341. The views and conclusions contained herein are those of the authors only and should not be interpreted as representing those of ONR, the U.S. Navy or the U.S. Government.

Grant or Contract Number: N00014-18-1-2341
Date Prepared: 26NOV2018
Project Title: Novel High Power Microwave System Designs Using Nonlinear Transmission Lines
Annual Summary Report: [FY2018]
Principal Investigator: Allen L. Garner, (office): 765-494-0618, algarner@purdue.edu, Purdue University

Section I: Project Summary

1. Overview of Project

Abstract: Nonlinear transmission lines (NLTLs) are of great interest to the Navy for solid state high repetition rate directed energy systems. This project investigates the suitability of novel composite materials for NLTLs in a high power microwave (HPM) source. Since understanding the current state of NLTL research will guide potential areas of improvement, we have performed an extensive review of current NLTL technology and topologies. This report provides an executive summary of the review paper that will be edited and submitted for publication in the coming months. We have constructed preliminary composite materials and are currently optimizing their design for future testing. We also report preliminary measurements of the dielectric properties of composites containing various volume fractions of barium strontium titanate (BST), which our discussions with engineers at TPL Inc. indicate will provide the greatest nonlinear performance at room temperature. This report summarizes the experimental setups for measuring the dielectric parameters and summarizes the results for composites with various volume loadings of BST. Proposed circuits for measuring nonlinear electromagnetic properties are also presented.

Objective: The goal of this project is to evaluate the feasibility of creating novel nonlinear dielectric materials by mixing nonlinear inclusions into a polymer base dielectric. The resulting composite dielectric properties will be measured using a vector network analyzer (VNA) to determine the complex permittivity and permeability of the composite. This will provide a baseline for determining the relationship between the volume loading of the nonlinear electric and nonlinear magnetic inclusions in a material to the dielectric properties of the composite. These measurements will be used to develop a model based on common effective medium theories, such as the Maxwell Garnett model, to guide material design. This model can be coupled with electromagnetic simulations to optimize an NLTL system as a radio frequency (RF) source.

Introduction: Increased global volatility motivates the development of devices for nonlethal deterrence. Directed energy devices can provide forceful persuasion at a distance for both civilian and military peacekeepers. Additionally, increasing occurrences of vehicular terrorism further drive the development of technology to stop vehicles from a distance before they can injure civilians or destroy property. Militarily, disabling motorized attacks before contact with troops is critical for reducing casualties while keeping the attackers alive for future interrogation. Directed energy technology can provide these capabilities, although system size often limits application in the field.

Thus, developing compact HPM devices could facilitate fielding devices for nonlethal defense with increased standoff range or for radar or weapons systems for aircraft or ships. This effort assesses the design of novel NLTLs by examining the impact of composites comprised of various

combinations of dielectric and magnetic inclusions and leveraging various geometries, such as tapering, used in conventional transmission lines for matching. This may increase efficiency and energy in the RF output as it relates to pulse width while also providing additional flexibility in design.

Background:

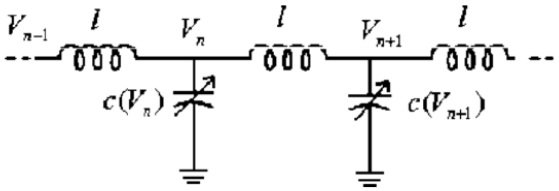

Fig. 1 Representative circuit model for a NLTL with nonlinear capacitors.

Materials are a challenge for NLTL design. Figure 1 shows a simple example of a NLTL. One may represent a conventional transmission line with lumped elements as an inductor in series with a resistor on the top line and a capacitor in parallel with a shunt conductor in the vertical lines with the resistor and conductor representing losses. An NLTL has a similar setup, as shown in Figure 1, except that either the inductor or capacitor (or both) vary with current or voltage, respectively. This modulates the delivered pulse to generate an RF signal with tunability of the NLTL important for controlling the frequency of the resulting RF.

While NLTLs are growing in importance for generating RF, challenges remain in constructing them with high voltage and power capabilities, as required in many HPM applications, and in tunability for wideband applications or capability to be used at multiple frequencies. Based on the definitions above and the circuit diagram in Figure 1, one method to generate an NLTL involves using a varactor, whose capacitance varies with applied voltage, generally sigmoidally (rapidly increasing over a narrow voltage range). Understanding the importance of this dependence is critical for understanding the potential flexibility in design. Early NLTLs often used nonlinear capacitance to induce this phenomena, resulting in soliton formation. This mathematical result arises from writing the circuit equation for the NLTL in Figure 1 as

$$L\frac{\partial}{\partial t}\left[C(V)\frac{\partial V}{\partial t}\right] = \frac{\partial^2 V}{\partial x^2} + \frac{\delta^2}{12}\frac{\partial^4 V}{\partial x^4}, \quad (1)$$

where $\square$ is the length of each segment of the NLTL, L is the inductance, C is the capacitance, and V is the voltage.

Varactors are generally low voltage devices, which presents a challenge for high power applications. Additionally, the frequency cannot be tuned for a given varactor. A recent alternative growing in popularity involves using ferrites to provide nonlinear inductance in meandering NLTLs. Texas Tech University (TTU), the Air Force Research Laboratory (AFRL), and others have also developed and applied such approaches for gyromagnetic NLTLs for HPM and high power radiofrequency applications. The initial TTU NLTLs provided peak voltages of approximately 50 kV with 15% power efficiency and frequencies of a few GHz. TTU next considered the impact of material, such as nickel-zinc, yttrium iron garnet, magnesium-zinc, and

lithium ferrites, on performance. They demonstrated that varying the material's bias magnetic field provided active delay control and that the material's ferromagnetic resonance line width played a significant role in microwave generation. TTU next showed that one could effectively tune the output by controlling the bias voltage, which subsequently impacted the electrical properties of the NLTL due to its nonlinear nature, enabling the construction of a single, frequency-agile device capable of operating from 1.8 to 2.6 GHz with powers from 1 MW to 3 MW; however, higher voltages (on the order of 40 kV) resulted in corona discharge, limiting application at higher voltages. Thus, attaining higher powers required combining multiple NLTLs, which they demonstrated for arrays of either two or four NLTLs. The NLTL could then be incorporated into a solid-state HPM source to generate microwave pulses with a microwave frequency of 2.1 GHz with a pulse repetition frequency of 65 MHz. AFRL designed a spatially dispersive ferrite NLTL with axial bias that was frequency tunable from 0.95 to 1.45 GHz with instantaneous power levels of tens of MW and durations from 4 to 17 ns.

A Russian group from the Institute of High Current Electronics has also studied gyromagnetic RF sources using NLTLs. Their early work used saturated NiZn ferrites as an active nonlinear medium and found an optimum length of approximately 1 m for producing a 1000 pulse burst at 200 Hz repetition rate for a peak RF power of 260 MW with a central frequency of 1.2 GHz and of 0.25 GHz at -3 dB level and 0.4 GHz at -10 dB level. They have also demonstrated electronically controlled beam steering by connecting two NLTLs to one high voltage driver with each NLTL capable of producing RF pulses from 50-700 MW at frequencies from 0.5 to 1.7 GHz with 100 Hz repetition rate. Gyromagnetic NLTLs have also generated high power ns RF pulses with field strengths up to 40 kV/cm, durations from 4 to 25 ns, and frequency from 0.6 to 1.0 GHz to provide flexible output at laboratory scale for biological experiments. They have also subsequently extended their frequency output to 4 GHz with a peak voltage of 175 kV for 100 Hz repetition rates during one second. Their ferrite line in the NLTLs implements a continuous unit of NiZn rings of M200VNP type of a total length of 700 mm. At lower frequencies (~300 MHz), they have also used a gyromagnetic NLTL as a peak power amplifier of an input pulse. They applied a 500 kV pulse with a full-width-half-max duration of 7 ns to the NLTL to increase the pulse amplitude to 740 kV while reducing the pulse duration to ~2 ns. This increased the power from ~ 6 GW on the input to ~13 GW on the output at a 1 kHz pulse repetition rate in burst mode.

Another approach explored by the University of New Mexico entails developing a hybrid line consisting of both nonlinear capacitors and inductors. While this is a promising approach that could provide some ability for tunability, one must attain appropriate inductance and capacitance behavior to achieve a constant transmission line impedance.

2. Activities and Accomplishments

We have reviewed the relevant literature and drafted a summary of the current state of NLTL work, focusing on modeling and experiment for the three main NLTL topologies: nonlinear lumped element circuits (LEC), split ring resonators (SRRs), and coaxial/planar geometries with nonlinear dielectrics. The executive summary of the current draft undergoing revision follows.

Interest in NLTLs has greatly increased over the past decades because they can sharpen pulses to rise times below 100 ps and produce radio frequency (RF) oscillations from 100s MHz to low GHz once their permittivity and permeability have saturated, forming an electromagnetic shock wave. The development of solid state switching both in materials and structures has created a need for a high power RF source that can operate at fast duty cycles. The tunability of NLTLs has shown

promise as a high duty cycle RF source at various frequencies of interest. The three main topologies used to construct NLTLs are lumped element circuits consisting of nonlinear capacitors and/or inductors, split ring resonators (SRRs) with nonlinear gap capacitance, and planar and coaxial transmission lines composed of nonlinear dielectric materials.

Using LECs for NLTLs permits a more detailed examination of the physics involved in the transmission of electromagnetic waves. These NLTLs can be built using commercial off-the-shelf (COTS) components or novel nonlinear components. LECs permit the testing of mathematical circuit models and the development of methods to solve the resulting coupled nonlinear equations. These mathematical models were derived in the second half of the 20th century to separate the propagating wave into various arrays based on their magnitude. This separation elucidated how the traveling waves sharpen in rise time since a higher amplitude wave results in a higher permittivity, causing a lower impedance to the wave.

The resulting equations may be solved using the Runge-Kutta or Bulirsch-Stoer method. The Runge-Kutta method is more useful and efficient in solving the coupled differential equations and evaluating the wave propagation due to its simpler step calculations required. These results facilitated the optimization of NLTL design by constructing the shortest NLTL that will induce oscillations and produce RF power. Other methods for simplifying the nonlinear partial differential equations (PDEs) also provide a more efficient method for solving the wave propagation while incorporating nonlinear properties. The Korteweg-de Vries equation simplifies the nonlinear PDEs for hybrid NLTLs comprised of both nonlinear permittivity and nonlinear permeability to yield a solvable system of equations. These mathematical models have also been compared to simulations using different numerical solvers, including SPICE and COMSOL.

Experimental evaluation of LEC NLTLs comprised of COTS components to achieve peak power of 20 MW at a repetition rate of a few kHz at RF frequencies in the low GHz regime agree well with the mathematical models. Systems composed of nonlinear ceramic capacitors using a lead-manganese-niobate ceramic work very well when evaluating mathematical models and circuit simulations; however, the failure of a single component causes the whole device to fail, limiting system reliability to the weakest component.

Due to their inherent structure resonance, SRRs have been a viable option for adding a nonlinear capacitance that can be placed in various topologies in NLTL design. SRRs can also be combined in numerous geometries, ranging from coplanar to edge coupled. The small size of these structures greatly limits their output power; however, they generate very narrowband frequencies with a great deal of control through device design.

Various methods for modeling SRRs have assessed their resonant structure to determine appropriate nonlinear capacitance placement within the design. HFSS and CST Microwave Studios, which are commercial electromagnetic packages, have modeled these structures. The circuit model of an SRR can also be solved using finite integration method (FIM) and finite element method (FEM) to analyze how altering the geometries of the devices changes the output frequencies. The structures can be simulated individually or as inclusions in a bulk material once the material properties of the individual SRR have been established.

The experimental applications of SRRs has been made possible as manufacturing techniques have improved for constructing microscale and nanoscale devices. In addition to their implementation in NLTLs, SRRs have been used as waveguide filters and antennas to provide RF

output. Some studies have evaluated the feasibility of SRRs as high power microwave (HPM) devices and showed that they would fail if 1 W of RF power was applied to the structure. This would differ depending on the size of the structure. In low power NLTLs, controlling the nonlinear capacitance of a varactor can control the system's frequency output.

While using nonlinear materials in a NLTL seems obvious, designing, characterizing, and manufacturing these materials is nontrivial. The challenge of using nonlinear materials arises from understanding the physics of the nonlinearities and accurately predicting them to optimize system design. These nonlinear materials can also be a composite with a linear base material and nonlinear inclusions. Typical nonlinear materials include barium titanate (BT), barium strontium titanate (BST), and nickel zinc ferrites (NZF).

Theoretically, the nonlinear materials can be examined by using finite difference time domain (FDTD) to examine the wave propagation through the nonlinear materials. Ikezi, et al. demonstrated the feasibility of generating high-power microwave bursts by creating a soliton pulse train in nonlinear-dispersive system. They proposed the design of a modulated transmission line with a nonlinear dielectric and analyzed the nonlinear wave evolution and the requirements for the nonlinear dielectric necessary to create this pulse. While a model designed by Brown has also been used to evaluate NLTLs, some of the material constraints are not constrained by electrostatics, making it less reliable than the physics based model by Ikezi, et al. Another model developed by Crowne solves Kirchhoff's circuit laws using *Mathematica* to evaluate wave propagation.

Various NLTL topologies can be constructed using nonlinear ferroelectric capacitors or ZnO microvaristors. The dielectric properties of microvaristors placed in a rubber matrix can be controlled by varying the inclusion concentration. Dielectric mixing laws provide a means to predict the material properties of the materials with loadings below the percolation threshold, which corresponds to the concentration at which the composite electrically resembles the inclusion. The most commonly applied mixing rule is the Maxwell Garnett law, which generally agrees well with experiment. A high frequency mixing rule has also been developed for materials with inclusions and small structures, such as SRRs. The generalized effective medium theory, developed by MacLachlan's research group, provides a semi-empirical means to predict effective electromagnetic properties and has been applied at AC frequencies for conducting inclusions of various geometries.

NLTLs using nonlinear dielectrics has been studied experimentally for over thirty years to achieve pulse sharpening and RF generation depending on the input power and rise time. These materials may be incorporated into various topologies, primarily coaxial and planar geometries. These NLTLs have been used in conjunction with other components to increase power output through beam combining and adding slow wave structures. The output powers of just the lines have produced peak powers of hundreds of MW and rise times of less than 500 ps. They can operate at kHz repetition rates with output frequencies up to low GHz. The main issue with these NLTLs is that the RF output is only a few nanoseconds in duration. More recent studies are exploring methods to increase the RF envelope and power output while maintaining GHz frequencies.

a) Initial experimental results

Figure 2 shows preliminary dielectric measurements using an LCR meter to determine the relative permittivity of samples comprised of a host material of PDMS with various volume loadings of BST and/or NZF inclusions. The measurements were taken by applying metal

electrodes to the top and bottom of the sample using a silver paste adhesive to ensure good electrical contact. We measured the capacitance and calculated the relative permittivity using $\varepsilon_r = Cd/\varepsilon_0 A$, where C is the capacitance, ε_0 is the permittivity of free space, ε_r is the relative permittivity, A is the electrode cross sectional area, and d is the thickness of the material. We generally achieved good reproducibility although further studies on appropriate loading techniques are necessary to obtain consistent behavior with inclusion volume loading.

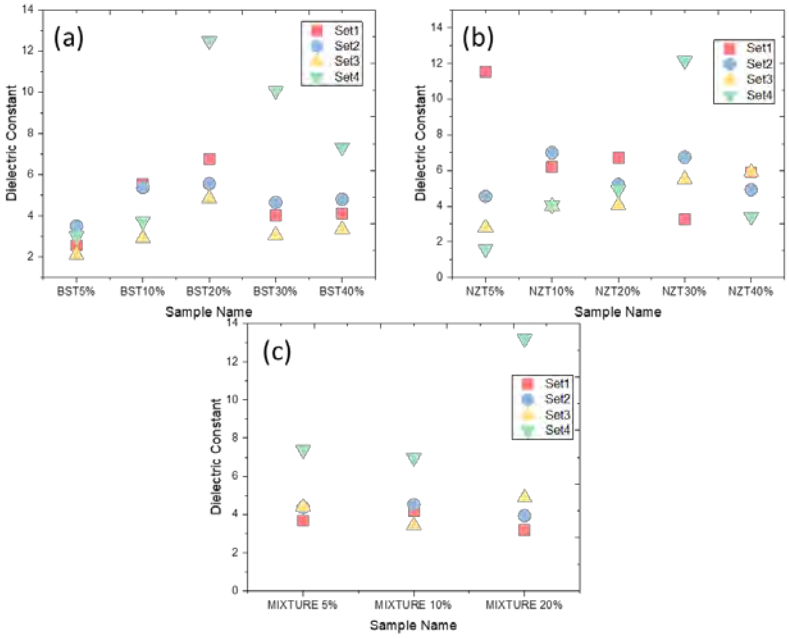

Fig. 2 Preliminary dielectric measurements of samples with varying volume fractions of (a) BST, (b) NZF, and (c) a mixture of both.

We used a CT scan to assess the homogeneity of the initial sample, which is critical for the validity of applying effective medium theories and controlling effective electromagnetic behavior. The images in Figure 3 demonstrate the homogeneity of the samples.

Figure 4 shows the dielectric measurement system purchased for this grant to perform baseline dielectric measurements of the composites. The system was placed on an anti-static mat to eliminate potential shock damage and the cables were secured to the mat using tape to prevent potential movement that would invalidate the calibration performed before each measurement.

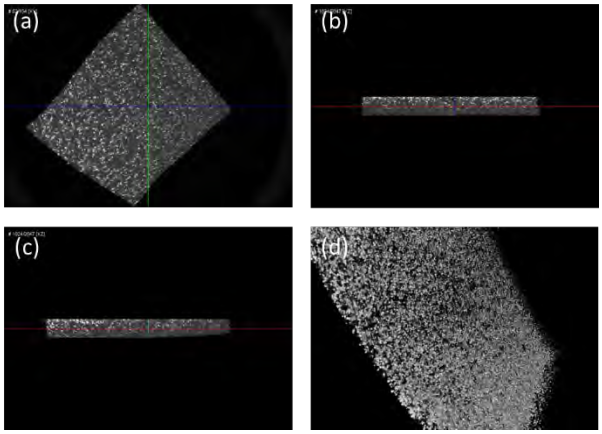

Fig. 3 CT scan of 10% NZT composite showing homogeneity (a) top view, (b) right side view, (c) left side view, and (d) 3 dimensional illustration.

Fig 4 Experimental test setup for dielectric measurements

Figure 5 shows proposed circuits for measuring the nonlinear permittivity and permeability of the composites. We are currently collaborating with Brad Hoff (AFRL) and Jack Chen (NSWCDD) to determine the suitability of these designs.

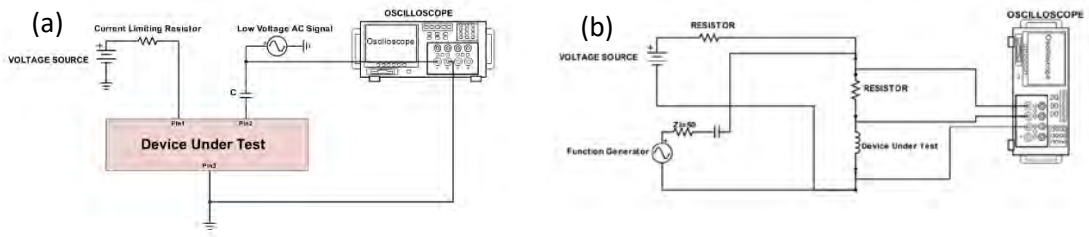

Fig 6 Proposed circuit designs for measuring nonlinear (a) permittivity and (b) permeability.

3. Findings and Conclusions

Preliminary results have shown that the dielectric properties of the sample vary with changes in the volume fraction of the sample. Future studies will assess this with more sensitive dielectric measurements and at higher frequency ranges.

4. Plans and Upcoming Events

We will be reevaluating the dielectric properties of the samples with different volume loadings using more precise measurements as a function of frequency. We will then apply various effective medium theories, starting with Maxwell-Garnett, to predict composite behavior. This will provide a means to predict composite behavior to guide future designs to optimize NLTL designs. We plan to use this data to evaluate various mixing models, starting with the Maxwell Garnett mixing model, and adjusting the parameters to achieve proper fits to the measured data. We will continue to work with Brad Hoff and Jack Chen to finalize designs of nonlinear dielectric testing circuits and constructing these test circuits. Also, we will start utilizing CST Microwave Studios with the help of Walter Sessions from GTRI.

5. Transitions and Impacts

Not Applicable

6. Collaborations

Brad Hoff, Air Force Research Laboratory
Jack Chen, Naval Surface Warfare Center Dahlgren Division
Eagle Harbor Technologies
Ryan McBride, University of Michigan

7. Personnel

Principal Investigator: Allen L. Garner, 0.5 person-month, National Academy Member (N).
Co-PI: Wenzhuo Wu, <0.5 person-month, National Academy Member (N).
Teams Members:
Amanda M. Loveless, graduate student, 1.5 person-months, National Academy Member (N).
Russell S. Brayfield, graduate student, 0.2 person-months, National Academy Member (N).
Adam M. Darr, graduate student, 0.2 person-months, National Academy Member (N).
Andrew J. Fairbanks, graduate student, 1.7 person-months, National Academy Member (N).
Xiaojun Zhu, graduate student, 1.3 person-months, National Academy Member (N).
Shengjie Gao, graduate student, 1.5 person-months, National Academy Member (N).
Business Contact: Jill Clauson
Subs: GTRI: <1 person-month.

8. Students

Graduate Students: 6

9. Technology Transfer

We are working with Jack Chen from NSWCDD concerning the incorporation of NLTLs into high power microwave systems and Brad Hoff from AFRL concerning NLTL physics and

characterization of the electromagnetic properties. We will continue to work with them as we finalize the review and begin measuring nonlinear electromagnetic properties.

10. Products, Publications, Patents, License Agreements, etc.

Not Applicable

11. Point of Contact in Navy

Jack Chen, NSWCDD, yeongjer@navy.mil, 07SEP2018
Brad Hoff, AFRL, brad.hoff@us.af.mil, 07SEP2018.

12. Acknowledgement/Disclaimer

This work was sponsored by the Office of Naval Research (ONR), under grant (or contract) number N00014-18-1-2341. The views and conclusions contained herein are those of the authors only and should not be interpreted as representing those of ONR, the U.S. Navy or the U.S. Government.

Nanoscale Effects on Gas Breakdown and Electron Emission

Grant No. N000014-17-1-2702

Period of Performance: October, 1, 2017 to September 30, 2018

Prepared by:

Dr. Allen L. Garner, Principal Investigator
Assistant Professor, School of Nuclear Engineering
Purdue University
400 Central Drive
West Lafayette, IN 47907-2017
Tel: (765) 494-0618
Email: algarner@purdue.edu

This work was sponsored by the Office of Naval Research (ONR), under grant number N000014-17-1-2702. The views and conclusions contained herein are those of the authors only and should not be interpreted as representing those of ONR, the U.S. Navy or the U.S. Government.

Grant or Contract Number: N000014-17-1-2702
Date Prepared: 21NOV18
Project Title: Nanoscale Effects on Gas Breakdown and Electron Emission
Annual Summary Report: FY2018
Principal Investigator: Allen L. Garner, 765-494-0618, algarner@purdue.edu
Purdue University

Section I: Project Summary

1. Overview of Project

Abstract: Accurately predicting gas breakdown voltage is becoming increasingly important as the trend toward electronics miniaturization increases. Microelectromechanical systems (MEMS), such as microactuators, pressure sensors, and high-frequency circuits, require microscale gaps and high operating voltages. Accurate breakdown voltage predictions for these systems will prevent discharges that could damage or destroy the device. Conversely, microplasmas use microdischarges for various applications, such as electric micropropulsion and environmental mitigation. From a directed energy perspective, present research trends focus on developing micro- and nano-vacuum electronics for providing increased power densities and frequency for directed energy applications, including radar platforms for shipboard and aircraft systems. In particular, the Air Force and Navy have ongoing efforts exploring the field emission characteristics of arrays of carbon nanotubes, particularly exploring the implications of distance between emitters and variation of work function on electric field characteristics.

Objective: This effort will elucidate the impact of nanoscale effects on gas breakdown for microscale and smaller gaps by combining experiment, numerical analysis, and theoretical analysis. Specifically, it will assess the impact of surface irregularities, which alter the work function and field enhancement factors that drive field emission. This research fills a gap in understanding the influence on surface structure for electron emission and breakdown, which have significant implications for efficiency and equipment durability.

Introduction: Accurately predicting gas breakdown voltage is becoming increasingly important as the trend toward electronics miniaturization increases. From a directed energy perspective, which is critical for Navy and Air Force applications, present research trends focus on developing micro- and nano-vacuum electronics for providing increased power densities and frequency for shipboard and aircraft radar platforms. In particular, the Air Force and Navy have ongoing efforts exploring the field emission characteristics of arrays of carbon nanotubes, particularly exploring the implications of distance between emitters and variation of work function on electric field characteristics. Directed energy systems using laser or intense electromagnetic systems, including pulsed power and high power microwave technologies, are constantly striving to achieve very high power densities using high frequency and more compact systems. As one goes to these smaller systems, higher electric fields arise and issues concerning breakdown, field emission, and space-charge limited flows increase significantly.

Background: Elucidating the impact of nanoscale effects on gas breakdown for microscale and smaller gaps requires combining experiment, numerical analysis, and theoretical analysis. Initial efforts involve the following:

- Assessing and applying analytic models relating field emission and space-charge limited flow, both at vacuum and general pressure, will elucidate the potential impact of space charge on field enhancement to determine the point at which pressure no longer contributes.
- Performing experiments and developing analytic models will determine the impact of surface roughness and various flaws on surface on the work function and field enhancement, which measures the energy necessary to remove an electron from the cathode and plays a crucial role in the determining the field emission current.
- Performing molecular dynamics simulations to determine the implications of surface roughness on both electron emission and space charge effects to provide data to put into continuum models of gas breakdown.

These results will then be applied to understand experimental and theoretical analyses of gas breakdown for microscale gaps and smaller. Specific next steps will include:
- Further coupling the existing electron emission and breakdown models to the one-dimensional Schrödinger equation to develop a universal breakdown model from the classical Paschen law to quantum scale for multiple gases.
- Analytic and numerical models developed by the Principal Investigator's group will be modified to incorporate the effects of surface roughness and space charge on field enhancement and work function and compared to the parametric experiments.
- Experimental measurements will be performed for gaps from microscale to approximately 100 nm from vacuum to atmospheric pressure to provide a full parametric study of the mechanisms responsible for breakdown across a wide range of parameters.

This effort will ultimately pave the way for future work unifying all relevant modes of breakdown and electron emission across gap pressure and distance for numerous applications relevant to the Department of Defense, including directed energy, field emission, and micropropulsion.

2. Activities and Accomplishments

While our previous studies derived closed form solutions unifying field emission and Townsend-driven breakdown mechanisms that agreed with experiment and simulation at microscale, they were only valid at atmospheric pressure. In Year 1, we generalized this model to account for any pressure, gas, and gap distance (above the mean free path of the electron to avoid quantum considerations and below Meek's criterion to avoid streamer effects) to derive a new, universal (true for any gas) model that is valid at classical length scales and unifies Paschen's law (PL) and the coupled field emission-Townsend breakdown model.

TABLE 1**.** Calculated scaling parameters for argon, nitrogen, neon, and xenon.

Gas	p_* [Torr]	L [m]	j_0 [A/m^2]	ϕ_* [eV]	E_* [V/m]	τ_* [K]
Argon	3.44×10^8	2.42×10^{-12}	2.24×10^{18}	96.81	6.20×10^{12}	8476
Nitrogen	1.81×10^8	4.60×10^{-12}	2.24×10^{18}	96.81	6.20×10^{12}	11288
Neon	6.20×10^8	4.03×10^{-12}	2.24×10^{18}	96.81	6.20×10^{12}	21409
Xenon	1.77×10^8	2.17×10^{-12}	2.24×10^{18}	96.81	6.20×10^{12}	11539

We derived the exact equation for dimensionless breakdown field, $\bar{E}$, obtained from this analysis by

$$\frac{\exp\left[\bar{\phi}^{3/2}/(\beta\bar{E})\right]}{\beta\bar{\phi}^{1/2}\exp(\bar{\phi}^{-1/2})}\sqrt{\frac{\bar{\tau}\bar{E}}{\bar{p}\bar{d}^2}}\frac{\left\{1-\gamma_{SE}\left[\exp\left(\bar{\alpha}\bar{d}\right)-1\right]\right\}}{\left[\exp\left(\bar{\alpha}\bar{d}\right)-1\right]}=\frac{\exp(x_o)(1+2\bar{E}x_o)}{x_o}, \tag{1}$$

which depends on the dimensionless work function, $\bar{\phi}$, field enhancement factor, □, dimensionless temperature, $\bar{\tau}$, dimensionless pressure, $\bar{p}$, secondary emission coefficient, γ_{SE}, dimensionless ionization coefficient, $\bar{\alpha}$, dimensionless gap distance, $\bar{d}$, and $x_0=\left[(1+8\bar{E})^{1/2}-1\right]/(4\bar{E})$. Table 1 shows the calculated scaling parameters necessary for converting dimensionless units back to dimensional using $\phi=\bar{\phi}\phi_*$, $p=\bar{p}p_*$, $d=\bar{d}L$, $\alpha=\bar{\alpha}/L$, and $\tau=\bar{\tau}\tau_*$.

Performing a matched asymptotic analysis of (1) yields

$$\bar{V}=\bar{d}\left[\frac{-\Delta_1-\sqrt{\Delta_1^2-2\Lambda_1\left(\bar{\phi}^{3/2}/\beta+\gamma_{SE}\bar{p}^2\bar{d}+\bar{p}\right)}}{\Lambda_1}\right], \tag{2}$$

for $\bar{\alpha}\bar{d}\ll 1$, where

$$\Delta_1=\frac{\ln\left[\bar{\tau}\bar{p}^{-1}\bar{d}^{-2}\right]}{2}-\ln\left[\beta\bar{\phi}^{1/2}\right]-\bar{\phi}^{-1/2}-\frac{\ln[\Lambda_1]}{2}-\ln\left[\bar{p}\bar{d}\right]-\gamma_{SE}\bar{p}\bar{d}-\frac{3}{2} \tag{3}$$

and $\Lambda_1=4\times10^4$, and

$$\bar{V}=\bar{d}\left[\frac{-\Delta_2-\sqrt{\Delta_2^2-2\Lambda_2\,\bar{\phi}^{3/2}/\beta}}{\Lambda_2}\right], \tag{4}$$

for $\bar{\alpha}\bar{d}\gg 1$ where

$$\begin{aligned}\Delta_2=\frac{\ln\left[\bar{\tau}\bar{p}^{-1}\bar{d}^{-2}\right]}{2}-\ln\left[\beta\bar{\phi}^{1/2}\right]-\bar{\phi}^{-1/2}-\frac{\ln[\Lambda_2]}{2}+\ln\left\{1-\gamma_{SE}\left[\exp\left(\frac{\bar{p}\bar{d}}{\exp(1)}\right)\right]\right\}\\-\ln\left[\exp\left(\frac{\bar{p}\bar{d}}{\exp(1)}\right)-1\right]-\frac{3}{2},\end{aligned} \tag{5}$$

and $\Lambda_2=1\times10^5$. Finally, rearranging (1) as

$$1-\gamma_{SE}\left[\exp\left(\bar{\alpha}\bar{d}\right)-1\right]=\frac{\beta\bar{\phi}\exp\left(\bar{\phi}^{-1/2}\right)}{\exp(\bar{\phi}^{3/2}/\beta\bar{E})}\sqrt{\frac{\bar{p}\bar{d}^2}{\bar{T}\bar{E}}}\frac{\exp(x_0)\,(1+2\bar{E}x_o)\left[\exp\left(\bar{\alpha}\bar{d}\right)-1\right]}{x_0} \tag{6}$$

highlights the term that drives the breakdown behavior back to the classical PL. Once the transition to Paschen's law occurs, the field emission term—shown as the first quotient on the right-hand side (RHS) of (6)—drives the RHS to ≈ 0. Substituting $\bar{\alpha}=\bar{p}\exp(-\bar{p}/\bar{E})$ and solving for $\bar{V}$ yields

$$\bar{V}=\frac{\bar{p}\bar{d}}{\ln\left[\bar{p}\bar{d}\right]-\ln[\ln(1+\gamma_{SE}^{-1})]}, \tag{7}$$

which is a dimensionless, universal form of PL (UPL). Thus, we can recover the classical PL from the coupled field emission-Townsend breakdown of (1) under appropriate conditions and, therefore, link field emission and Paschen's law by a series of analytic expressions across classical length scales. Fig. 1 shows the results of the numerical equation, the analytic limiting equations, and the UPL law for different pressure and gap distances.

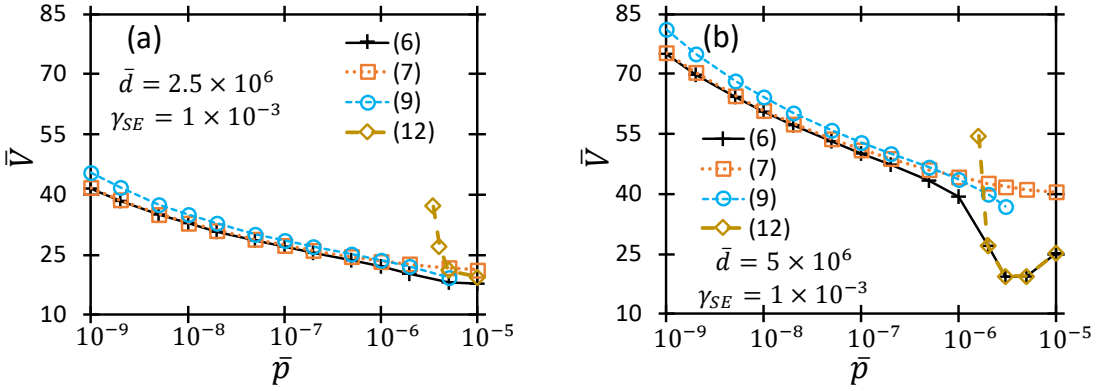

FIG. 1. Comparison of dimensionless breakdown voltage, $\bar{V}$, as a function of dimensionless pressure, $\bar{p}$, determined from numerically solving (6), and calculating (7), (9), and (12) for (a) $\bar{d} = 2.5 \times 10^6$ and $\gamma_{SE} = 0.001$, (b) $\bar{d} = 5 \times 10^6$ and $\gamma_{SE} = 0.001$ (from Ref. [3]).

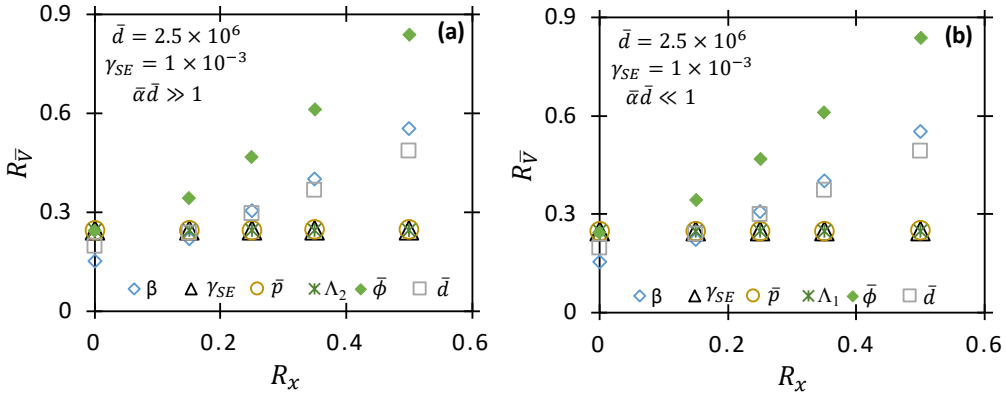

FIG. 2. Relative error in calculated voltage, $R_{\bar{V}}$, as a function of the relative error in □, □$_{SE}$, $\bar{p}$, □, $\bar{\phi}$ □□and $\bar{d}$ for (a) $\bar{\alpha}\bar{d} \gg 1$ and (b) $\bar{\alpha}\bar{d} \ll 1$ with $\bar{p}$ =10^{-6} for $\bar{\alpha}\bar{d} \gg 1$ and $\bar{p}$ =10^{-7} for $\bar{\alpha}\bar{d} \ll 1$, using $\beta = 55$, $\bar{\phi} = 0.0532$, and $\bar{T} = 0.0354$. Of these parameters, predicted $\bar{V}$ is most sensitive to $\bar{\phi}$, □□□$\bar{d}$ and least sensitive to □$_{SE}$, $\bar{p}$, and □ for both large and small $\bar{\alpha}\bar{d}$.

While numerical and analytic models can demonstrate this transition, a quantitative understanding of the relative importance of each parameter remains unclear. Starting from the closed form solutions in (2) through (5), we applied the concept of error propagation from ionizing radiation measurements to determine the relative impact of each factor on the predicted breakdown voltage. Considering $\bar{V}(\bar{p}, \bar{d}, \beta, \bar{\phi}, \gamma_{SE}, \Lambda_1, \Lambda_2, \text{and } \bar{T})$ with the each variable and its standard deviation independent, the standard deviation of $\bar{V}$, $\sigma_{\bar{V}}$, is

$$\sigma_{\bar{V}}^2 = \sum_{n=1}^{8} \left[\left(\frac{\partial \bar{V}}{\partial x_n} \right) \sigma_{x_n} \right]^2 \tag{8}$$

where x_n represents the variables upon which $\bar{V}$ depends and σ_{x_n} is the standard deviation of each variable. It is often more convenient to assess the relative error, $R_{\bar{V}} = \sigma_{\bar{V}}/\bar{V}$. Using typical values, Fig. 2 shows that the electrode work function has the largest relative effect on the predicted breakdown voltages with a deviation of 50% in work function resulting in an uncertainty in the calculated breakdown voltage of ~84% for both $\bar{\alpha}\bar{d} \gg 1$ and $\bar{\alpha}\bar{d} \ll 1$. This quantifies the significance that nonuniformities in material surfaces and changes in surface structure during multiple electric field applications can have on predicting the breakdown voltage for small gaps, motivating better electrode characterization both initially and during repeated operation.

FURTHER DEVELOPMENT OF FIELD EMISSION DRIVEN BREAKDOWN

Additional assessment of data collected from our collaborator Dr. Guodong Meng yielded a further simplified breakdown equation in the field emission regime based on (1), given by

$$\bar{V} \approx \left(\frac{\bar{\phi}^{3/2}}{\beta \Delta_1} \right) \bar{d}, \tag{9}$$

where Δ_1 is given by (3). This indicates that breakdown voltage varies linearly with gap distance with the slope a function of field emission quantities. Fig. 3 shows the matched asymptotic results from (2) (presented as (1) in the figure), analytic results from (9) (presented as (8) in the figure), and the UPL from (7) (presented as (9) in the figure), along with the corresponding β values and experimental results from Dr. Meng. Note that β varies linearly in the regime where field emission drives breakdown ($d \lesssim 15\mu$m) and is constant upon transition to Townsend avalanche and PL.

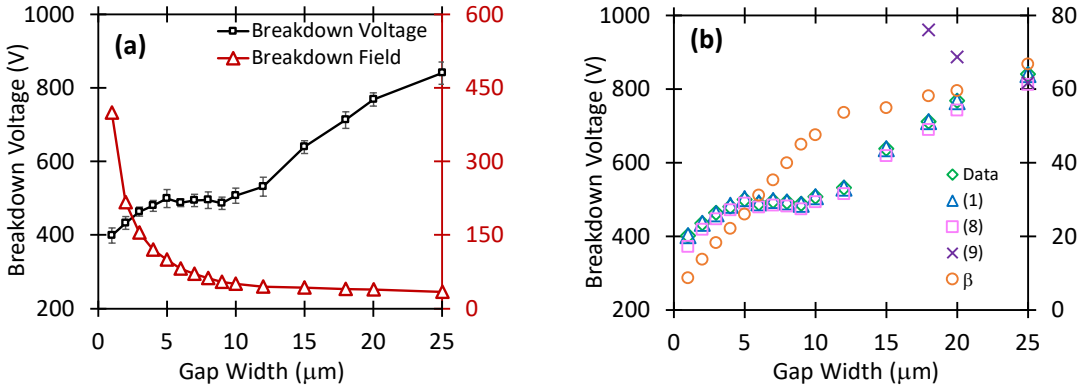

FIG. 3 (a) Measured breakdown voltage and electric field as a function of gap width. (b) Comparison of measured breakdown voltage, matched asymptotic prediction of breakdown voltage using (2) {1 in the figure}, simplified equation for breakdown voltage using (9) {(8) in the figure}, and UPL using (7) {(9) in the Figure} with the fitted field enhancement factor, □, used in (1) and (8) as a function of gap width.

We have recently extended our assessment with Dr. Meng to subatmospheric pressure (3 kPa, 50 kPa, and 101 kPa) breakdown. We derived a similar equation to (8) in the □d >> 1 limit based on this experimental data, leading to □$_2$ replacing □$_1$, and fit the exact solution of (1) to the experimental data in Fig. 5a. The analytic equation above agrees with the exact numerical solution

within 4%. Fig. 5b shows that β varied linearly with d in the field emission regime before becoming constant at gap distances corresponding to the transition to Townsend avalanche and the UPL. In this case, the 50 kPa data intersect with the UPL to the *left* of the classical UPL minimum while the 101 kPa data intersect with the UPL almost exactly at the minimum. The lower pressure of 1 kPa does not intersect with the UPL under the conditions currently examined as Dr. Meng's pulse generator could not achieve sufficient voltage. These results suggest that pressure and gas (since we are considering a universal curve that is independent of material) may contribute to what appears to be an extended plateau in breakdown voltage. An alternative explanation for this extended plateau could involve the combined PL solutions from two sharp tips; however, our experimental results below suggest that this may not be the complete solution.

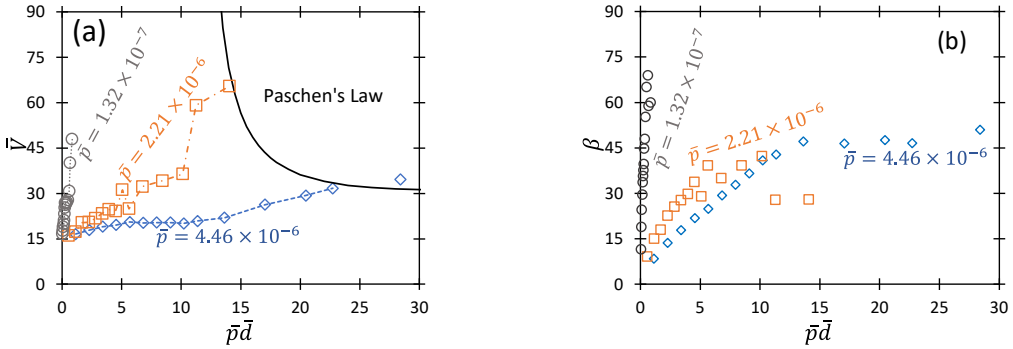

FIG. 4: (a) Dimensionless breakdown voltage, $\bar{V}$, as a function of the product of dimensionless pressure and gap distance, $\bar{p}\bar{d}$, for various pressures compared to results from the UPL determined from (7) with $\gamma_{SE} = 10^{-5}$. The symbols represent experimental data points and the dashed lines represent the numerical solution of (1), using field enhancement factor β as a fitting parameter. (b) Field enhancement factor, β, as a function of the product of the dimensionless pressure and gap distance, $\bar{p}\bar{d}$, obtained by fitting the experimental data.

EXPERIMENTAL AND THEORETICAL ASSESSMENT OF SURFACE ROUGHNESS ON GAS BREAKDOWN

Table 2 Average surface features before tests and depth of the observed ablative feature at the breakdown voltage for the anodes polished at each grit where measurable ablation occurred.

Grit	Number of Samples (initial/ablated)	Initial Surface Height (μm)	Average Crater Depth (μm)
400	9/6	1.47±1.08	22.0±14.6
800	9/5	0.26±0.18	7.3±2.7
1200	9/4	0.24±0.23	6.5±3.3

The experimental setup consisted of tungsten dissection needles (Roboz Surgical Instrument Co., RS-6065) mounted into polyethylene to ensure electrical isolation. The copper plates were mounted to polyethylene blocks mounted to a micromanipulator and moved in increments of 1μm. We used atomic force microscopy (AFM) to quantify the change in surface roughness by measuring the average height of surface features before and after the breakdown events. We used optical microscopy to measure crater depth for larger, post-breakdown craters. Table 2 summarizes the average values for various initial surface roughnesses.

Fig. 5 shows the impact of the cathode surface roughness (grit), gap distance, and number of breakdown events on breakdown voltage without error bars, since they cluttered the plot. A statistical analysis demonstrated no statistical significance between measured breakdown voltage and the various grits and gap distances. Thus, gap distance did *not* influence breakdown voltage, which seems counterintuitive.

We hypothesized that this arose because the breakdown events at the smaller gap distances are driven by field emission, which leads to concentration of breakdown voltage at the relatively sharp tips in the surface roughness on the cathodes. These higher electric fields are more likely to create more extensive cathode damage, resulting in larger craters of depth □ at smaller gap distances. When combined with the initial gap distance, this results in an effective gap distance d_{eff} = d+ □□that are equivalent to the gap separation distance at larger gaps. In fact, Fig. 6 shows that the measured breakdown voltage, extrapolated β, and calculated □d all behave similar as functions of d_{eff} as they would if plotted as a functions of d for a smooth electrode. Thus, while cathode erosion will definitely impact β by destroying sharp tips and ϕ by altering the cathode structure, d_{eff} appears to be the major factor impacted. Future studies will explore the impact of crater formation on ϕ and the impact of anode surface roughness.

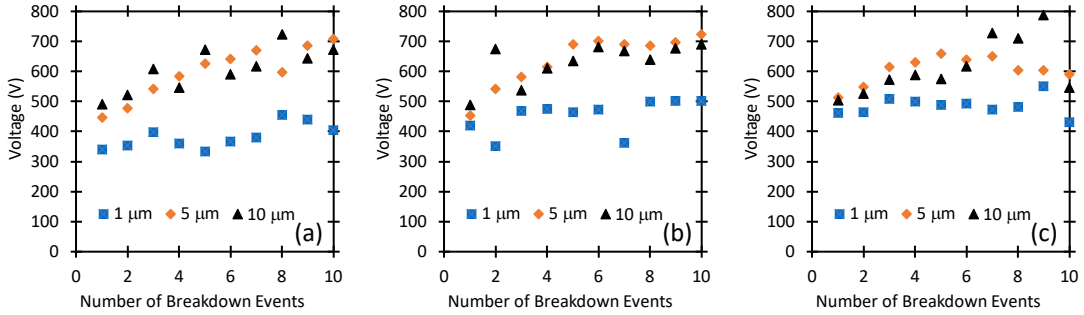

FIG. 5. Average breakdown voltage as a function of number of breakdown events for (a) 400 grit (b) 800 grit and (c) 1200 grit with measurements of three samples each.

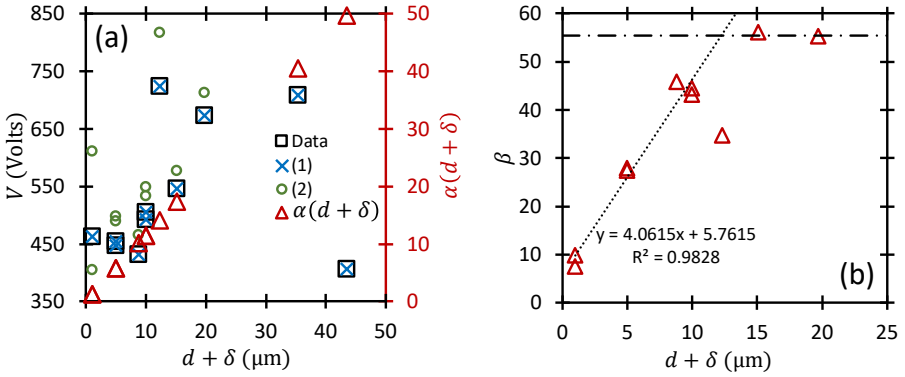

FIG. 6. (a) Average breakdown voltage, V, as a function of effective gap distance, $d_{eff} = d + \delta$, where d is the anode-cathode gap and δ is the breakdown induced crater depth, compared to numerical results from (1) and analytic results from (2). The product of the ionization coefficient and effective gap distance, $\alpha(d + \delta)$, is displayed on the secondary vertical axis as a function of effective gap distance, $(d + \delta)$. The largest two gap distance points exceed Meek's criterion for streamer formation. (b) Field enhancement factor, β, as a function of effective gap distance,

$(d + \delta)$, showing that β is approximately linear until the larger gap distances corresponding to the transition to Townsend avalanche, where it becomes constant.

3. Findings and Conclusions

These efforts have provided important insight into the mechanisms behind gas breakdown, driven by electron emission, at microscale. Of particular note is our collaboration with Dr. Meng, where our theory demonstrated the experimental transitions observed using his novel in-situ optical diagnostic method. This work was selected as a featured article in *Physics of Plasmas* (https://publishing.aip.org/publishing/journal-highlights/researchers-unravel-path-electrical-discharges-scales-are-phenomenally). Our recent results assessing surface roughness indicate that field emission at smaller gap distances and higher surface roughness can increase the effective gap distance and cause a transition in breakdown regime for a given gap distance. This has implications for high voltage devices where multiple breakdowns may damage the cathode. Future work will explore the impact of multiple breakdown events on □ or electrode shape on □.

4. Plans and Upcoming Events

Upcoming significant events:

1) Completion of theory connecting quantum breakdown to Paschen's law.
2) Experimental assessment of sub-microscale gaps to characterize field enhancement.
3) Assessment of anode surface roughness to compare to cathode surface roughness.
4) Experimental assessment of relative changes in work function following breakdown.

Future transitions:

1) Continue discussions with AFRL – particularly concerning sub-microscale breakdown experiments as this expands to sub-atmospheric pressure.
2) Work with NRL to transition breakdown theory (Kevin Jensen) and surface roughness effects (Ray Allen) for larger devices.
3) Continue discussions with NSWCDD (Matt McQuage and Jack Chen) concerning relevant 6.2 applications of the studied phenomena.

5. Transitions and Impacts

None at present, although future goals for Year 2 are outlined in Section 4.

6. Collaborations

Guodong Meng, international collaborator, N/A, National Academy Member (N), China
Ágúst Valfells, international collaborator N/A, National Academy Member (N), Iceland,
Wenzhuo Wu, Purdue University, N/A, National Academy Member (N), USA

7. Personnel

Principal Investigator: Allen L. Garner, 1 person-month, National Academy Member (N).
Teams Members:
Amanda M. Loveless, graduate student, 3 person-months, National Academy Member (N).
Russell S. Brayfield, graduate student, 4.5 person-months, National Academy Member (N).
Andrew J. Fairbanks, graduate student, 3.5 person-months, National Academy Member (N).

Business Contact: Jill Clauson
Subs: None

8. Students

4 graduate students (1 graduate student unfunded)/4 undergraduate students assisting (research for credit or visiting students) during reporting period

9. Technology Transfer

None.

10. Products, Publications, Patents, License Agreements, etc.

Publications resulting from this project:
Archival Publications:

1. A. M. Loveless and A. L. Garner, "A Universal Theory for Gas Breakdown from Microscale to the Classical Paschen Law," *Physics of Plasmas*, **24**, 113522 (2017). Peer-reviewed, Distribution A, Federal Funding Acknowledged. https://doi.org/10.1063/1.5004654

2. G. Meng, X. Gao, A. M. Loveless, C. Dong, D. Zhang, K. Wang B. Zhu, Y. Chen, and A. L. Garner, "Demonstration of Field Emission Driven Microscale Gas Breakdown for Pulsed Voltages using In-situ Optical Imaging," *Physics of Plasmas* **25**, 082116 (2018). (Selected for AIP Press Release: https://publishing.aip.org/publishing/journal-highlights/researchers-unravel-path-electrical-discharges-scales-are-phenomenally) Peer-reviewed, Distribution A, Federal Funding Acknowledged. https://doi.org/10.1063/1.5046335

3. S. Dyanko, A. M. Loveless, and A. L. Garner, "Sensitivity of Modeled Microscale Gas Breakdown Voltage due to Parametric Variation," *Physics of Plasmas* **25**, 103505 (2018). Peer-reviewed, Distribution A, Federal Funding Acknowledged. https://doi.org/10.1063/1.5042270

4. A. M. Darr, A. M. Loveless, and A. L. Garner, "Unification of field emission and space charge limited emission with collisions," *Applied Physics Letters*, Under Review, 12 October 2018.

5. G. Meng, Q. Ying, A. M. Loveless, F. Wu, K. Wang, Y. Fu, A. L. Garner, and Y. Cheng "Pulsed Gas Breakdown Dynamics in Microgaps," *Applied Physics Letters*, Under Review 01 November 2018.

6. R. S. Brayfield II, A. J. Fairbanks, A. M. Loveless, S. Gao, A. Dhanabal, W. Li, C. Darr, W. Wu, and A. L. Garner, "The Impact of Cathode Surface Roughness and Multiple Breakdown Events on Microscale Gas Breakdown at Atmospheric Pressure," *Journal of Applied Physics*, Under Preparation.

7. A. M. Loveless, G. Meng, Q. Ying, F. Wu, K. Wang, Y. Cheng, and A. L. Garner, "The Transition to Paschen's Law for Microscale Gas Breakdown at Subatmospheric Pressure," *Applied Physics Letters*, Under Preparation.

Invited Conference Oral Presentations

1. A. L. Garner, A. M. Loveless, R. S. Brayfield II, A. J. Fairbanks, S. D. Dyanko, S. Gao, W. Wu, R. S. Bean, and G. Meng, "Gas Breakdown at Microscale and Smaller Gaps: Theoretical Unification of Mechanisms and Experimental Assessment of Surface Roughness," iPlasmaNanoIX, New Buffalo, MI, 27 August 2018.

Conference Oral Presentation Abstracts

1. A. M. Loveless, A. M. Darr, S. D. Dyanko, and A. L. Garner, "Transition from Microscale to Nanoscale Breakdown Dynamics," 2018 IEEE International Conference on Plasma Sciences, O3A-2, 26 June 2018, Denver, CO USA.

2. A. L. Garner, R. S. Brayfield II, A. J. Fairbanks, A. M. Loveless, S. Gao, R. S. Bean, Y. Xuan, and W. Wu, "Microscale Gas Breakdown and Implications to Electron Emission," 20th Annual Directed Energy Science & Technology Symposium, High Power Microwave (HPM) Technologies, 01 March 2018, Oxnard, CA, USA.

3. A. M. Loveless, A. M. Darr, S. D. Dynako, and A. L. Garner, "Gas Breakdown Dynamics: From Microscale to Nanoscale," 20th Annual Directed Energy Science & Technology Symposium, Education Workshop I, 27 February 2018, Oxnard, CA, USA.

4. A. Loveless, A. Darr, and A. Garner, "Gas Breakdown: Across Length Scales and Frequency," Bull. Am. Phys. Soc. Vol. 62, No. 10, ET2.00002 (2017).

Conference Poster Presentation Abstracts

1. A. L. Garner, A. M. Darr, and A. M. Loveless, "Incorporating Collisions into the Transition from Field Emission to Space Charge Limited Flow," 2018 IEEE International Conference on Plasma Sciences, P2A-1346-1, 27 June 2018, Denver, CO USA.

2. R. Brayfield II, A. Fairbanks, A. Loveless, S. Gao, R. Bean, Y. Xuan, W. Wu, and A. Garner, "The Impact of Electrode Surface Roughness on Field Emission Driven Breakdown for Microscale Gaps," 04 June 2018, Jackson Lake Lodge, WY, USA, Poster 1P02 (2018).

Invited Colloquia and Seminars:

1. A. L. Garner, "Unification of Breakdown Theories across Gap and Pressure," Army Research Laboratory, Aberdeen, MD, 12 July 2018.

2. A. L. Garner, "The Influence of Gap Size and Electrode Surface on Gas Breakdown and Electron Emission," Naval Surface Warfare Center Dahlgren Division, Dahlgren, VA, 11 July 2018.

3. A. M. Loveless, "Unification of gas breakdown laws across frequency and gap distance," Naval Research Laboratory, 10 July 2018.

4. A. L. Garner, "The Influence of Gap Size and Electrode Surface on Gas Breakdown and Electron Emission," Varex Imaging, Salt Lake City, UT, 07 June 2018.

5. A. L. Garner, "Gas Breakdown and Electron Emission for Microscale and Smaller Gaps," Naval Surface Warfare Center Crane, Crane, IN, 03 May 2018.

11. Point of Contact in Navy

Kevin Jensen, NRL, 19SEP2018; Joe Schumer, NRL, 10JUL2018; Tom Mehlhorn, NRL, 10JUL2018; Jack Chen, NSWCDD, 10JUL2018; Wilkin Tang, AFRL, 07SEP2018; Don Schiffler, AFRL, 05JUN2018; Alex Sheets, AFRL, 15JUN2018.

12. Acknowledgement/Disclaimer

This work was sponsored by the Office of Naval Research (ONR), under grant number N000014-17-1-2702. The views and conclusions contained herein are those of the authors only and should not be interpreted as representing those of ONR, the U.S. Navy or the U.S. Government.

Compact High-Power Microwave Oscillators

Grant No. N62909-18-1-2122– GRANT12538355, N00014-18-S-B001

Period of Performance: June 15, 2018 to September 30, 2018

Prepared by:

Dr. Alan Phelps, Principal Investigator
Physics Department
University of Strathclyde
John Anderson Building
107 Rottenrow East
Glasgow, Scotland, UK G4 0NG
Tel: +44 141 548 3166
Email: a.d.r.phelps@strath.ac.uk

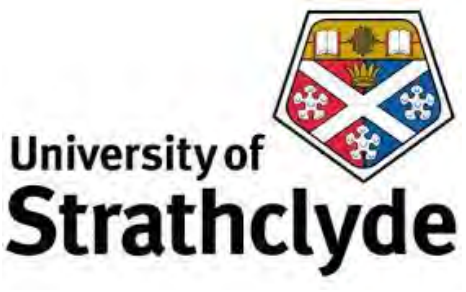

This work was sponsored by the Office of Naval Research (ONR), under grant number N00014 - 18-S-B001. The views and conclusions contained herein are those of the authors only and should not be interpreted as representing those of ONR, the U.S. Navy or the U.S. Government.

Grant or Contract Number: N62909-18-1-2122– GRANT12538355, N00014-18-S-B001
Date Prepared: 30th November 2018
Project Title: Compact High-Power Microwave Oscillators
Annual Summary Report: ONR HPM 2018 Program – End of Year report
Principal Investigator: Alan Phelps, +44141 548 3166, a.d.r.phelps@strath.ac.uk
University of Strathclyde, Scotland, UK

Section I: Project Summary

1. Overview of Project

Abstract:
This report details work carried out between 15 June and 30 September 2018, at the University of Strathclyde, Scotland, UK, developing a novel high-power X-band ($8-12\,GHz$) microwave source. Nominally it is a variant of the Backward-Wave Oscillator, designed to propagate its electron beam with no externally applied magnetic insulation. This greatly reduces the energy requirements, physical size, and weight of the resultant device. Current numerical modeling of the source indicates output powers of $200-300\,MW$ should be obtainable for a source driven by a mildly-relativistic $500\,kV, \sim 4.5\,kA$ electron beam, corresponding to an electronic efficiency of $\sim 13\%$. At this stage in development approximate dimensions for the source (excluding driving supply but including launch antenna and required shielding) are expected to be on the order of $2-3$ feet in length and $1-1.5$ feet in diameter.

Objective:
Develop an experimental prototype of a high-power, frequency-stable, microwave oscillator, operating in the X-band that does not required an externally applied magnetic confinement system.

Introduction:
The University of Strathclyde (UoS) has been under contract from June 15 – September 30 2018, of the current FY2018 reporting year, tasked with the development of an X-band (defined between $8-12\,GHz$) high-power Self-Insulating variant of the Backward-Wave Oscillator (SIBWO). The SIBWO offers the potential to significantly reduce the complexity and footprint required to obtain output $>100\,MW$ from a genuinely practical directed energy source. This has taken the form of an analytic and numerical study of the operational parameter space of the source, along with commissioning work on the power supply, intended for use in driving the future source prototype.

Figures List:

Abbreviations List:

(r,z)	Cross-sectional plane, r = radius, z = longitudinal axis.
2.5D modeling	2 dimensional (e.g. r,z) numerical representation of the EM-fields with conservation of particle momentum in 3 dimensions (e.g. r, θ, z)
3D modeling	Numerical representation of both the EM-fields and particles in 3 dimensions (e.g. x, y, z)
AK gap	Anode Cathode gap
BWO	Backward-Wave Oscillator
$CuSO_4$	Copper-Sulfate solution
Deionized water	"Pure", low electrical conductivity water
e-beam	Electron beam
EM	Electromagnetic (field / wave / pulse / spectrum)
KARAT	PiC code used to predict the time-dependent evolution of the interaction of charged particles with electromagnetic fields[1]
MATLAB	"Matrix Laboratory", MATLAB is a commercial numerical software package, used for solving complex numerical problems
MIDEL 7131	An insulating fluid used in applications with very high electrical stresses (e.g. in high voltage transformers, or in the UoS PPS)
PiC	Particle in Cell
PPS	Pulsed Power Supply
PVC	PolyVinyl Chloride – a synthetic plastic polymer.
PVCu	PolyVinyl Chloride–unplasticized (also alternatively termed 'uPVC')
S-band	A subset of the electromagnetic spectrum between 2 GHz and 4 GHz
SIBWO	Self-Insulating Backward-Wave Oscillator
SWS	Slow Wave Structure
UoS	University of Strathclyde
X-band	A subset of the electromagnetic spectrum between 8 GHz and 12 GHz

Background:

Over the current reporting period, the work carried out at the UoS was progressed in two main sections: Analytic and numerical investigation of the SIBWO operational parameter space; and preparations for experimental investigations of a prototype source.

Numerical work:

To characterize the operation of the SIBWO, the UoS has made use of the Particle in Cell (PiC) code KARAT [Tarakanov[1]], using the 2.5D (r,z) solver. While this assumes azimuthal symmetry in the EM-field-pattern, it is sufficient to obtain an initial scoping of the parameter space, from which a targeted, fully 3D, numerical study may be taken forward. This study has been aided by the use of analytic tools, developed in MATLAB, to obtain "sets" of values for the key design parameters of the SIBWO.

Experimental work:

In preparation for testing of a prototype source, planned to start at the end of Project Year 2/beginning of Project Year 3 of the current work program, the UoS has undertaken commissioning and tuning of the required power supply, for use with the effective load presented by the new electron accelerator of the SIBWO.

2. Activities and Accomplishments

Numerical investigation of SIBWO:

The SIBWO consists of a relativistic electron accelerator and an interaction region, formed jointly by a periodic-corrugation on the drift-tube wall (Slow-Wave Structure (SWS)) and a smooth-bore modulation cavity (defined between the anode-grid and the start of the SWS). An example of the SIBWO, as modelled in KARAT[1], is given in Figure 1, with key components annotated.

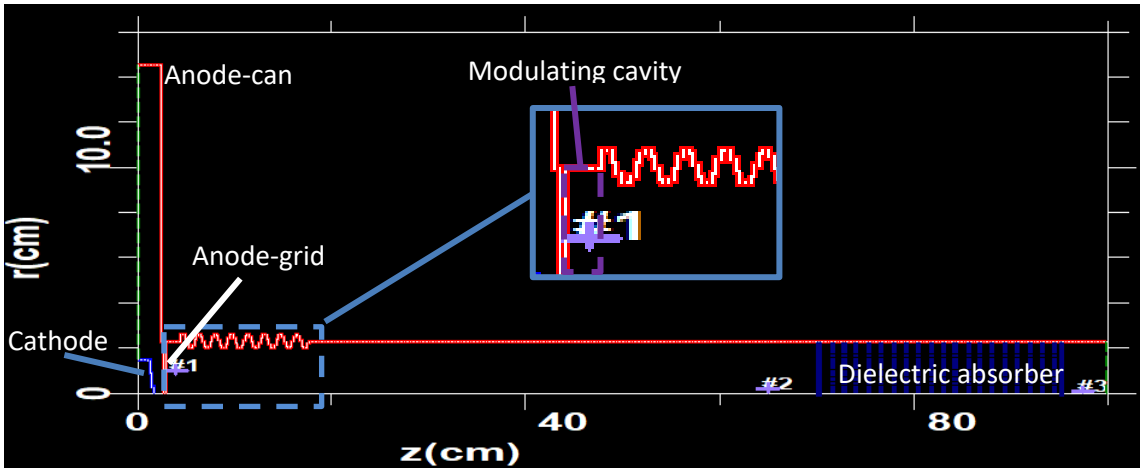

Figure 1. Shows the (r,z) cross-section of an X-band SIBWO, as modelled using the 2.5D KARAT[1] PiC code. Key components are annotated along with the location of the code's diagnostic locations (#1 – 3).

The electron accelerator is formed by the cathode and bounding anode-can, with the emitted electron beam propagated into the interaction region through the anode-grid (in KARAT[1] defined as transparent to the particles but as an electrical short to the EM-field). A dielectric absorber is located downstream of the interaction region to prevent the onset of parasitic oscillations within the code, which may otherwise grow in amplitude and influence the predicted performance.

Initial modeling of the SIBWO involved scaling of model geometry from an existing S-band ($2-4\ GHz$) variant, resulting in a saturated output power of $\sim 300\ MW$ at a resonant frequency of $\sim 8.5\ GHz$ operating in the intended TM_{01} mode. The applied potential on the electron accelerator was $500\ kV$, generating transported beam currents of $\sim 4.5\ kA$.

The E-field stress at the surface of the interaction was dominated by the radial E_r field component, peaking at $\sim 800\ kV/cm$, which puts operation of the source into the "possible spark" range, as historically described by Kilpatrick[2] (for example, see Figure 2 in [Kilpatrick 1957]), indicating a risk of electrical breakdown occurring in a physical source. While much can be done to mitigate against the occurrence of a vacuum arc/spark (through surface processing etc.), the most effective means is to reduce the E-field stress as far as is practicable. The numerical work package is therefore currently looking at the effect on operation of increasing the mean diameter of the drift-space, with suitable scaling of the SWS and modulating cavity parameters to maintain the approximate resonant frequency. At the time of writing, best performance, from an over-sized source, has been obtained for an interaction region of mean radius $23\ mm$, corrugation period $17\ mm$, of amplitude $\pm 3\ mm$, and modulator cavity length $17\ mm$. The E-field components, power envelope and spectral content are shown in Figure 2.

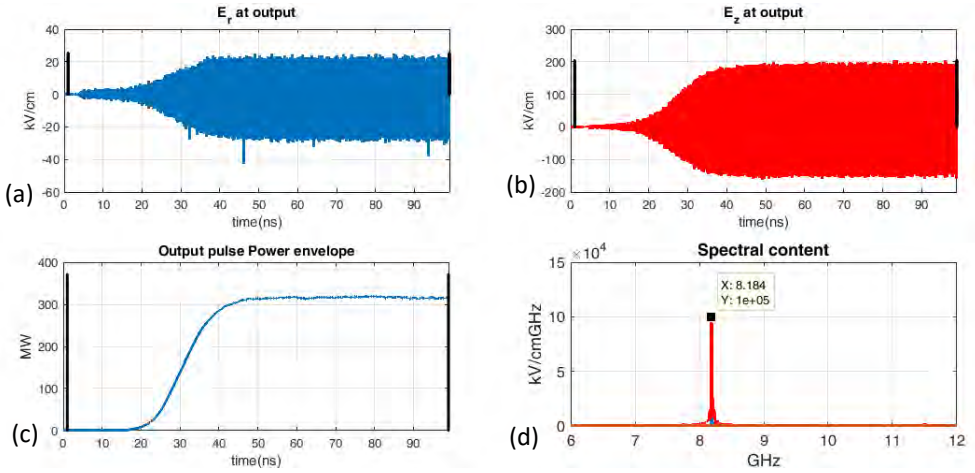

Figure 2. Shows (a) – (b) the components of the E-field at the source output (#2 in Figure 1), along with (c) the associated output power envelope and (d) spectral content in the pulse [taken within the time window indicated by the black bars in (a) – (c)].

This maintained an output power of $\sim 300\ MW$, albeit at a slight down-shift in operating frequency to $\sim 8.2\ GHz$. The E-field stress at the surface was reduced to $\sim 500\ kV/cm$, which is closer to the "no-spark" region described by Kilpatrick[2], but still shows a risk; ideally one would like a decrease of at least a further factor of 2. To aid in reducing this further a MATLAB code was written that produces "maps" of the required corrugation parameters for a given value of mean radius and intended operating frequency. This generated sets of parameters which may now be used to focus the numerical study, aimed at maintaining/maximizing the output power whilst further reducing the surface field stress. It is noted that increasing the mean radius introduces the risk of reduced mode-control (the source may begin to oscillate at multiple frequencies). The extent of this risk can only be assessed through full 3D numerical simulation, which the UoS will undertake after determining a suitable subset of the operation parameter space via the existing 2.5D study.

Collaborative numerical work with NRL

The electron accelerator, as modelled in KARAT[1], is not currently optimized; rather it is a geometric simplification of an existing S-band SIBWO accelerator, scaled to match the reduced dimensions of the X-band source. While a degree of optimization of the accelerator is being carried out at the UoS, as part of the above mentioned numerical study, the UoS is involved in a collaboration with researchers at NRL, who are looking at maximizing the transport of the generated current, through into the drift-space, while minimizing variation in the particle momentum vectors. This combined work effort, between the UoS and NRL researchers, should allow for a reduction in the total current emitted by the cathode assembly and potentially for an uplift in the achievable electronic efficiency, as the transport of a higher quality electron beam, into the drift-space would enhance the operation of the source.

Experimental work:

In preparation for testing of a prototype X-band SIBWO, the UoS has begun commissioning of the laboratory experimental space, focusing primarily on the preparation of the required driving pulsed-power supply (PPS). This is composed of two main sections; a 15-stage inverting Marx-generator (charged at positive potential, but discharged negative), discharging to a deionized-water filled pulse-forming transmission line. It is important to note that this pulsed-power supply is being used because it is already available in our laboratory and it therefore avoids requiring the purchase of major new capital equipment that would have incurred significant extra costs to the present project.

A much smaller, more compact, smaller mass, pulsed-power supply could be employed to drive the SIBWO in any eventual application, or deployment.

The Marx- generator.

Due to the high electrical stresses involved, the Marx- generator is charged and discharged within a grounded metallic tank, filled with an electrically insulating fluid. In previous work programs the UoS employed mineral oil for this purpose, however new operating guidelines required a move to the higher flashpoint, more environmentally friendly, MIDEL 7131. The sensitivity of the MIDEL to some components in use (and vice versa), led to a redesign of the discharge spark-gap and various copper-sulfate ($CuSO_4$) resistor assemblies. The $CuSO_4$ resistors (formed using $CuSO_4$ solution- filled flexible tubing) were prone to leakage over time. This issue was expected to increase when placed in MIDEL due to increased leaching of the plasticizers from the resistor tubes. To mitigate against this, the UoS replaced all such resistors with PVCu equivalents. Sight-glasses were added at the top of each resistor, with an expansion gap left to prevent damage due to over-pressure (due to heating of the $CuSO_4$ solution during the charge / discharge cycle). Further, the UoS replaced, in all places of high-stress, any brass components with copper equivalents. This mitigated the risk of introducing zinc into the MIDEL, which is known to degrade its performance. The re-assembled Marx-generator is shown in Figure 3(a).

Pulse forming transmission line.

When fired, the Marx-generator shows the typical characteristics of a capacitive discharge, with a (relatively) sharp rise in the output potential of $\sim 250\,ns$, a short peak, following by a long decaying tail of multiple microseconds. This means the majority of the energy in the pulse is not located at a potential that is of use to the attached source. To remedy this, the output from the Marx-generator, first passes through a "pulse former", in the form of a deionized-water filled transmission-line, terminated in a high-voltage spark-gap. While the spark-gap remains open, the Marx output charges the transmission line as if it were a coaxial capacitor; however when the spark-gap closes, the transmission line acts as a simple length of coaxial cable, discharging at a uniform potential into a matched load for a duration set by its electrical length. The pulse former at the UoS typically produces fast rising, flat-top output pulses of $200 - 250\,ns$, at $\sim 60\%$ of the peak output voltage of the Marx-generator, dependent on the load presented, with its power handling being a strong function of the quality of the deionized water filling the line. The deionized water system is shown in Figure 3(b).

Figure 3. Shows (a) Marx-generator, formed of fifteen $100\,kV$ $25\,kA$ capacitors, (b) The deionized water system and PPS as a whole.

For stable operation the PPS requires a minimum water quality of $14\ M\Omega\ cm$ when operating at $\sim 500\ kV$. The pre-existing water purification system was sufficient to maintain the water quality at a level of $16 - 17\ M\Omega\ cm$ when the system was at rest (i.e. in between experimental runs) and to keep it above $14\ M\Omega\ cm$, provided no more than ~ 30 shots were taken during a typical experimental run (over a period of a single working day). The upgraded system, shown in Figure 3(b), maintains the same level of water quality, when the system is a rest, and has a higher flow-rate, meaning more shots should be obtainable in a single experimental run.

Overall progress on the PPS.
At the time of writing the UoS is finalizing construction of the matching resistors, used on the output spark-gap of the pulse former. When these are complete, the PPS will be ready for commissioning tests, which are expected to commence in FY2019.

3. Findings and Conclusions

The numerical study of a SIBWO, operating in the X-band, has produced a preliminary source design, capable of generating $\sim 300\ MW$ of output power, at a resonant frequency in the region of $8 - 8.5\ GHz$, from a driving electron beam of $\sim 500\ kV$, $\sim 4.5\ kA$, corresponding to an electronic efficiency of $\sim 13\%$. This was predicted from a numerical model that indicates E-field stresses in a range that risk potential arc-formation in the operation of a physical source, indicating a move to a more over-sized source geometry is required. The analytic groundwork for investigating this has been performed and simulations are currently underway to address this issue.

An outstanding issue relates to the overall predicted energy efficiency, which at present is lower than the electronic efficiency, due to the non-optimized nature of the electron accelerator. The field-stresses in the accelerator are such that emission occurs on all surfaces of the cathode, as opposed to just the intended emitter, resulting in the deposition of $\sim 2/3$ of the total emitted current onto the face of the anode. The predicted electronic efficiency therefore relates only to the energy extracted from the remaining $\sim 1/3$ of the beam current that successfully propagated into the drift region. It should be noted that suppressing emission from the non-emitter regions of the cathode assembly has, in previous work, shown to have little impact on the electronic efficiency of the source – i.e. when this spurious emission is mitigated, the electronic and overall efficiencies become analogous and source performance is not detrimentally affected.

In terms of the experimental work, preparations for construction and testing of the prototype SIBWO are underway, with the required power supply undergoing a comprehensive upgrade to key components. This upgrade is near completion, with commissioning expected in the near future; including characterization and tuning of the supply output pulse-shape, when driving a load comparable to that presented by the expected electron accelerator design.

The key finding from the work to date is that a high frequency (X-band) source, operating without the application of an external magnetic confinement system, appears feasible, with output powers in the region of $\sim 300\ MW$ obtainable at a reasonable electronic efficiency. While issues are outstanding in reducing the total emission current and E-field stress in the source, the latter should be accountable via further adjustment and optimization of the drift-space, and it should be possible to greatly reduce/mitigate the former, through redesign of the electron accelerator and proper choice of materials in the experiment. Further, the presence of stray emission in the accelerator, does not

appear to decrease the electronic efficiency of the source, indicating that, while desirable to reduce/mitigate this stray emission in a final deployable source, this is not presently an issue for the continued development of the first X-band prototype.

References:

1. Tarakanov V. P., *User's Manual for Code KARAT*, Distributed by Berkeley Research Associates Inc.: Springfield, VA.
2. Kilpatrick W. D., 1957, Criterion for Vacuum Sparking Designed to Include both rf and dc, *Review of Scientific Instruments*, **28**(10), pp. 824–826.

4. Plans and Upcoming Events

The next stage in the numerical work program will be to conclude the 2.5D study of the SIBWO parameter space, determining a sub-set of values for the geometry that maintain output powers of $\sim 300\ MW$, but with reduced E-field stresses within the interaction region. This would be carried out in tandem with the numerical work underway at the NRL to optimize the design of the electron accelerator. A teleconference, with researchers at the NRL, is scheduled for October 2018, to discuss current progress and routes for synergy between the two numerical programs.

Following the 2.5D study, the UoS plan to progress to fully 3D PiC modeling of the SIBWO, based on the parameters sets identified, to check for, and mitigate against, operation in higher-order modes that cannot be accounted for in the 2.5D study (i.e. those modes showing azimuthal asymmetry). This is on schedule for completion by the end of $12\ months$ from the commencement date of the current project program i.e. by 14 June 2019, with progression to design for manufacture intended to occur directly thereafter.

It is intended that the design of the accelerator will be close to being finalized by this same date (14 June 2019), for progression of the accelerator design to manufacture. Hot testing of the accelerator is expected for the end months of calendar year 2019, corresponding to the early months of ONR FY2020. Similarly, in the course of the numerical study, the requirements for ancillary components, (e.g. tapers and output horn antenna) will be identified and progressed to manufacture, with cold-testing performed as appropriate, in preparation for assembly of the source as a whole.

Hot testing of the SIBWO X-band prototype is expected to start by the end of $24\ months$ from the commencement date of the current project program i.e. by 14 June 2020, corresponding to 3 to 4 months before the end of ONR FY2020.

5. Transitions and Impacts

Not yet applicable at this early stage

6. Collaborations

Collaboration with Dr. Simon Cooke at NRL in modeling and design of the electron accelerator.

7. Personnel

Principal investigator: Prof. Alan D. R. Phelps
Person months worked: 1
National Academy Member: Yes

Nationality: UK

Co-investigator and Co-PI: Dr. Kevin Ronald
Person months worked: 1
National Academy Member: Yes
Nationality: UK

Co-investigator: Dr. Philip MacInnes
Person months worked: 4
National Academy Member: No
Nationality: UK

Business Contact: Mrs. Alison McFarlane, RKES, University of Strathclyde

8. Students

No students engaged with the project at this stage

9. Technology Transfer

We have undertaken collaborative discussions with Dr. Simon Cooke, NRL, in relation to modeling of the electron accelerator.

10. Products, Publications, Patents, License Agreements, etc.

Publications resulting from this project: 0

11. Point of Contact in Navy	**Date of last contact (in period 15 June – 30 Sept 2018)**
Ryan Hoffman ONR Code 35, ryan.hoffman@navy.mil	23 & 28 August 2018
Tim Andreadis NRL, tim.andreadis@nrl.navy.mil	
Jesus GilGil NRL, jesus.gilgil@nrl.navy.mil	23 August 2018
Dave Abe NRL, david.abe@nrl.navy.mil	23 August 2018
Simon Cooke NRL, simon.cooke@nrl.navy.mil	September 2018
Isaac Bankman ONRG (up to Sept 2018), isaac.n.bankman.civ@mail.mil	27 September 2018
Predrag Milojkovic ONRG (from Oct 2018), predrag.milojkovic.civ@mail.mil	

12. Acknowledgement/Disclaimer

This work was sponsored by the Office of Naval Research (ONR), under grant number N00014-18-S-B001. The views and conclusions contained herein are those of the authors only and should not be interpreted as representing those of ONR, the U.S. Navy or the U.S. Government.

High-Power Microwave Generation by Compact Linear Transformer Driver Technology

Grant No. N00014-18-1-2499

Period of Performance: June, 1, 2018 to September 30, 2019

Prepared by:

Professor Ryan McBride, Principal Investigator
University of Michigan
Department of Nuclear Engineering and Radiological Sciences
2355 Bonisteel Blvd
1906 Cooley Building
Ann Arbor, MI 48109-2104
Tel: (734) 763-7504
Email: mcbride@umich.edu

This work was sponsored by the Office of Naval Research (ONR), under grant number N00014 - 18-1-2499. The views and conclusions contained herein are those of the authors only and should not be interpreted as representing those of ONR, the U.S. Navy or the U.S. Government.

Grant or Contract Number: N00014-18-1-2499
Date Prepared: November 30, 2018
Project Title: High-Power Microwave Generation by Compact Linear Transformer Driver Technology
Annual Summary Report: CY2018
Principle Investigator: Ryan McBride, 734-763-7504, mcbrider@umich.edu
University of Michigan, Department of Nuclear Engineering and Radiological Sciences

This work was sponsored by the Office of Naval Research (ONR), under grant (or contract) number N00014-18-1-2499. The views and conclusions contained herein are those of the authors only and should not be interpreted as representing those of ONR, the U.S. Navy or the U.S. Government.

Section I: Project Summary

1. Overview of Project

Abstract: The efficient generation of high-power microwaves (HPM) from compact generating equipment is of critical importance to the United States Navy and Department of Defense (DoD). Applications include: radar, signal jamming, electronic warfare, counter IED (improvised explosive device), and vehicle stoppers. Example systems where HPM is critical include the Patriot Missile and the Aegis Combat/Weapon System. This project will explore the use of compact linear transformer driver (LTD) technology to drive various gigawatt-class, narrow-band (~1 GHz), HPM sources. LTDs are low-voltage, low-impedance drivers. An LTD-driven HPM source could become one of the most compact, low-voltage, GW-class HPM sources available for Office of Naval Research (ONR)/DoD directed energy programs. To obtain this performance, a rich assortment of physics issues will be studied. For example, as we increase the driver power, electrode plasmas (particularly from contaminants adsorbed onto electrode surfaces) can become problematic. If plasmas form in the anode-cathode gap with densities >1e10 electrons/cc, then L-band microwaves (1 GHz) can become attenuated significantly. We will study these low-density power flow plasmas by combining particle-in-cell (PIC) simulations with experimental measurements from a vast array of diagnostics, including energetic particle detectors, Zeeman and Stark spectroscopy, self-emission imaging, and laser-based probing and imaging techniques. The use of LTD technology to drive an HPM source is advantageous for several reasons: First, the driver impedance and driver voltage is tunable, because LTD systems are modular. The PI will be assembling a 4-cavity LTD facility called BLUE (Bestowed LTD from the Ursa-minor Experiment) at the University of Michigan (UM). The driver impedance of BLUE can be varied from 1 to 30 ohms. Second, the pulsed-power components in LTDs are completely encased in metal, thus minimizing stray high-voltage fields and electrical interference. Third, LTDs can be rep-rated up to (and possibly beyond) 0.1 Hz, thus increasing the average power. Additionally, rep-rating has the potential benefits of electrode conditioning and decontamination, therefore allowing us to emulate standard industry practices in the fabrication of commercial microwave tubes. The effects of various rep-rates will be tested directly.

Objective: To explore the use of linear transformer driver (LTD) technology for driving high-power microwave (HPM) sources, including GW-class recirculating planar magnetrons (RPM) and other crossed-field devices.

Introduction: This project will study GW-class, narrow-band HPM devices, operating at a frequency ~1 GHz. Such devices are driven by pulsed power technology. Pulsed power involves the use of high-voltage capacitors and fast switching techniques to store electrical energy over long time scales and discharge the energy over fast time scales; because power is the rate at which energy is delivered, the fast discharge time leads to power amplification. Often the peak powers obtainable in HPM can be quite large (~GW), but this usually comes at the expense of high average powers. This project will explore the use of LTD technology (an exciting new compact and efficient pulsed power technology) to drive various HPM sources. An important attribute of LTD technology is that it has the potential to be rep-rated up to (and possibly beyond) 0.1~Hz.

In narrow-band HPM, the pulsed-power driver is used to apply a large, fast-rising voltage pulse across a vacuum-filled anode-cathode gap (A-K gap). This A-K gap then serves as the load for the pulsed-power driver, sometimes being referred to as a "diode" load. The large applied voltage (and its associated electric field) can cause electrons to be emitted from the cathode surface. This is especially true if the cathode is treated in a way that favors field emission of electrons (e.g., velvet covered cathodes). If the voltage applied across the A-K gap is an appreciable fraction of the electron's rest mass energy (511 keV), then the predominantly vacuum-filled region within the A-K gap can become populated with relativistic electrons. Longer timescale electromagnetic fields [~DC fields relative to the faster radio frequency (RF) timescales of interest] can then be applied to direct these electrons into a well-formed electron beam. The electron beam can then be modulated to amplify and/or excite RF electromagnetic waves.

In crossed-field devices (CFDs) – such as relativistic magnetrons and crossed-field amplifiers – an approximately DC electric field **E** and an approximately DC magnetic field **B** are applied at right angles to one another, so that the well-known $\mathbf{E}\times\mathbf{B}$ drift velocity ($\mathbf{v} = \mathbf{E}\times\mathbf{B}/B^2$, where B is the scalar magnitude of the magnetic field) can be used to drive and steer the electron beam. To get the beam to interact with an RF field, the beam is driven in close proximity to a slow-wave structure (i.e., an anode structure with periodically spaced metal vanes). A synchronized, modulating interaction between the beam and the RF wave can then be obtained if the magnitude of the drift velocity $v=E/B$ is well matched to the phase velocity of the RF wave propagating in the slow-wave structure. A bunching instability, called the phase-focusing mechanism, causes the beam to become modulated, enhancing the RF output.

To drive the electron beams, this project will use a pulsed-power technology called linear transformer drivers. The LTD concept was pioneered in 1995-1997 at the High Current Electronics Institute (HCEI), in Tomsk, Russia, by Kovalchuk, Vizir, Kim, and colleagues. Since then, the LTD concept has been advanced further by HCEI as well as researchers at Sandia National Laboratories and many others worldwide. LTDs have been called the greatest advance in prime-power generation since the invention of the Marx generator in 1924.

In the late 2000's, a collaboration was developed between HCEI, Sandia National Laboratories, and the University of Michigan (UM) to bring LTD technology to the United States. In 2006--2007, five 3-m-diameter, 1-MA, 100-ns LTD cavities were tested at HCEI with resistive and electron-beam diode loads. In July of 2007, one of these HCEI cavities was shipped to UM, becoming the MAIZE facility and the first 1-MA, 100-ns LTD in the United States. In 2008, ten more 1-MA, 100-ns LTDs cavities were shipped to Sandia, becoming part of the Mykonos facility. Additionally, smaller (1.25 m in diameter), lower-current cavities were shipped to Sandia, becoming the Ursa

Minor facility. The Ursa Minor facility stacked 21 of these 1.25-m-diameter cavities together to obtain a high-impedance driver for high-energy x-ray source development: https://www.sandia.gov/Pulsed-Power/research_facilities/Ursa_Minor.html

Four of the Ursa Minor cavities were recently shipped to UM, where we are now assembling them into the BLUE facility (Bestowed LTD from the Ursa-minor Experiment) to drive HPM sources for this project (see *Figure 8*).

Figure 22. The BLUE pulsed power facility being received at the University of Michigan. These four LTD cavities were previously part of the 21-cavity Ursa Minor facility at Sandia National Laboratories. This technology transfer is part of Sandia's Stevenson-Wydler Gift Program. [Pictured from left to right: Prof. Ryan McBride (PI), Dr. Nick Jordan (lab manager, research scientist, and Co-I), Steven Exelby (HPM PhD student of Prof. Gilgenbach), and Mark Perreault (senior lab technician and safety coordinator).

Background: Over the past three decades, the University of Michigan (UM) has developed an expertise in both experimental and theoretical investigations of HPM devices under the supervision of Professors Ron Gilgenbach and Y. Y. Lau. Most of the experiments have been carried out on the Michigan Electron Long-Beam Accelerator (MELBA), which is a Marx-generator-based pulsed-power machine at UM. Some of the experimental CFDs studied recently with MELBA include the recirculating planar magnetron (RPM), the multi-frequency recirculating planar magnetron (MFRPM), and the recirculating planar crossed-field amplifier (RPCFA), all of which have been met with success.

This new project, using LTDs to drive HPM sources, is both basic and applied research, involving HPM design and optimization with PIC simulations and experimental optimization of driver impedance using the 4-cavity BLUE LTD facility. BLUE will provide a variable drive voltage of 50–800 kV and a variable drive impedance of 1–30 Ω. Our approach will also involve the study of electrode plasmas (particularly from contaminants adsorbed onto electrode surfaces), which can become problematic. If plasmas form in the anode-cathode gap with densities $>10^{10}$ electrons/cc, then L-band microwaves (1 GHz) can become attenuated significantly. We will study these low-density power flow plasmas by combining particle-in-cell simulations with experimental measurements from a vast array of diagnostics, including energetic particle detectors, Zeeman and Stark spectroscopy, self-emission imaging, and laser-based probing and imaging techniques.

2. Activities and Accomplishments

This project just began this past summer (June 2018), thus these are interim activities and accomplishments.

First and foremost, we have successfully recruited a new (first-year) PhD student, Brendan Sporer (see *Figure 9*), to build/assemble the BLUE Linear Transformer Driver (LTD) pulsed power facility at Michigan. Brendan, along with PI Ryan McBride and Co-I Nick Jordan, traveled to Sandia National Laboratories to visit the LTD development labs there. This gave us a chance to ask the lab scientists questions about the BLUE cavities and the latest developments for LTD technology in general. We learned about the benefits of using trigger inductors (rather than trigger resistors). The BLUE cavities were previously used at Sandia's Ursa Minor facility to produce bright x-ray sources.

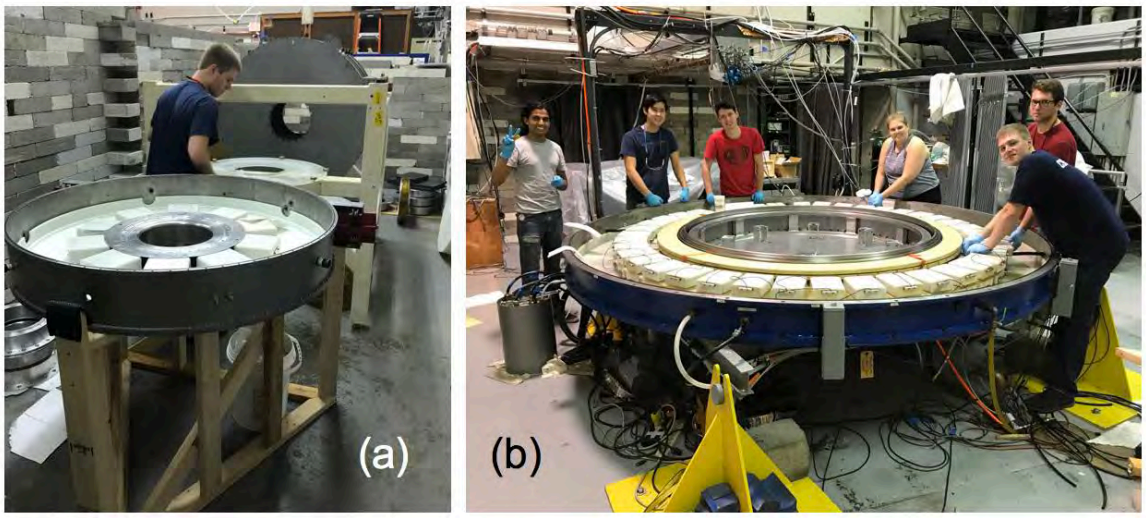

Figure 23. (a) Newly recruited PhD student Brendan Sporer assembling the first BLUE LTD cavity. Brendan has reconfigured the concrete shielding wall to accommodate BLUE and has built the wooden test stand to facilitate the assembly of BLUE cavities. (b) Brendan Sporer and other lab graduate students reassembling the MAIZE LTD cavity to test BLUE's L3 gas switches.

Brendan has reconfigured a concrete shielding wall in our lab to accommodate the BLUE facility [see *Figure 9*(a)]. We have begun pricing/performance analysis for new power supplies to allow rep-rating BLUE, and we are about to order two new Spellman power supplies (one positive and one negative supply). Brendan has begun LTD training (and general pulsed power training) by helping with the rebuild of our other LTD facility, MAIZE [see *Figure 9*(b)]. This allowed Brendan to understand the basic power units of LTDs, which are the "bricks" (2 caps connected in series with a high-power spark-gap switch). Brendan tested and conditioned BLUE's L3 gas switches in our LTD brick tester and in MAIZE. He has also learned the overall assembly procedure for MAIZE [see *Figure 9*(b)], which will help him immensely as he begins to assemble BLUE for the first time [see *Figure 9*(a)].

Brendan has constructed a maintenance stand for servicing the LTD cavities, and he has used this stand to begin assembling the first BLUE cavity [see *Figure 9*(a)]. For the assembly of the larger overall 4-cavity BLUE *module* (where a *module* is multiple cavities stacked together in series),

design work is required to compress the stack, since all of the cavities must share a common vacuum. To help with this, Sandia recently sent us SolidWorks CAD models of the Ursa Minor facility, which will help our design and construction efforts immensely. Brendan has completed his own initial SolidWorks CAD model of BLUE, but we may need to reassess after further reviewing the Sandia models.

PhD Student Brendan Sporer, PI Ryan McBride, and Co-I Nick Jordan (along with the rest of the LTD students in the UM pulsed power lab) hosted two researchers (LTD specialists) from Sandia National Labs (Jon Douglass and Tommy Mulville) (see *Figure 10*). The goal of the visit was for Sandia to help UM with UM's LTD facilities (MAIZE & BLUE). The outcomes of the visit were that cleaner transformer oil (with oil recirculation) is needed. This could help alleviate some pre-firing issues UM has been having with BLUE's new L3 switches, which are presently being tested in the MAIZE cavity. Sandia is donating roughly $5k worth of solid-state charging-resistor assemblies (improved components over the more standard copper-sulfate charging resistors typically used). Other outcomes include better/cleaner zero-air switch gas and gas line plumbing. A list of safety improvements is also being provided. All recommendations from Sandia have been written up in a post-visit report by Douglass and Mulville. Significant progress was made in improving the operation and reliability of BLUE's new L3 switches in MAIZE, despite the poor conditions of the insulating transformer oil.

Figure 24. PI Ryan McBride (front left) and Sandian Jon Douglass (front right) as well as Co-I Nick Jordan (back left), Sandian Tommy Mulville (back center), and applied physics PhD student Akash Shah (back right) working on the MAIZE LTD cavity. The L3 switches for BLUE are presently being tested in MAIZE. Significant improvements to UM's LTD facilities were made during this visit.

For the HPM device side of this project, we have recruited a PhD student, Drew Packard, to begin cold tube and PIC simulations of crossed-field HPM devices on BLUE. Drew has mentored an undergraduate student, Anna Cooleybeck, who has run several new simulations of various devices intended for BLUE.

3. Findings and Conclusions

This project just began this past summer (June 2018), thus these are interim results and conclusions.

From the visit of Sandia LTD experts (Dr. Jon Douglass and Mr. Tommy Mulville), a key finding was that an oil processing unit is needed to remove impurities from the insulating transformer oil. This is needed to keep BLUE's L3 gas switches from pre-firing, which is a surprising (non-intuitive) result. We also learned that solid-state charging-resistor assemblies are now the preferred approach over the more standard copper-sulfate charging resistor approach. Other outcomes include the need for better/cleaner zero-air switch gas and gas line plumbing, which has now been implemented, along with a list of safety improvements, which are now in the process of being implemented. All recommendations from Sandia have been written up in a post-visit report by Douglass and Mulville, which has been delivered to UM. Significant progress was made in improving the operation and reliability of BLUE's new L3 switches in the MAIZE facility, despite the poor conditions of the insulating transformer oil. These techniques will be used as we bring up the full BLUE facility.

As for HPM device simulations, we now have working simulation results in hand demonstrating HPM operation (spoke formation) in slow wave structures driven by electrical pulses representative of those which will be provided by BLUE. These preliminary results will continue to be refined in the upcoming year.

In addition to the development of our own LTD facility construction and HPM device design and fabrication, the Air Force Research Laboratory (AFRL) in Albuquerque, NM, is sending us a mini-LTD for further testing (courtesy of Dr. Brad Hoff, AFRL) and a working crossed-field HPM device (along with CAD models) for testing on BLUE (courtesy of Dr. Kyle Hendricks, AFRL). These devices will provide further opportunities for research outputs and student training in areas relevant to the DoD, Navy (ONR/NRL), and Air Force (AFOSR/AFRL).

4. Plans and Upcoming Events

Our plans for the near-term future begin with assessing Sandia's SolidWorks CAD model of the Ursa Minor facility and incorporating any useful ideas into Brendan Sporer's SolidWorks CAD model of BLUE. We will also complete our high-level block diagram designs for the overall layout of the BLUE facility; as part of this high-level design, we are evaluating various options such as pure LTD architectures versus an impedance-matched Marx generator (IMG) architecture.

In parallel with the design and facility layout work, we will complete our assembly of a single BLUE LTD cavity and begin testing this single cavity. Once the operation of a single cavity has been demonstrated, we will begin incorporating additional cavities and building a multi-cavity LTD module.

In parallel with these facility construction activities, we will be developing an LT-SPICE model for BLUE, and we will use this model to run circuit simulations for the overall system, including triggering units.

We will also continue to develop our cold-tube electromagnetic simulations and PIC simulations of various crossed-field HPM devices on BLUE.

Our goal is to have a working BLUE facility, with a preliminary (point design) HPM device tested on BLUE by the end of 2019. We will also make use of the mini-LTD device and the crossed-field HPM device provided by the AFRL.

5. Transitions and Impacts

This project just began in June 2018, thus all of the transitions and impacts have been in the direction from Sandia National Labs and the AFRL, both in Albuquerque, NM, to the University of Michigan. Upon testing the donated equipment, we will begin to transition research outputs, technology products, and trained students/PhDs back to these labs.

6. Collaborations

As part of this program/project, we are collaborating with Dr. Brad Hoff of the AFRL, who is providing guidance on what is important to directed energy programs in the Navy and Air Force and who is also sending us a mini-LTD pulser for HPM device testing. Similarly, we are collaborating with Dr. Kyle Hendricks of the AFRL, who is sending us a working crossed-field HPM device (along with its CAD models) for testing on BLUE.

We have also been collaborating with Dr. Jon Douglass, Mr. Tommy Mulville, Mr. Matt Sceiford, Dr. Josh Leckbee, and (previously) Dr. Matt Wisher, all of Sandia National Laboratories, who have been working to help us with the transition of the four Ursa Minor cavities to the University of Michigan, where they will be part of the BLUE LTD facility. It is of strategic importance to Sandia's pulsed-power development labs that students are being trained in new LTD technology.

This program is also allowing us to collaborate with Prof. Allen Garner of Purdue University, who has his own ONR HPM funding to test out a non-linear transmission line (NLTL) HPM source on an LTD. We will be providing the LTD and Prof. Garner's group will be providing the NLTL source.

7. Personnel

Principal investigator
Prof. Ryan McBride
~1.25 person months worked
National Academy Member: No

Co-investigator or Co-PI
Dr. Nicholas Jordan
~1.25 person months worked
National Academy Member: No

Business Contact
Ms. Tawny Dekar

~0.25 person months worked
National Academy Member: No

Team Members
Mr. Brendan Sporer
~2.5 person months worked
National Academy Member: No

Team Members
Mr. Drew Packard
~0.25 person months worked
National Academy Member: No

Team Members
Ms. Anna Cooleybeck
~1 person months worked
National Academy Member: No

8. Students

2 graduate students, 1 undergraduate student:

Mr. Brendan Sporer: PhD student
Fully supported by this ONR YIP HPM project

Mr. Drew Packard: PhD student
Assisting with HPM device simulations and experimental diagnostics/setups on this ONR YIP HPM project (supported by other ONR HPM project: Multi-Frequency RPM project)

Ms. Anna Cooleybeck: Undergraduate student
Conducting HPM device simulations on this ONR YIP project. Her laboratory research is for academic credit; thus, her work is presently at no cost to this ONR YIP project.

9. Technology Transfer

We are presently perusing a patent for a crossed-field device that we would like to test on an LTD. This effort is being led by Prof. Y. Y. Lau, as the device design is his. Presently, the UM Office of Technology Transfer is conducting a "prior art search". We will know more about our chances of obtaining a patent after we review these results.

Regarding LTD work in general, we have been in communication with folks at the Naval Research Lab (Joe Schumer, Jacob Zier, and Tom Mehlhorn), Sandia National Labs (see above), and the AFRL (see above). We recently published an invited tutorial on LTDs with Joe Schumer and Jacob Zier of the NRL and Jon Douglass and Josh Leckbee of Sandia National Laboratories (see Section 10 below).

10. Products, Publications, Patents, License Agreements, etc.

Publications resulting from this project:
Archival Publications (publication reference information (article title, authors, journal, date, volume, issue) can be automatically entered using a DOI)

a. A Primer on Pulsed Power and Linear Transformer Drivers for High Energy Density Physics Applications
b. IEEE Transactions on Plasma Science
c. R. D. McBride, W. A. Stygar, M. E. Cuneo, D. B. Sinars, M. G. Mazarakis, J. J. Leckbee, M. E. Savage, B. T. Hutsel, J. D. Douglass, M. L. Kiefer, B. V. Oliver, G. R. Laity, M. R. Gomez, D. A. Yager-Elorriaga, B. M. Kovalchuk, A. A. Kim, P.-A. Gourdain , S. N. Bland, S. Portillo, S. C. Bott-Suzuki, F. N. Beg, Y. Maron, R. B. Spielman, D. V. Rose, D. R. Welch, J. C. Zier, J. W. Schumer, J. B. Greenly, A. M. Covington, A. M. Steiner, P. C. Campbell, S. M. Miller, J. M. Woolstrum, N. B. Ramey, A. P. Shah, B. J. Sporer, N. M. Jordan, Y. Y. Lau, and R. M. Gilgenbach
d. Equation of state, high-energy-density physics (HEDP), inertial confinement fusion (ICF), laboratory astrophysics, linear transformer driver (LTD), magnetized liner inertial fusion (MagLIF), material properties, pulsed power, radiation effects, radiation science, radiation sources.
e. Unrestricted distribution (open access)
f. Published
g. DOI
h. 10.1109/TPS.2018.2870099
i. November 8, 2018
j. Volume 46
k. Issue 11
l. Page 3928
m. Piscataway, New Jersey
n. Acknowledgement of Federal Support: Yes
o. Peer Reviewed: Yes

Conference Papers

a. Construction of the BLUE Linear Transformer Driver System at the University of Michigan
b. Brendan Sporer, Nick Jordan, and Ryan McBride
c. 60th Annual Meeting of the APS Division of Plasma Physics
d. November 5-9, 2018
e. Portland, OR, USA
f. Abstract published, poster presented
g. Friday, November 9, 2018
h. None
i. None
j. Acknowledgement of Federal Support: Yes

Books: None

Book Chapter: None

Theses: None

Websites: None

Patents: None (yet)

Other Products: Identify any other significant products that were developed under this project. Describe the product and how it is being shared.

a. Description: Developed models and simulations of crossed-field devices for use on the BLUE LTD facility. Also developed a SolidWorks CAD model of the BLUE LTD facility.
b. Product Type: models

11. Point of Contact in Navy

Dr. Joseph Schumer
Head, Pulsed Power Physics Branch
Plasma Physics Division
Naval Research Laboratory
(202) 841-2766
joe.schumer@nrl.navy.mil

Date we last discussed HPM research: June 1, 2018

12. Acknowledgement/Disclaimer

This work was sponsored by the Office of Naval Research (ONR), under grant (or contract) number N00014-18-1-2499. The views and conclusions contained herein are those of the authors only and should not be interpreted as representing those of ONR, the U.S. Navy or the U.S. Government.

Improved Computational Tools for Navy High Power Microwave Applications

Grant No. N68335-18-C-0060

Period of Performance: November, 14, 2017 to September 30, 2019

Prepared by:

Dr. Peter Stoltz, Principal Investigator
Tech-X Corporation
5621 Arapahoe Ave
Boulder, CO, 80303
Tel: (720) 563-0336
Email: pstoltz@txcorp.com

This work was sponsored by the Office of Naval Research (ONR), under grant number N00014 - 17-1-2848. The views and conclusions contained herein are those of the authors only and should not be interpreted as representing those of ONR, the U.S. Navy or the U.S. Government.

Section I: Project Summary

1. Overview of Project

Abstract: In this document, we show recent progress on applying modern plasma simulation tools to projects of interest to the Navy. We show results of a kinetic code (VSim) and a fluid code (USim) to four problems: high power microwave transmission line gap closure, a dense plasma focus neutron source, a relativistic planar magnetron microwave source, and a klystron microwave source.

Objective: The objective of this work is to undertake a comprehensive study of where in the Navy modeling space, given recent advances in plasma modeling, one can apply fluid approaches with sufficient accuracy and where kinetic models are required. We will compare the trade-off of accuracy of results with computational speed, attempting where we can to use automated optimization tools to tailor both approaches.

Introduction: Modeling and simulation play a critical role in the design and evaluation of high power microwave (HPM) devices. However, many of the most recent simulation methods have yet to be adopted by Navy scientists in their design process, in part because these methods need additional improvements and need to be shown to work on problems of interest to the Navy. Magnetohydrodynamics (MHD) and Particle-in-Cell (PIC) are two standard techniques that Navy researchers have relied on for many decades. More recently, however, the Air Force Office of Scientific Research (AFOSR) has sponsored the development of two-fluid electromagnetic models that bridge the gap between these two regimes, in a fashion that enables DoD researchers to solve problems of interest in the hypersonics and high energy density plasma community. However these new two-fluid electromagnetic models require further improvement to solve the range of problems involved in HPM design. With regard to kinetic PIC modeling, embedded boundaries are a new advance with promise for significantly improving modeling of HPM sources.

Background: Our approach is to modify two existing simulation tools, a multifluid modeling tool USim and a kinetic modeling tool VSim, to meet the needs of Navy high power microwave research. In collaboration with Naval Research Laboratory (NRL) scientists, we will identify representative problems on which we can apply these tools to demonstrate the improved capabilities.

2. Activities and Accomplishments

Our activities and accomplishments include simulation results on high power microwave transmission lines, dense plasma focus neutron sources, relativistic planar magnetron microwave sources, and klystron microwave sources. We discuss these each briefly below.

A standard problem for all high power devices is delivery of the power from the high voltage source to the load. For example, the delivery mechanism is frequently metallic vacuum transmission lines, and at high power the strong fields cause plasma emission from the transmission lines. That plasma eventually fills the vacuum gap in the transmission line, disrupting the power transmission. The exact rate at which the plasma expands across the gap is important to HPM design, and that is the problem we addressed here. We compare fluid and kinetic models, and demonstrate a hybrid model of transitioning from fluid to kinetic. We show in Fig. 1 both the parameters and the results from

USim and previously published results [C. Sack and H. Schamel, Plasma expansion into vacuum - A hydrodynamic approach, Physics Reports, 156:311–395, December 1987].

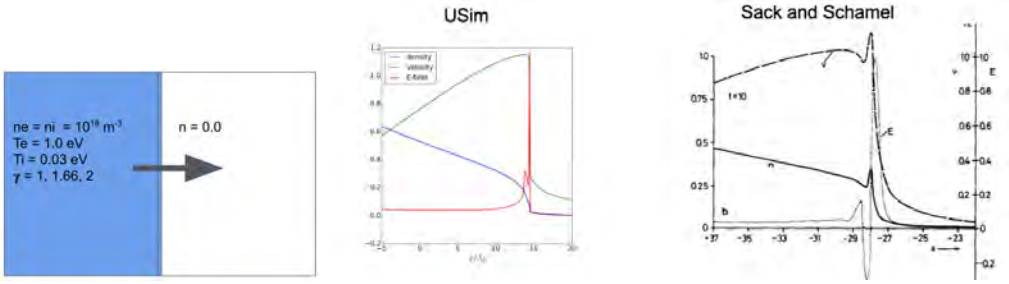

Fig 1: (left) Parameters for HPM transmission line gap closure. (center and right) Density, velocity and electric field (blue, green and red respectively) versus position at ten ion plasma times, comparing USim to published results.

We developed in the USim multifluid code an initial simulation model of the Hawk pulsed power machine, configured to operate as a dense plasma focus neutron source. Because this machine is well diagnosed, simulations of this device provide excellent benchmark opportunity that will give confidence in the other models of high power microwave devices.

We developed both three dimensional and two dimensional geometries and meshes. In Fig. 2 on the left, we show the two dimensional geometry with color contours of the plasma density. We are investigating the fraction of density that assembles on axis and how this fraction depends on anode shape, pulse shape, plasma and neutral gas distributions. We have developed a number of synthetic diagnostics for comparing simulation to experiment. In particular, we have synthetic photon emission (that can also be a proxy for x-ray emission), plasma inductance, and thermal neutron yield. We show in Fig. 2 on the right the time resolved and time integrated synthetic thermal neutron yield for a Hawk simulation.

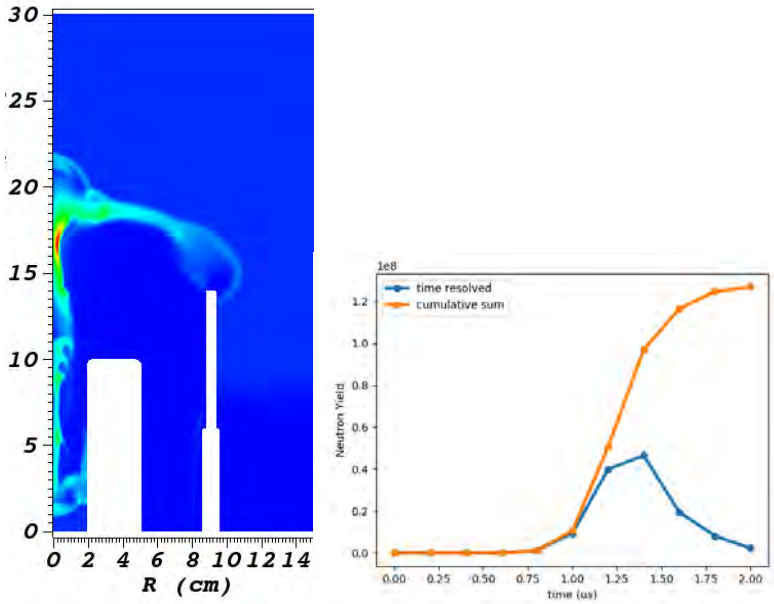

Fig 2: (left) Density contours in the Hawk dense plasma focus modeled with USim. (right) Thermal neutron yield, both time resolved in blue and time integrated in orange.

We developed in the kinetic code VSim an initial simulation model of a planar magnetron design based on recent work from the University of Michigan. We see the formation of the pi-mode and spokes. We added diagnostics for important quantities such as voltage, RF power, current, and current density. In Fig. 3 we show on the left a picture of the geometry for the planar magnetron with particles forming spokes and the RF fields oscillating (as color contours). In Fig. 3 on the right we show a Fourier transform of the time series of one of the field components, showing the operating frequency of 1 GHz.

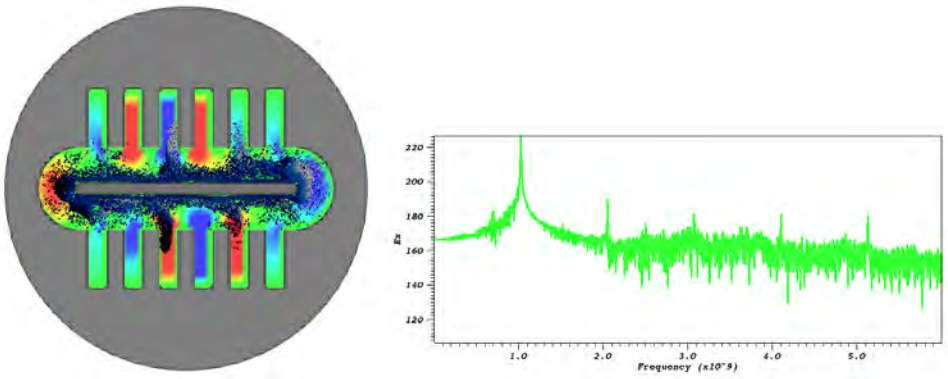

Fig 3: (left) Particles and fields in a planar magnetron modeled with VSim. (right) Fourier transform of the time series of a field component in one of the cavities showing the operating and harmonic frequencies.

We have models of a 5 GHz klystron in USim for comparison of advanced fluid models with PIC models and theory. Our first simulations were cold tests of the cavity modes in a planar geometry. Cold tests are important to understand how cavity frequencies and Qs shift under different beam currents and powers. We show in Fig. 4 the klystron geometry and various electric and magnetic field components modeled using USim.

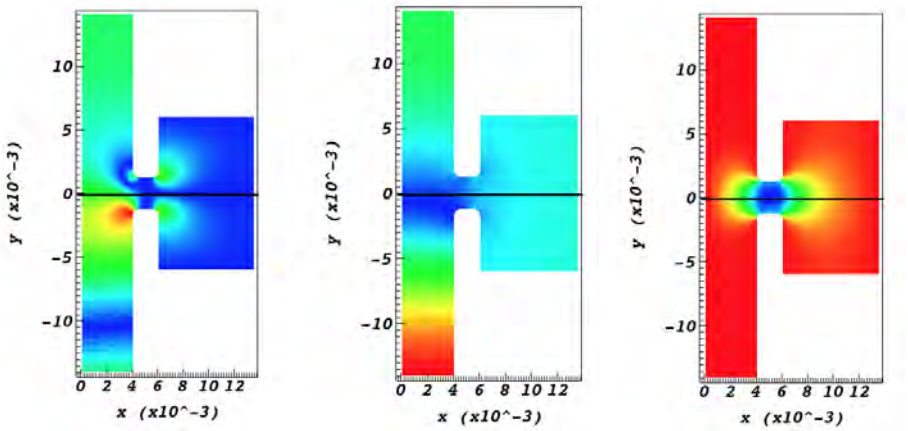

Fig 4: Electromagnetic field components for USim models of a 5 GHz magnetron.

3. Findings and Conclusions

Our conclusions are that USim and VSim are capable of modeling devices relevant to the Navy mission, specifically high power microwave devices and dense plasma focus neutron sources. We have transitioned these capabilities to scientists at the NRL.

4. Plans and Upcoming Events

A broad description of our upcoming work includes how best to validate emission models. This will include work on electron beam collectors and continued work on microwave sources such as the planar magnetron.

We have a February meeting planned with our NRL collaborators at the NRL facilities. We also plan a series of posters and talks at the Pulsed Power and Plasma Science meeting in June (http://www.ppps2019.org).

Recommendations for Future Work: We feel we are making sufficient progress at this time.

5. Transitions and Impacts

We believe we have transitioned to NRL the capability to model magnetrons. This concluded with a successful presentation at the International Conference on Plasma Science in May 2018. The lead author of the presentation was Ian Rittersdorf of NRL. We demonstrated specifically that VSim models of a relativistic planar magnetron agreed with results from other established codes (Neptune and ICEPIC).

We also believe we have transitioned to NRL the capability to model a dense plasma focus. This will conclude with two November presentations at the American Physical Society Division of Plasma Physics meeting in Portland, one with Steve Richardson of NRL as the lead author. Specifically, we have demonstrated the ability to model key diagnostics such as x-ray pinhole images, neutron yield and plasma inductance using the USim multifluid code.

6. Collaborations

We have an ongoing collaboration with Naval Research Laboratories. We began with a kickoff meeting held at NRL on Dec 15 2017, where we collaborated with NRL researchers to identify exact details of the simulations we would perform as part of the tasks outlined in our contract. The NRL attendees included Joe Schumer, Ian Rittersdorf, Steve Richardson, Dave Abe, Sasha Vlasov, and Simon Cooke. Tech-X attendees included Christine Roark and Peter Stoltz. The Michigan State attendee was John Luginsland. Ryan Hoffman from ONR attended as well. During this reporting period, we compare simulation results with NRL experimental results, specifically to the Hawk Dense Plasma Focus. We also compared with other NRL simulation results, specifically to ICEPIC and Neptune simulation results of a planar magnetron.

We also have a collaboration with Verus Research on work funded by ONR. This work is to model plasma-based switches in L-band and S-band waveguides. We compare with experiment and simulation done by Verus scientists.

7. Personnel

Principal investigator: Peter Stoltz, Tech-X Corp., 8.6 person months worked, not a National Academy Member, US citizen

Co-PI: John Luginsland, Confluent Sciences LLC, 6.75 person months worked, not a National Academy Member, US citizen

Business Contact: Laurence Nelson, Tech-X Corp., 0 person months worked, not a National Academy Member, US citizen

Team Members: Anton Spirkin, Tech-X Corp., 8.3 person months worked, not a National Academy Member, US citizen; Christine Roark, Tech-X Corp., 6.4 person months worked, not a National Academy Member, US citizen

Subs: see Co-PI

8. Students

N/A

9. Technology Transfer

We have an ongoing collaboration with Naval Research Laboratories that includes Joe Schumer, Stuart Jackson, Ian Rittersdorf, and Steve Richardson. We compare simulation results with NRL experimental results, specifically to the Hawk Dense Plasma Focus. We also compare with other NRL simulation results, specifically to ICEPIC and Neptune simulation results of a planar magnetron.

We also collaborate with Air Force Research Laboratory on code-to-code comparison between ICEPIC and VSim.

Regarding commercialization efforts, we are working with Verus Research scientists on models of plasma switches. We believe this effort may lead to future software sales and contract work.

10. Products, Publications, Patents, License Agreements, etc.

Publications resulting from this project:

Conference Papers

Higher Order Fluid Moments, And Their Ability To Capture Beam-Wave Interaction In High Power Microwave Sources, John Luginsland, JH Shin, Ryan Marcus, Christine Roark, Peter Stoltz, Anton Spirkin, International Conference on Plasma Science, June 24-28, 2018, Denver, CO, USA, other, N/A, abstract number, P2A1346-36, Yes

Modeling Of The Hawk Dense Plasma Focus (DPF) Device Using USim, Christine Roark, Peter Stoltz, Anton Spirkin, John Luginsland, Stuart Jackson, John Giuliani, Joey Engelbrecht, International Conference on Plasma Science, June 24-28, 2018, Denver, CO, USA, other, N/A, abstract number, P1A257-28, Yes

Comparison Of High Power Microwave Source Performance Between Different Particle-In-Cell Codes At The Naval Research Laboratory, Ian Rittersdorf, Steve Richardson, Steve Swanekamp, Joseph Schumer, Peter Stoltz, Christine Roark, John Luginsland, International Conference on Plasma Science, June 24-28, 2018, Denver, CO, USA, other, N/A, abstract number, P1A257-29, Yes

Hybrid Fluid-Kinetic Simulations Of Magnetized Plasma Systems, Peter Stoltz, Anton Spirkin, John Luginsland, Kris Beckwith, Uri Shumlak, International Conference on Plasma Science, June 24-28, 2018, Denver, CO, USA, other, N/A, abstract number, P2A1346-35, Yes

11. Point of Contact in Navy

Joseph Schumer, PhD
Head, Pulsed Power Physics Branch
Plasma Physics Division
Naval Research Laboratory, Code 6770
4555 Overlook Ave SW
Washington, DC 20375
email: joseph.schumer@nrl.navy.mil
work: (202) 404-4359 (DSN 354)

We last discussed our research with Dr. Schumer at a collaboration team meeting on Sept. 17-19 at the NRL facilities.

12. Acknowledgement/Disclaimer

This work was sponsored by the Office of Naval Research (ONR), under grant number N00014-18-C-0060. The views and conclusions contained herein are those of the authors only and should not be interpreted as representing those of ONR, the U.S. Navy or the U.S. Government.

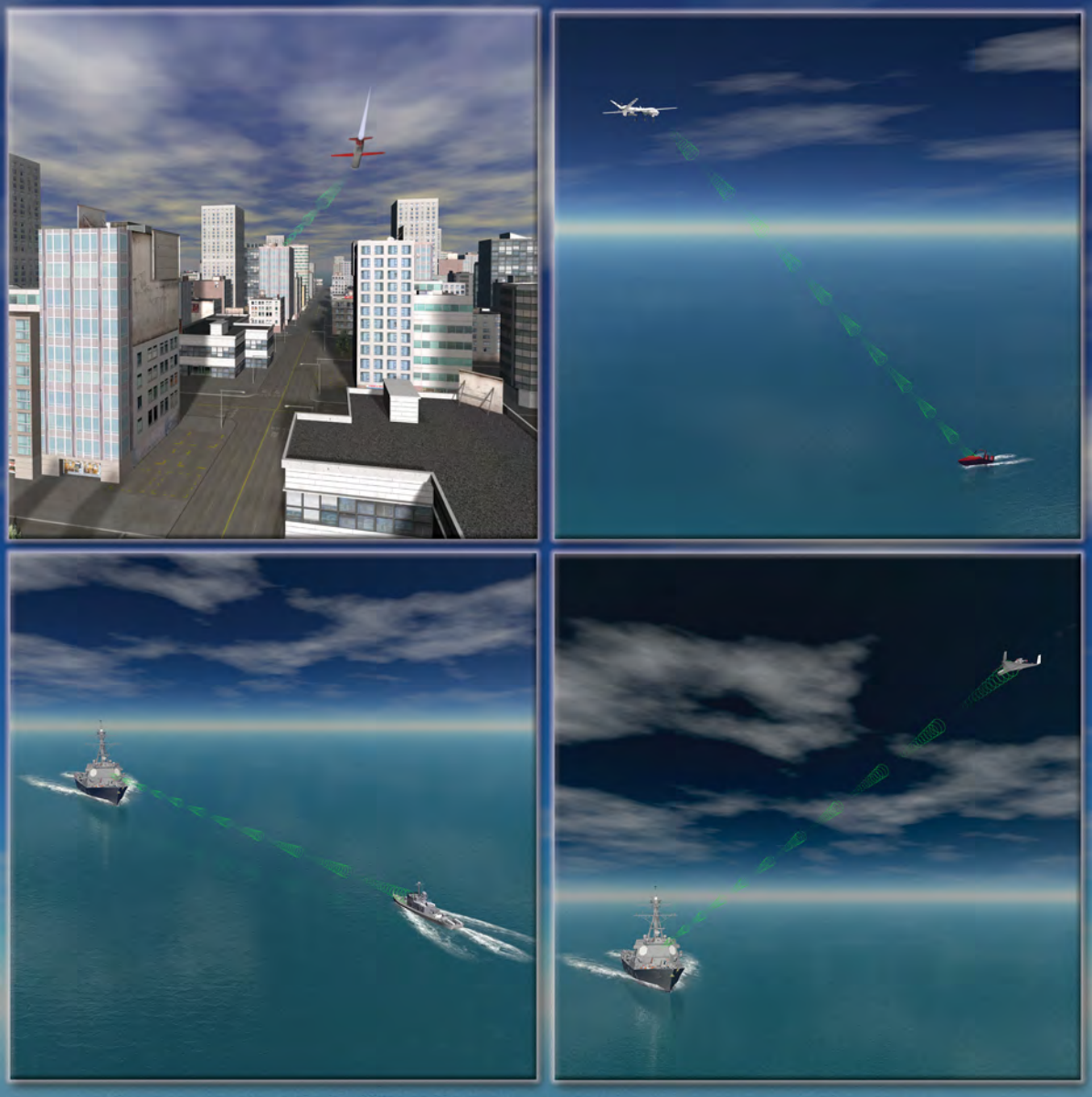

Office of Naval Research
875 N. Randolph Street
Arlington, VA 22203-1995
www.onr.navy.mil